Hyainailourine and teratodontine cranial material from the late Eocene of Egypt and the application of parsimony and Bayesian methods to the phylogeny and biogeography of Hyaenodontida (Placentalia, Mammalia) (#10831)

First submission

Please read the **Important notes** below, and the **Review guidance** on the next page.
When ready **submit online**. The manuscript starts on page 3.

Important notes

Editor and deadline

Hans-Dieter Sues / 28 Jun 2016

Files	23 Figure file(s)
	10 Table file(s)
	7 Raw data file(s)
	Please visit the overview page to **download and review** the files not included in this review pdf.
Declarations	**Describes a new species.**

For assistance email **peer.review@peerj.com**

Review guidelines

Please in full read before you begin

How to review

When ready **submit your review online**. The review form is divided into 5 sections. Please consider these when composing your review:

1. **BASIC REPORTING**
2. **EXPERIMENTAL DESIGN**
3. **VALIDITY OF THE FINDINGS**
4. General comments
5. Confidential notes to the editor

📄 You can also annotate this **pdf** and upload it as part of your review

To finish, enter your editorial recommendation (accept, revise or reject) and submit.

BASIC REPORTING

- Clear, unambiguous, professional English language used throughout.

- Intro & background to show context. Literature well referenced & relevant.

- Structure conforms to **PeerJ standard**, discipline norm, or improved for clarity.

- Figures are relevant, high quality, well labelled & described.

- Raw data supplied (See **PeerJ policy**).

EXPERIMENTAL DESIGN

- Original primary research within **Scope of the journal**.

- Research question well defined, relevant & meaningful. It is stated how research fills an identified knowledge gap.

- Rigorous investigation performed to a high technical & ethical standard.

- Methods described with sufficient detail & information to replicate.

VALIDITY OF THE FINDINGS

- Impact and novelty not assessed. Negative/inconclusive results accepted. *Meaningful* replication encouraged where rationale & benefit to literature is clearly stated.

- Data is robust, statistically sound, & controlled.

- Conclusion well stated, linked to original research question & limited to supporting results.

- Speculation is welcome, but should be identified as such.

The above is the editorial criteria summary. To view in full visit **https://peerj.com/about/editorial-criteria/**

Hyainailourine and teratodontine cranial material from the late Eocene of Egypt and the application of parsimony and Bayesian methods to the phylogeny and biogeography of Hyaenodontida (Placentalia, Mammalia)

Matthew R Borths [Corresp., 1] , Patricia A Holroyd [2] , Erik R Seiffert [3]

[1] Department of Biomedical Sciences, Ohio University, Athens, Ohio, United States

[2] Museum of Paleontology, University of California, Berkeley, Berkeley, California, United States

[3] Department of Cell and Neurobiology, University of Southern California, Los Angeles, California, United States

Corresponding Author: Matthew R Borths
Email address: borths.1@gmail.com

Hyaenodontida is a diverse, extinct group of carnivorous mammals that included weasel-to rhinoceros-sized species. The oldest-known hyaenodontidan fossils are from the middle Paleocene of North Africa and the antiquity of the group in Afro-Arabia lead to the hypothesis that it originated there and dispersed to Asia, Europe, and North America. Here we describe two new hyaenodontidan species based on the oldest hyaenodontidan cranial specimens known from Afro-Arabia. The material was collected from the latest Eocene Locality 41 (L-41, ~34 Ma) in the Fayum Depression, Egypt. *Akhnatenavus nefertiticyon* sp. nov. has specialized, hypercarnivorous dentition and an elongate cranial vault. In *A. nefertiticyon* the tallest piercing cusp on M^1–M^2 is the paracone. *Brychotherium ephalmos* gen. et sp. nov. has more generalized dentition that retains a metaconid and complex talonid on M_1–M_3. In *B. ephalmos* the tallest piercing cusp on M^1–M^2 is the metacone. We incorporate this new material into a series of phylogenetic analyses using a character-taxon matrix that includes novel dental, cranial, and postcranial characters, and samples extensively from the global record of the group. The phylogenetic analysis includes the first application of Bayesian methods to hyaenodontidan relationships. *B. ephalmos* is consistently placed close to members of Teratodontinae, an Afro-Arabian clade with several generalist and hypercarnivorous forms. *Akhnatenavus* is consistently recovered in Hyainailourinae as part of an Afro-Arabian radiation. The phylogenetic results suggest that hypercarnivory evolved independently three times within Hyaenodontida: in Teratodontinae, in Hyainailourinae, and in Hyaenodontinae. Teratodontines are consistently placed in a close relationship with Hyainailouridae (Hyainailourinae + Apterodontinae) to the exclusion of "proviverrines," hyaenodontines, and several basal North American clades, and we propose that the superfamily Hyainailouroidea be used to

describe this relationship. Using the topologies recovered from each phylogenetic method, we reconstructed the biogeographic history of Hyaenodontida using parsimony optimization, likelihood optimization, and Bayesian Binary MCMC to examine support for the Afro-Arabian origin of Hyaenodontida. Across all analyses, we found that Hyaenodontida originated on northern continents (Europe or North America), rather than Afro-Arabia. The clade is estimated by tip-dating analysis (given a ~K-Pg boundary prior on root age) to have undergone a rapid radiation in the Paleocene; a radiation currently not documented by fossil evidence. During the Paleocene lineages are reconstructed as dispersing to Asia, Afro-Arabia, and either Europe or North America. The place of origin of Hyainailouroidea is ambiguous but at least three of the constituent clades — Hyainailourinae, Apterodontinae, and Teratodontinae — are estimated by tip-dating to be established in Afro-Arabia by the middle Eocene.

1 **Hyainailourine and teratodontine cranial material from the**
2 **late Eocene of Egypt and the application of parsimony and**
3 **Bayesian methods to the phylogeny and biogeography of**
4 **Hyaenodontida (Placentalia, Mammalia)**
5
6 Matthew R. Borths[1], Patricia A. Holroyd[2], Erik R. Seiffert[3]

7 [1]Department of Biomedical Sciences, Heritage College of Osteopathic Medicine, Ohio University,

8 Athens, Ohio, USA

9 [2]Museum of Paleontology, University of California, Berkeley, California, USA

10 [3]Department of Cell and Neurobiology, Keck School of Medicine, University of Southern California, Los

11 Angeles, California, USA

12

13 Corresponding Author:

14 Matthew Borths[1]

15 228 Irvine Hall, Department of Biomedical Sciences, Heritage College of Osteopathic Medicine, Ohio

16 University, Athens OH 45701

17 Email address: borths.1@gmail.com

18   ABSTRACT

19   Hyaenodontida is a diverse, extinct group of carnivorous mammals that included weasel-

20   to rhinoceros-sized species. The oldest-known hyaenodontidan fossils are from the middle

21   Paleocene of North Africa and the antiquity of the group in Afro-Arabia lead to the hypothesis

22   that it originated there and dispersed to Asia, Europe, and North America. Here we describe two

23   new hyaenodontidan species based on the oldest hyaenodontidan cranial specimens known from

24   Afro-Arabia. The material was collected from the latest Eocene Locality 41 (L-41, ~34 Ma) in

25   the Fayum Depression, Egypt. *Akhnatenavus nefertiticyon* sp. nov. has specialized,

26   hypercarnivorous dentition and an elongate cranial vault. In *A. nefertiticyon* the tallest, piercing

27   cusp on M^1–M^2 is the paracone. *Brychotherium ephalmos* gen. et sp. nov. has more generalized

28   dentition that retain the metacone and complex talonids on M_1–M_3. In *B. ephalmos* the tallest,

29   piercing cusp on M^1–M^2 is the metacone. We incorporate this new material into a series of

30   phylogenetic analyses using a character-taxon matrix that includes novel dental, cranial, and

31   postcranial characters, and samples extensively from the global record of the group. The

32   phylogenetic analysis includes the first application of Bayesian methods to hyaenodontidan

33   relationships. *B. ephalmos* is consistently placed close to members of Teratodontinae, an Afro-

34   Arabian clade with several generalist and hypercarnivorous forms, and *Akhnatenavus* is

35   consistently recovered in Hyainailourinae as part of an Afro-Arabian radiation. The phylogenetic

36   results suggest that hypercarnivory evolved independently three times within Hyaenodontida: in

37   Teratodontinae, in Hyainailourinae, and in Hyaenodontinae. Teratodontines are consistently

38   placed in a close relationship with Hyainailouridae (Hyainailourinae + Apterodontinae) to the

39   exclusion of "proviverrines," hyaenodontines, and several basal North American clades, and we

40   propose that the superfamily Hyainailouroidea be used to describe this relationship. Using the

41 topologies recovered from each phylogenetic method, we reconstructed the biogeographic

42 history of Hyaenodontida using parsimony optimization, likelihood optimization, and Bayesian

43 Binary MCMC to examine support for the Afro-Arabian origin of Hyaenodontida. Across all

44 analyses, we found that Hyaenodontida originated on northern continents (Europe or North

45 America), rather than Afro-Arabia. The clade is estimated by tip-dating analysis (given a ~K-Pg

46 boundary prior on root age) to have undergone a rapid radiation in the Paleocene; a radiation

47 currently not documented by fossil evidence. During the Paleocene lineages are reconstructed as

48 dispersing to Asia, Afro-Arabia, and either Europe or North America. The place of origin of

49 Hyainailouroidea is ambiguous but at least three of the constituent clades — Hyainailourinae,

50 Apterodontinae, and Teratodontinae — are estimated by tip-dating to be established in Afro-

51 Arabia by the middle Eocene.

52   INTRODUCTION

53   Hyaenodontida is an extinct clade of carnivorous mammals whose members were broadly

54   distributed across Europe, North America, Asia, and Afro-Arabia during the Paleogene (Rose,

55   2006). In Eurasia and Afro-Arabia, some hyaenodontidan lineages persisted into the Miocene

56   (Lewis & Morlo, 2010). Hyaenodontidans ranged in body mass from small weasel-sized species

57   like North American *Thinocyon* (Gunnell, 1998) and European *Eoproviverra* (Godinot, 1981) to

58   gigantic, bear-sized species like North American *Hemipsalodon* (Mellet, 1969) and Afro-Arabian

59   *Megistotherium* (Savage, 1973). In Europe, Asia, and North America, hyaenodontidans shared

60   carnivorous niche space with species from Carnivoramorpha, Mesonychia, and Oxyaenida

61   (Morlo, Gunnell & Nagel, 2010), but in Afro-Arabia, a continent that was largely isolated from

62   all others from the Albian (Early Cretaceous, ~100 Ma, Gaina et al., 2013) to the Miocene (~16

63   Ma, Partridge, 2010), terrestrial carnivore niches were occupied almost exclusively by

64   Hyaenodontida (Lewis & Morlo, 2010).

65   Historically, the first hyaenodontidans recovered from Afro-Arabia were found in the

66   early Oligocene beds of the Fayum Depression, Egypt, and were placed in genera known from

67   Europe (*Apterodon, Pterodon,* and *Hyaenodon*) and North America (*Sinopa*) thereby implicitly

68   linking hyaenodontidans from the northern continents to the Fayum fauna (Andrews, 1904,

69   1906). The dominant phylogenetic hypothesis at the time (Matthew, 1901; Matthew, 1906;

70   Matthew, 1915) placed *Pterodon* and *Hyaenodon* (genera with specialized hypercarnivorous

71   dentitions [Van Valkenburgh, 2007]) in the subfamily Hyaenodontinae, and *Sinopa* in the more

72   generalized Proviverrinae. In this taxonomic arrangement, proviverrines were distinguished from

73   other hyaenodontidans by their retention of prominent metaconids on the lower molars and

74   separated paracones and metacones on the upper molars; Proviverrinae was therefore seen as the

75   generalized "stock" that gave rise to the more specialized hyaenodontines, which were derived in

76   having lost lower molar metaconids, and having fused the paracone and metacone on the upper

77   molars. Schlosser (1911) built on this phylogenetic framework in his analysis of the Fayum

78   hyaenodontidans, arguing for a North American origin of hyaenodontidans from a *Sinopa*-like

79   ancestor, some of which then dispersed to Europe and gave rise to *Pterodon* and *Apterodon*,

80   before members of *Pterodon*, *Apterodon*, and *Sinopa* dispersed to Afro-Arabia from Europe

81   during the late Eocene. This biogeographic hypothesis framed Afro-Arabia as something of a

82   cul-de-sac for hyaenodontidan lineages that evolved during the early and middle Eocene on

83   northern continents.

84   This scenario had to be reevaluated when Crochet (1988) described *Koholia atlasense,* a

85   hyaenodontidan from the late early Eocene of Algeria that they argued had no obvious links to

86   North American, European, or Asian taxa. By providing evidence for the great antiquity of

87   Hyaenodontida in Afro-Arabia, the presence of *Koholia* complicated the biogeographic history

88   of the clade. The presence of Hyaenodontida in Afro-Arabia was pushed even deeper into time

89   when Gheerbrant et al. (2006) described the early Eocene *Boualitomus marocanensis*, and Solé

90   et al. (2009) described the middle Paleocene (Kocsis et al., 2014) *Lahimia selloumi*, both small-

91   bodied species from Morocco that were hypothesized to be closely related to *Koholia* (Solé et al.,

92   2009). *Lahimia* is the oldest-known hyaenodontidan from any continent, and multiple authors

93   have recently advocated for the Afro-Arabian origin of Hyaenodontida in large part based on the

94   great age of *Lahimia* (Solé, 2013; Morlo et al., 2013; Solé et al., 2014b).

95   In addition to the discovery of ancient Afro-Arabian hyaenodontidans, the reframing of

96   the biogeographic history of Hyaenodontida has also been spurred by new phylogenetic

97   hypotheses generated by parsimony-based cladistic analyses. Barry (1988) was the first to apply

98   cladistic methodology to hyaenodontidan systematics. Barry (1988) employed 40 dental

99   characters in his study of the relationships within Proviverrinae, particularly among the Afro-

100   Arabian proviverrines *Masrasector*, *Anasinopa, Metasinopa,* and *Dissopsalis*, which were found

101   to be paraphyletic with respect to the proviverrines *Proviverra*, *Cynohyaenodon*, *Prodissopsalis*,

102   *Paracynohyaenodon*, and *Allopterodon.* The results of his analysis implied multiple dispersal

103   events between Europe and Afro-Arabia, and between Asia and Afro-Arabia.

104   Polly (1996) conducted the first cladistic study that included proviverrines as well as

105   more specialized hyaenodontidans like *Pterodon* and *Hyaenodon* in the same character-taxon

106   matrix. His study was also the first to incorporate cranial and postcranial characters. Polly found

107   Proviverrinae to be paraphyletic, and to include at least two lineages that independently evolved

108   specialized carnivory — Hyaenodontinae, which includes *Hyaenodon*, and Hyainailourinae,

109   which includes *Pterodon*. Importantly, the cranial characters (particularly the construction of the

110   nuchal crest) and postcranial characters (particularly the morphology of the astragalar-calcaneal

111   joints) that he employed provided non-dental support for the hypothesis that hypercarnivory had

112   evolved independently multiple times within Hyaenodontida.

113   More recent phylogenetic studies have focused on specific lineages within

114   Hyaenodontida — Limnocyoninae (Morlo & Gunnell, 2003), Afro-Arabian and Asian

115   proviverrines (Egi et al., 2005), early North American and European proviverrines (Zack, 2011;

116   2015), possible relatives of *Apterodon* (Grohé et al., 2012), European proviverrines (Solé, 2013;

117   Solé, Falconnet & Yves, 2014a), and Hyainailourinae (Solé et al., 2015) — but each of these

118   studies was limited in its biogeographic scope, and restricted its character sample to dental

119   morphology. This restriction is understandable because much of the hyaenodontidan record is

120   composed of isolated dentaries, rostral fragments, and isolated teeth, and the inclusion of cranial

121   and postcranial characters leaves a great deal of missing data, though simulation studies have

122   shown that missing data is less problematic than might be expected (Wiens, 2003; Kearney &

123   Clarke, 2003; Wiens & Moen, 2008; Prevosti & Chemisquy, 2010).

124   Rana et al. (2015) was the first study that used the cranial and postcranial characters

125   described by Polly (1996) as part of an expanded cladistic analysis, an effort expanded by Zack

126   & Rose (2015) in their study of North American hyaenodontidans. The study of Rana et al.

127   (2015) was the first since that of Polly (1996) to include both *Hyaenodon* and *Pterodon* in the

128   same analysis. Two clades recovered by Rana et al. (2015) are particularly relevant to the present

129   study — Teratodontinae and Hyainailourinae. Teratodontinae is a subfamily that was first

130   proposed by Savage (1965) to accommodate *Teratodon*, a strange early Miocene hyaenodontidan

131   from East Africa with massive premolars. Solé et al. (2014b) found that many Afro-Arabian taxa

132   formally considered to be proviverrines by Barry (1988) and Egi et al. (2005) — including

133   *Masrasector*, *Anasinopa*, and *Dissopsalis* — formed a clade with *Teratodon*. In the topology

134   recovered by Solé, Falconnet & Yves (2014a), Teratodontinae was the sister clade to European

135   Proviverrinae and North American *Arfia*, implying that dispersal had occurred between Afro-

136   Arabia and Europe. Rana et al. (2015) also recovered a monophyletic Teratodontinae, but found

137   that it was more closely related to *Apterodon* and Hyainailourinae, two predominantly Afro-

138   Arabian clades. In Rana et al.'s study, Hyainailourinae (similar to Polly's Pterodontinae [=

139   Hyainailourinae; Lewis & Morlo, 2010]) groups *Pterodon* species with Miocene

140   *Megistotherium/Hyainailouros* and Eocene-Oligocene *Akhnatenavus* in an unresolved polytomy.

141   Hyainailourinae is a cosmopolitan clade that was closely examined by Solé et al. (2015) that

142   includes North American *Hemipsalodon*, several European forms (*Paroxyaena, Kerberos*, and

143   *Pterodon dasyuroides*), Afro-Arabian "*Pterodon*" *africanus* and *Akhnatenavus*, and possibly

144   Asian *Orienspterodon* (Egi, Tsubamoto & Takai, 2007). Rana et al. (2015) constructed the first

145   character-taxon matrix since that of Polly (1996) that employed cranial characters, though

146   Hyainailourinae was part of a polytomy with European *Oxyaenoides*, Afro-Arabian *Koholia*, and

147   Afro-Arabian *Metapterodon*. Solé et al. (2015) proposed additional cranial features that

148   distinguish Hyainailourinae from Hyaenodontinae, but these features were not incorporated into

149   the Solé et al. (2015) phylogenetic analysis.

150   Here we describe several hyaenodontidan fossils from the latest Eocene of Egypt that

151   bear on the content, interrelationships, and biogeography of Teratodontinae and Hyainailourinae,

152   as well as Hyaenodontida generally. A new teratodontine genus and species is represented by

153   two rostra and well-preserved mandibular remains, while a new hyainailourine species is

154   represented by a largely complete, but crushed, crania. Both are known from sufficient dental

155   material to facilitate estimations of body mass based on regression equations used by Van

156   Valkenburgh (1990) and Morlo (1999). To place these species into phylogenetic context, we

157   employed a character taxon matrix that includes 134 morphological characters and 76 taxa that

158   builds upon previous analyses of hyaenodontidan systematic efforts. This matrix was analyzed

159   using parsimony and Bayesian approaches.

160   As part of the Bayesian analysis, we employ a recently developed expansion of Bayesian

161   phylogenetic inference that has been called "tip-dating" (Pyron, 2011; Ronquist et al., 2012b;

162   Beck & Lee, 2014). In standard Bayesian phylogenetic inference, a posterior distribution of

163   unique topologies with different branch lengths is generated using Markov chain Monte Carlo

164   (MCMC) sampling, taking into account the data (character-taxon matrix), a model of evolution

165   (for morphology typically the M_k model [Lewis, 2001]), and a parameter for evolutionary rate

166   (Huelsenbeck et al., 2002, Archibald, Mort & Crawford, 2003). Clades are sampled by the

167   MCMC process in proportion to their posterior probabilities. Tip-dating is a logical extension of

168   standard Bayesian inference that more realistically constrains rates of evolution across the tree

169   by taking into account the actual ages of fossil taxa (Beck & Lee, 2014; Arcila et al., 2015);

170   therefore, tip-dating provides additional information that contributes to the comparative

171   likelihood of the branch-length-scaled topologies, and it can also be used to estimate divergence

172   times among living and extinct taxa. This method has recently been applied to phylogenetic

173   analysis of several clades (Schrago, Mello & Soares, 2013; Wood et al., 2013; Beck & Lee,

174   2014; Lee et al., 2014; Dembo et al., 2015; Arcila et al., 2015; Close et al., 2015; Sallam &

175   Seiffert, 2016; Gorscak & O'Connor, 2016) and is applied here for the first time to

176   hyaenodontidan systematics.

177

178   **A Note on the taxonomic terms "Creodonta" and Hyaenodontida**

179   Hyaenodontida is discussed in this study as an elevation of the clade Hyaenodontidae,

180   which has traditionally been nested within Creodonta along with another extinct family,

181   Oxyaenidae (e.g., Matthew, 1915; Gunnell, 1998; Rose, 2006). Creodonta is then traditionally

182   considered sister clade to Carnivoramorpha in the larger clade Ferae (McKenna & Bell, 1997;

183   Wesley-Hunt & Flynn, 2005; Spaulding & Flynn, 2012; Halliday, Upchurch & Goswami, 2015).

184   Cope (1875) originally defined Creodonta and modified its definition through time, eventually

185   determining that the Creodonta was part of Insectivora and that Insectivora also included

186   Miacidae, Mesonychidae, Chrysochloridae, Centetidae, Talpidae, Mythomyidae, Oxyaenidae,

187   and Hyaenodontidae (Cope, 1884). With additional fossil, osteological, and eventually genetic

188   information, each of these families was moved to other orders and clades (Miacidae to

189   Carnivoramorpha [Spaulding & Flynn, 2012]; Mesonychidae as a sister group of artiodactyls and

190   perissodactyls [Spaulding, O'Leary & Gatesy, 2009]; "Centetidae" and "Mythomyidae" [tenrecs]

191   and Chrysochloridae to Afrosoricida, and Talpidae to Eulipotyphla or Lipotyphla [Stanhope et

192   al., 1998]) except Oxyaenidae and Hyaenodontidae, which have been retained as members of

193   Creodonta by Gunnell & Gingerich (1991) and Gunnell, (1998).

194   Multiple authors, first Van Valen (1966) then later Polly (1996), raised the possibility

195   that Oxyaenidae and Hyaenodontidae are not sister taxa and that Creodonta is not a clade. This

196   suggestion has been adopted in many recent studies (Grohé et al., 2012; Morlo et al., 2013; Solé

197   et al., 2014b), but there has been little discussion of what the sister taxon of Hyaenodontidae is if

198   not Oxyaenida as a whole or if these groups of mammalian carnivores are each indeed clades.

199   Spaulding, O'Leary & Gatesy (2009), O'Leary et al. (2013), and Halliday, Upchurch &

200   Goswami (2015) each applied cladistic methodology to an examination of large-scale

201   relationships within Placentalia which included representatives of Ferae (Carnivora + Pholidota

202   and possibly Creodonta). Ferae and Creodonta were monophyletic in Spaulding, O'Leary &

203   Gatesy (2009), but their study was focused on the relationships within Cetartiodactlyla, rather

204   than Ferae, and only included four species from Creodonta (and did not include Pholidota).

205   O'Leary et al. (2013) also resolved a monophyletic Ferae, but only included one representative

206   from Creodonta, the hyaenodontidan *Sinopa rapax*, thus this large-scale examination of

207   Placentalia did not test for the monophyly of Creodonta. Halliday, Upchurch, & Goswami (2015)

208   focused on Paleocene mammal groups and found a monophyletic Ferae and a monophyletic

209   Creodonta when all topological constraints were applied to the analysis, though their analysis

210   was limited to four North American creodonts: the hyaenodonts *Prolimnocyon* and *Pyrocyon* and

211   the oxyaenidans *Dipsalidictis* and *Tytthaena*.

212   Recent phylogenetic studies that have examined relationships among non-oxyaenid

213   creodonts have employed the order Hyaenodontida, and named clades (families and subfamilies)

214   that reflect their inclusion in that order (Grohé et al., 2012; Solé, 2013; Solé et al., 2014b; Solé et

215   al., 2015). These studies cite Van Valen (1967) as the source of Hyaenodontida, but Van Valen

216   (1967) actually used the suborder Hyaenodonta, a taxon that he employed to encompass

217   Oxyaenidae, Hyaenodontidae, and Palaeoryctoidea. The name Hyaenodontida in the sense used

218   in the present study was first used by Solé (2013) to encompasses placental mammals with a

219   carnassial complex between P^4 and M_1, M^1 and M_2, and M^2 and M_3 that were previously placed

220   in Hyaenodontidae. Future analyses that sample broadly from Oxyaenida, Hyaenodontida, and

221   other placental orders are required to rigorously test the monophyly or polyphyly of Creodonta

222   and the phylogenetic definition of Hyaenodontida; such an analysis is, however, beyond the

223   scope of the current study.

224

225   **Institutional Abbreviations**

226   **AMNH**, American Museum of Natural History, New York; **BSPG**, Bayerische

227   Staatssammlung für Paläontologie und Historische Geologie, Munich; **CGM,** Cairo Geological

228   Museum, Cairo; **DPC,** Duke Lemur Center, Division of Fossil Primates, Durham; **KNM,**

229   National Museums of Kenya, Nairobi; **SMNS**, Staatliches Museum für Naturkunde, Stuttgart.

230

231   MATERIALS AND METHODS

232

233   **Geological Context**

234   The material described here was collected from Locality 41 (L-41) in the Fayum

235   Depression, Egypt (Fig. 1). The Fayum area preserves a near-continuous terrestrial record from

236   the early late Eocene through the early Oligocene (Bown & Kraus, 1988). Quarry L-41 is at the

237   top of the lower variegated sequence in the Jebel Qatrani Formation, and is interpreted to have

238   been deposited during a period of reversed magnetic polarity (Kappelman, Simons & Swisher,

239   1992) that has been correlated with the Eocene-Oligocene spanning Chron C13r (Seiffert, 2006).

240   The latest Priabonian (latest Eocene, ~37 Ma) age of L-41 is supported by the identification of a

241   major erosional unconformity just above L-41 that Seiffert (2006) hypothesized was caused by

242   the major drawdown in global sea level that occurred during the earliest Oligocene (e.g., Miller

243   et al., 2008). The age is also supported by biostratigraphic correlation with well-dated mammal

244   sites in Oman (Seiffert, 2006), and extinctions of multiple strepsirrhine primate lineages

245   upsection from L-41 that might have been due to earliest Oligocene cooling (Seiffert, 2007).

246   Many of the productive quarries in the Fayum are composed of a poorly consolidated

247   fine- to medium-grained sandstone and gravel that are quarried through aeolian weathering,

248   sweeping, and dry sieving (Bown & Krause, 1988). In contrast, L-41 is a well-consolidated

249   deposit that is dominated by green to yellow clay and postdepositional salt that is quarried in

250   sheets, with fossils exposed by carefully prying apart silt and claystone bedding planes (Simons,

251   Cornero & Bown, 1996). Vertebrate fossils are abundant at L-41 and the fine-grained matrix is

252   capable of preserving small fossils that are delicately prepared from the clay matrix. The larger

253   mammals known from the Fayum fauna, such as anthracotheres and hyraxes (Rasmussen &

254   Simons, 1991) are preserved at L-41, but the quarry is particularly important for preserving the

255   smaller components of the mammalian fauna, such as bats (Gunnell, Seiffert & Simons, 2008),

256   rodents (Sallam, Seiffert & Simons, 2011; Sallam, Seiffert & Simons, 2012; Sallam & Seiffert,

257   2016), tenrecoids (Seiffert & Simons, 2000; Seiffert et al., 2007) and small primates (Simons,

258   1990, 1997; Simons & Rasmussen, 1996; Simons et al., 2001). Complete crania, jaws, and

259   isolated skeletal elements are preserved in abundance, though most are crushed through post-

260   depositional taphonomic processes (Simons, Cornero & Bown, 1996). The quarry was likely

261   formed in the distal portion of a large freshwater lake, as suggested by the abundant preservation

262   of freshwater fish fossils. The vertebrate remains are hypothesized to have floated into the lake

263   during periodic flooding events and been buried with little disturbance from flowing water or

264   predation (Simons, Cornero & Bown, 1996).

265

266   **Taxonomy**

267   The electronic version of this article in Portable Document Format (PDF) will represent a

268   published work according to the International Commission on Zoological Nomenclature (ICZN),

269   and hence the new names contained in the electronic version are effectively published under that

270   Code from the electronic edition alone. This published work and the nomenclatural acts it

271   contains have been registered in ZooBank, the online registration system for the ICZN. The

272   ZooBank LSIDs (Life Sciences Identifiers) can be resolved and the associated information

273   viewed through any standard web browser by appending the LSID to the prefix

274   http://zoobank.org/. The LSID for this publication is urn:lsid:zoobank.org:pub:4EB91175-33FF-

275   4A6C-B5B2-2F9933C0DED9. The online version of this work is archived and available from

276   the following digital repositories: PeerJ, PubMed Central and CLOCKSS. The physical

277   specimens described here with a CGM specimen code are deposited at the Cairo Geological

278   Museum, Cairo, Egypt and specimens described here with a DPC specimen code are deposited at

279   the Duke Lemur Center, Division of Fossil Primates, Duke University, Durham, NC.

280

281   **Morphological Measurements and Nomenclature**

282   Dental measurements of the specimens were collected from digital photographs using

283   ImageJ (Schneider, Rasband & Eliceiri, 2012) or with digital calipers, following the methods of

284   Holroyd (1999). Dental nomenclature and measurements used in this description are illustrated

285   in Fig. 2.

286   Body mass was calculated using two sets of regression equations. The first is that of

287   Morlo (1999), which predicts body mass based on an average of the mesiodistal lengths of M_1-

288   M_3. The second regression equation was proposed by Van Valkenburgh (1990), which is based

289   on the mesiodistal lengths of M_1 in carnivorans. Although carnivorans show clear functional

290   parallels with hyaenodontidans due to their similar diets (Morlo, 1999; Van Valkenburgh, 2007;

291   Friscia & Van Valkenburgh, 2010), their capacity for dental shearing was achieved in a different

292   way, with carnivorans only having one pair of functional carnassials, and hyaenodontidans

293   having three (Rose, 2006). Many hyaenodontidan specimens have heavily worn M_1s and

294   shearing facets on M_2 and M_3, which suggests that the distal molars were used in adult

295   hyaenodontidans in the same way that the M_1 carnassial is used by carnivorans; therefore, any

296   results derived from Van Valkenburgh's (1990) equation must be viewed with caution. The Van

297   Valkenburgh (1990) equation was used in three ways, using 1) average mesiodistal molar length,

298   2) length of M_2, and 3) length of M_3. Because the L-41 hyainailourine is only known from upper

299   teeth, M_2 length is inferred from the distance between the postprotocrista of M^2 and the distal

300   aspect of the M^3 protocone.

301

302   **Specimen scanning**

303   All specimens presented in this analysis were micro-CT scanned on a Nikon XTH 225 ST

304   scanner housed in the Duke MicroCT lab in the Shared Materials Instrumentation Facility in the

305   Pratt School of Engineering at Duke University. All specimens described here are available for

306   viewing and download on MorphoSource, an NSF-supported repository for 3D scan data

307   <www.morphosource.org> in Project P200. Reviewers and editors can access this project before

308   publication by logging on to MorphoSource with the username

309   "morphsourcereviewer@gmail.com" and the password "reviewer." The voxel size, voltage, and

310   amperage used for each scan are are also accessioned in MorphoSource with with PLY files.

311   Three-dimensional surface models were constructed using Avizo 8.0 and are were visualized

312   using volume rendering or isosurface rendering for two-dimensional illustration.

313

Phylogenetic Analysis

315   Multiple phylogenetic analyses were conducted to place the two new L-41

316   hyaenodontidans into a broad phylogenetic framework. These analyses were also intended to test

317   existing hypotheses about relationships among multiple recently proposed hyaenodontidan

318   clades (e.g., Polly, 1996; Egi et al., 2005; Solé, 2013; Solé, Falconnet & Yves, 2014a; Solé et al.,

319   2014b; Solé et al., 2015; Rana et al., 2015) with new character data. Of particular interest for this

320   study are the structure of, and relationships within, Teratodontinae, Hyainailourinae, and

321   Hyaenodontinae, the latter clade having only been incorporated into two other cladistic analyses

322   (Polly, 1996; Rana et al., 2015) with an in-group expanded beyond *Hyaenodon* (note that Bastl,

323   Nagel & Peigné, [2014] limited their analysis to evaluation of the genus *Hyaenodon*). The

324   character taxon matrix used in this study includes 134 discrete dental, cranial, and postcranial

325   characters and 76 operational taxonomic units (OTUs — 4 outgroup taxa and 72

326   hyaenodontidans). For this study three basal eutherian taxa — Early Cretaceous *Eomaia*

327   *scansoria* from China (Ji et al., 2002), Late Cretaceous *Maelestes gobiensis* from Mongolia

328   (Wible et al., 2007, 2009), and Late Cretaceous *Cimolestes magnus* from North America

329   (Lillegraven, 1969; Kielan-Jaworowska, Cifelli & Luo, 2004) — were included as outgroups for

330   each analysis. This follows the outgroup selection used in previous phylogenetic analyses of

331   Hyaenodontida (Polly, 1996; Zack, 2011; Zack, 2015; Solé et al., 2014b; Rana et al., 2015; Zack

332   & Rose, 2015). Species level OTUs were used for all taxa except *Teratodon* and *Lesmesodon*

333   which were a composite of specimens referred to these genera.

334   Some of the characters used in this analysis were sampled from previous studies

335   including those of Polly (1996), Egi et al. (2005), Zack (2011), and Solé et al. (2014b). Some of

336   these characters were modified by concatenating similar characters and anatomical terminology

337   was modified to make the character descriptions consistent. Characters were expanded with

338   additional character states and 65 new characters are described, some initially proposed as

339   "features" in Solé et al. (2015). Inapplicable characters were reductively coded (Strong &

340   Lipscomb, 1999). Eighteen multistate characters were treated as ordered following the

341   recommendations of Slowinski (1993) in designating these characters and all characters were

342   equally weighted. All characters are listed in Table S1 with relevant citations, and ordered

343   characters are noted. All OTUs were rescored for each character in the analysis. Codings for

344   each taxon are provided in Data S1 and references, including age, formation, and locality, are

345   listed in Table S2. Character descriptions, nexus files, and photographs of the specimens

346   described in this study are also available on Morphobank (Project 2336)

347   <www.morphobank.org> and are accessible to editors and reviewers with the reviewer login

348   password "fayumreviewer."

349   **Parsimony Analysis**—Maximum parsimony analysis was performed in Tree Analysis

350   using New Technology software package (TNT) version 1.1 (Goloboff, Farris & Nixon, 2008).

351   The traditional search heuristic search algorithm was used across 10,000 replicates with random

352   addition sequence and TBR (tree bisection and reconnection) branch swapping, holding 10 trees

353   per TBR replicate. Consistency index (CI) and retention index (RI) values were calculated using

354   STATS.RUN in TNT. Support for each node in the maximum parsimony analysis was calculated

355   by running 10,000 bootstrap pseudoreplicates (Felsenstein, 1985) and Bremer support was

356   calculated for each node (Bremer, 1994) in TNT. Parsimony character optimization across all

357   MPTs was conducted in PAUP 4.0 (Swofford, 2003).

358   **Standard Bayesian Inference**—Bayesian phylogenetic inference analysis was

359   performed in MrBayes 3.2.3 (Ronquist et al., 2012a), using the CIPRES Scientific Gateway

360   (Miller, Pfeiffer & Schwartz, 2010). The M_k model (Lewis, 2001) for morphological data was

361   selected and the data type was set to "standard" with coding set to "variable" (Clarke &

362   Middleton, 2008). The analysis was run for 10×10^6 generations. Two runs were performed

363   simultaneously with four Markov chains, three of which were heated (temp = 0.02). A total of

364   2,000 generations were sampled (every 5000th generation of the 10×10^6 generations, to avoid

365   autocorrelation), the first 500 (25%) of which were discarded as burn-in. After the analysis was

366   run, convergence was examined using the effective sample sizes and average standard deviation

367   of split frequencies for the final generation. The resulting posterior probabilities (PP) for the

368   standard Bayesian analysis are listed to the right of the relevant node in the "allcompat"

369   (majority rule plus compatible groups) tree. Parsimony character optimization for the

370   "allcompat" tree was conducted in PAUP 4.0 (Swofford, 2003). PP values between 0 and 0.25

371   will be discussed as "very weakly supported," between 0.26 and 0.50 "weakly supported,"

372   between 0.51 and 0.75 "moderately supported," and between 0.76 and 1.00 "strongly supported."

373   **Bayesian "Tip-Dating"**—Bayesian "tip-dating" takes into account the relationships

374   between morphological character evolution and the temporal succession of fossil taxa to

375   simultaneously infer rates of morphological evolution and phylogenetic relationships. The

376   reconstructed evolutionary rates are taken into account in estimates of phylogenetic relationships,

377   and divergence dates between all included taxa are estimated (Ronquist et al., 2012b; Lee et al.,

378   2014). Note that this method does not operate directly upon a continuous temporal character as is

379   utilized in stratocladistic methods. Instead, the inferred branch length from the Bayesian

380   phylogenetic inference is divided by the tip-age to generate an implied rate along the branch and

381   estimate divergence dates for branches. Beck & Lee (2014) showed that when a temporal

382   constraint is imposed on an in-group, deeply nested but ancient taxa can be recovered at nodes

383   where rapid evolutionary change is taking place and evolutionary rates are consistent across

384   sister nodes. Tip-dating is an interesting alternative to parsimony analysis or standard Bayesian

385   inference for inferring phylogenetic relationships among members of "explosive" adaptive

386   radiations, such as those which are thought to have taken place in the placental mammalian

387   lineage near the K-Pg extinction event (O'Leary et al., 2013). Rapid radiations might be

388   expected to pose problems for parsimony analysis in particular, because rapid evolutionary

389   change near the base of a radiation might be overwritten by subsequent evolution along long

390   branches (Felsenstein, 1978) as lineages invade open niche space. Tip-dating seems especially

391   appropriate for Hyaenodontida, given the variable phylogenetic positions occupied by the oldest

392   Afro-Arabian hyaenodontidans *Lahimia*, *Boualitomus*, and *Tinerhodon* in the analysis by Rana et

393   al. (2015). These taxa were recovered deeply nested within Hyainailourinae in some MPTs and

394   in very basal positions in other MPTs, a result consistent with early phylogenetic experiments

395   performed with this data set using only dental characters.

396   The tip-dating analysis presented here was run in MrBayes 3.2.3 (Ronquist et al., 2012a)

397   following methods employed by Beck & Lee (2014). The M_k model was used to model

398   morphological character change and the independent gamma rates (IGR) relaxed clock model

399   (Lepage et al., 2007; Ronquist et al., 2012b), which assumes no autocorrelation of rates in the

400   phylogeny, was used to infer divergence ages from terminal taxa and reconstruct rates of

401   morphological evolution. Tip-dating requires specific dates for each terminal taxon. Each OTU,

402   with citations justifying its assigned date range, are listed in Table S2, from the oldest taxon in

403   the analysis (*Eomaia*, 129.7–122.1 Ma) to the youngest (*Dissopsalis*, 15–9 Ma). The root of the

404   tree was set with a prior of 120–130 Ma (Wible et al., 2009; O'Leary et al., 2013). Beck & Lee

405   (2014) demonstrated that, in the case of placental mammalian supraordinal phylogeny, node ages

406   tend to be reconstructed as particularly ancient and in extreme conflict with the fossil record if an

407   in-group constraint is not applied. The prior for the divergence date of Hyaenodontida was set

408   conservatively to be between 62 and 70 Ma, bracketing before and after the K/Pg boundary by

409   four million. This prior is also consistent with the estimated divergence date for Ferae, 63.8 Ma,

410   a divergence proposed by O'Leary et al. (2013). The analysis was run for 50×10^6 generations.

411   Shorter runs with 10×10^6 generations, the number of generations used in the standard Bayesian

412   analysis, had very low or inconsistent convergence parameters. Even with the greater number of

413   generations, convergence diagnostics remain low in this analysis (ESS 0.014). The priors that

414   produced the strongest convergence across all parameters was clockratepr = normal(0.01, 0.007),

415   and igrvarpr = exp(3). Two runs were performed simultaneously with four Markov chains, three

416   of which were heated (temp = 0.02). A total of 10,000 generations were sampled, the first 25%

417   of which were discarded as burn-in. The "allcompat" tree that results from the analysis includes

418   evolutionary rate estimates for each branch. Beck & Lee (2014:3) noted that rate estimates tend

419   to have "strongly positively skewed distributions" and they advocated for the use of the median

420   evolutionary rate rather than the mean evolutionary rate in discussions of branch evolution.

421   Relative rates for each node are calculated by comparing the % change/Ma for a given node to

422   the % change/Ma across the entire tree. The same definitions of the relative strength of posterior

423   probability support (PP) that were used in the standard Bayesian analysis, will be used to discuss

424   the results of the Bayesian tip-dating analysis.

425

426   **Biogeographic Methods**

427   Three separate biogeographic methods were applied to the phylogenetic topologies

428   recovered through parsimony analysis (strict consensus trees), standard Bayesian analysis

429   (allcompat tree), and tip-dating Bayesian analysis (allcompat tree). The three biogeographic

430   methods were ancestral state reconstruction using parsimony optimization (PO) (Brooks, 1990),

431   likelihood optimization (LO) (Maddison & Madison, 2015), and Bayesian Binary MCMC

432   (BBM) (Yu et al., 2015). Four continental areas were designated (Afro-Arabia, Asia, Europe,

433   and North America) for each analysis and each OTU was assigned to the continent where it was

434   found (Table S2).

435   Parsimony optimization of a continental biogeographic character not used in the

436   phylogenetic analysis was implemented in Mesquite (Maddison & Maddison, 2015) using

437   Mesquite's Parsimony Ancestral States reconstruction. Ambiguous reconstructions are

438   interpreted as equally parsimonious continental reconstructions for the origin of a clade.

439   Likelihood optimization of the continental biogeographic character was also implemented in

440 Mesquite using the Likelihood Ancestral States reconstruction with the model Mk1 (equally

441 probable state change). Likelihood analysis incorporated branch length information from the

442 standard Bayesian and tip-dating allcompat trees. Branch lengths for the maximum parsimony

443 tree were all equal.

444 BBM, a statistical method for inferring ancestral states such as biogeographic

445 distributions using Bayesian inference, was performed in RASP version 3.1 (Yu et al., 2015).

446 The number of areas from which a lineage could originate was was limited to one to model

447 dispersal rather than vicariance events. Dispersal is a more likely explanation for the distribution

448 of Hyaenodontida during the Late Cretaceous and early Paleogene than vicariance given global

449 paleogeography during this interval. Vicariance would imply an origin for Hyaenodontida that

450 proceeds the break-up of Pangea, which the fossil record does not currently support. The results

451 of the analysis are the probability of a given clade originating from one of four continental areas.

452 The MCMC analysis was performed over 10×10^6 generations with 10 Markov chains, sampling

453 every 100 generations, with the temperature set to 0.1. The first 100 trees were discarded as part

454 of the burn-in period, and the Jukes-Cantor model was used, with equal among-site rate

455 variation.

456

457 SYSTEMATIC PALEONTOLOGY

458 HYAENODONTIDA Solé, 2013

459 TERATODONTINAE Savage, 1965

460 *BRYCHOTHERIUM* Borths, Holroyd, and Seiffert, gen. nov.

461 urn:lsid:zoobank.org:act:A39C1414-CF72-4FDC-A087-9912FCEDB0C8

462 **Type Species**—*Brychotherium ephalmos,* sp. nov.

463　　　　**Etymology**—Meaning "greedily eating beast" in Greek from *brycho* (βρύχω) meaning to

464　eat greedily or noisily and thēríon (θηρίον) meaning beast. The name was first used by Holroyd

465　(1994) in her doctoral dissertation, and was subsequently used as a nomen nudum by Egi et al.

466　(2005) and Solé et al. (2014b).

467　　　　**Generic Diagnosis**—As for type species.

468　　　　**A Note on the Genus**—*Brychotherium* was originally coined and recognized as a distinct

469　genus in a dissertation (Holroyd, 1994), and was therefore not yet validly published under ICZN

470　rules. Subsequent studies (e.g., Egi et al., 2005; Solé et al., 2014b) have used the genus or

471　lumped it into "African *Sinopa* spp." (e.g., Rana et al., 2015), based solely on the lower

472　dentition. We formally name the taxon here, with a diagnosis that includes the more complete

473　sample now available including rostra and upper dentition. Notably, this formal diagnosis does

474　not include all specimens initially assigned to the genus in Holroyd (1994), as an expansion of

475　the L-41 sample in the last 22 years has further refined the understanding of the similarly-sized

476　hyaenodont fauna at the locality.

477

478　　　　*BRYCHOTHERIUM EPHALMOS* Borths, Holroyd, and Seiffert, sp. nov.

479　　　　　　　　　　　(Figs. 3–9, Table 1–2)

480　　　　　　　urn:lsid:zoobank.org:act:BCAACF37-E200-4172-A875-C4D5F6FFCEFB

481　　　　**Etymology**—Meaning "pickled in salty brine" in Greek from *ephalmos* (έφαλμος) in

482　reference to the high post-depositional salt content in the sediments of L-41.

483　　　　**Holotype**—CGM 83750, right dentary with canine–M_3.

484　　　　**Referred Specimens**—DPC 17627, right dentary with P_4-M_3 and rostrum with canine,

485　$dP4$-M^2, and erupting P^4. Specimens were associated and probably represent a single individual;

486   DPC 11990, rostrum with left and right P^4–M^3; DPC 11569A, right dentary with canine, P_2–M_3;

487   DPC 11569B, left dentary with P_2, P_3, M_1–M_3.

488   **Type Locality**—Locality 41 (L-41), Jebel Qatrani Formation, Fayum Depression, Egypt.

489   **Age and Distribution**—Late Eocene, latest Priabonian, ~34 Ma (Seiffert, 2006). Only

490   known from Locality 41, approximately 14.5 km west of Qasr el-Sagha Temple, and 2 km north

491   of the contact between the Qasr el-Sagha Formation and the Jebel Qatrani Formation.

492   **Diagnosis**—Differs from early Oligocene *Masrasector* species by being larger; having

493   relatively narrow talonid basins on the lower molars that taper distally toward the hypoconulids,

494   rather than being buccolingually wide and box-like; having tall lower molar trigonids that are

495   more than twice the height of the talonid, rather than being less than half the height of the

496   trigonid; having relatively small lower molar metaconids, rather than having metaconids that are

497   nearly subequal in height to paraconid; and having preprotocristids and postprotocristids that

498   more closely parallel the long axis of the horizontal ramus, rather than angling steeply lingually.

499   Differs from middle-late Miocene *Dissopsalis* by being smaller; having a pronounced metaconid

500   on M_3 rather than a metaconid that is very reduced or absent; having a larger and more complex

501   M_3 talonid rather than a very reduced M_3 talonid with poorly developed cusps; having

502   preprotocristid and postparacristid oriented somewhat lingually relative to the horizontal ramus

503   rather than being nearly parallel to the long axis of the horizontal ramus; having taller paracones

504   on M^1 and M^2 that are only slightly shorter than metacones, rather than having reduced

505   paracones that are distinctly shorter than metacones; and having wide upper molar protocones

506   that are more lingually placed relative to paracone, rather than having narrow protocones that are

507   shifted distally relative to the paracones. Differs from early Miocene *Anasinopa* by being

508   smaller; having taller, but mesiodistally short, lower molar trigonids rather than relatively low

509   and long trigonids; having a more buccolingually compressed P_4 rather than a buccolingually

510   broad P_4; having relatively elongate upper molar metastyles that form a deep and distinct

511   ectoflexus on M^2, rather than short metastyles that form a relatively shallow M^2 ectoflexus;

512   having more buccolingually compressed paracone and metacone cusps (with elliptical cross-

513   sections) on the upper molars, rather than having paracone and metacone cusps that are more

514   connate with rounded cross-sections; and having upper molar paracones that are relatively large,

515   when compared to the size of the metacone, rather than having paracones that are relatively low

516   and mesiodistally much shorter than metacones. Differs from early or middle Eocene *Furodon*

517   by having a relatively short P_4 with a more distinct paraconid; having a P_4 protoconid whose long

518   axis in buccal view is perpendicular to the alveolar margin, rather than being distally inclined;

519   having relatively low entocristids, rather than tall entocristids that close the lower molar talonids

520   lingually, especially on M_3; and having upper molar metacones that are mesiodistally longer and

521   taller than the paracones. Differs from early or middle Eocene *Glibzegdouia* by having an M_1

522   metaconid that is shorter than the M_1 paraconid, rather than an M_1 metaconid that is taller than

523   the M_1 paraconid; having an M_1-M_2 trigonid that is more than twice the height of the talonid,

524   rather than having an M_1-M_2 trigonid that is low compared to talonid; having M_1-M_2 talonids that

525   open lingually, rather than closed by a notched entocristid; having indistinct M_1-M_2 entoconids

526   rather than clear entoconid cusps; having M_1-M_2 trigonids that are buccolingually wider than the

527   talonids, rather than having M_1-M_2 trigonids that are of the same buccolingual width as the

528   talonids; and having a shallower M^1 ectoflexus and an elongate metastyle that is of

529   approximately the mesiodistal length of paracone/metacone base, rather than a deep M^1

530   ectoflexus with a metastyle that is shorter than the paracone/metacone base. Differs from early

531   Miocene *Teratodon* by having a P_4 with multiple cusps, rather than a bulbous P_4; having M_1-M_3

532   trigonids that are more than twice the height of the talonid; having buccolingually narrow upper

533   premolars that are not buccolingually wider than they are mesiodistally long; and having a

534   mesiodistally elongate M^2 metastyle that parallels the buccal margin, rather than a metastyle that

535   is shorter than the paracone/metacone base that angles lingually from buccal margin.

536

537   **Description**

538   **Rostrum**—DPC 11990 (Figs. 3 and 4) is a crushed rostrum referred to *Brychotherium*

539   *ephalmos*. The specimen preserves most of the anterior part of the cranium, from the premaxilla

540   back to the palatines, along with the left and right P^4–M^3. Like many specimens from L-41, the

541   specimen is crushed and many of the cranial bones are fragmentary, making sutures difficult to

542   interpret. Most of the distortion occurred through mediolateral crushing combined with minor

543   anterior-posterior shear. The left side of the rostrum is better preserved than the right. The rostral

544   remains of DPC 17627 also preserve dP^4-M^3; portions of the lateral and palatal aspects of the left

545   maxilla are relatively undistorted.

546   The premaxilla preserves the alveoli of I^2-I^3 and it frames the partially preserved nasal

547   aperture. Though the region is distorted, it is clear that the anterior and posterior borders of the

548   premaxilla incline dorsally and posteriorly and, as such, the nasals were somewhat retracted,

549   leaving the dorsal face of the palatal process of the premaxilla visible in dorsal view. The

550   premaxilla-maxilla suture traces the anterior margin of the canine alveolus. Neither canine is

551   preserved in DPC 11990 but the collapsed alveoli are present and indicate that the root of the

552   canine was wide and arched posteriorly over both roots of P^1 and the anterior root of P^2. From

553   the nasal aperture, the nasals become broader posteriorly. The nasal does not contact the

554   lacrimal; instead, there is an intervening maxilla-frontal suture. The facial process of the maxilla

555   is broad, and perforated by the infraorbital foramen dorsal to the anterior root of P^3. The maxilla

556   does not contribute to the anterior margin of the orbit; instead the dorsoventrally tall lacrimal has

557   a broad facial process that extends anteriorly at least as far as the distal root of P^4. A prominent

558   lacrimal tubercle is present on the anterior margin of the orbit, and a wide lacrimal canal is

559   completely contained within the orbit. The anterior margin of the orbit is positioned above the

560   distal root of M^1. The inferior margin of the orbit is formed by the jugal, which has a broad

561   contact with the lacrimal, excluding the maxilla from the orbital margin. The jugal process of the

562   maxilla is preserved along with fragments of the jugal. The zygomatic arch was robust and

563   dorsoventrally deep. The dorsal portion of the orbital margin is formed by the frontal, which

564   contacts the lacrimal dorsal to M^1. No postorbital process protrudes from the frontal. The linea

565   temporalis on the frontal has a low relief and trends medially from a lateral position near the

566   superior orbital margin toward the origin of the sagittal crest.

567   In ventral view, the palatal processes of the maxilla preserve the large alveolus of the

568   canine, two P^1 alveoli, two P^2 alveoli, and two P^3 alveoli. The rostral portion of the palate is

569   narrow, but the palate expands laterally near the distal root of P^3. The maxilla contacts the

570   palatine midway between the protocones of M^1 and M^2. A distinct palatine torus is present just

571   distal to the M^3 protocone. The internal choana originates posterior to M^3. As the choana opens

572   distally, it is framed by the left and right palatines, which trend laterally.

573   **Upper Dentition**—The alveoli of I^2 and I^3 are preserved in the premaxilla, but it is

574   difficult to discern whether an I^1 alveolus is present. The diameter of the I^3 alveolus is

575   approximately twice the size of the I^2 alveolus, while the diameter of the canine root and

576   alveolus is approximately twice the diameter of the I^3 alveolus. DPC 17627 preserves the crown

577   of the canine, which has crenulated enamel and is buccolingually compressed. The collapsed

578   alveolus of the canine is preserved in DPC 11990 and it arches posteriorly toward the nasal. P^1

579   had two roots, and the mesial root was smaller than the distal root and set very close to the root

580   of the canine. The crown of P^1 would have been close to, or in contact with, the base of the

581   canine. P^2 and P^3 also had two roots though the anterior alveolus of P^3 is not well preserved. The

582   premolars, from P^1 to the anterior root of P^3, were in the same anteroposterior plane and the

583   margins of the maxilla holding these teeth were parallel. At the posterior root of P^3 the palate

584   flares laterally and broadens distally.

585   P^4 is the only premolar whose crown is preserved. The parastyle is buccolingually

586   compressed, forming a crista that connects with the preparacrista. A thin buccal cingulum

587   surrounds the parastyle and runs along the base of the paracone to the base of the metastyle. The

588   preprotocrista connects the base of the parastyle to the protocone, forming a distinct mesial shelf

589   along the base of the paracone. The protocone is mesiodistally wide and connate, though much

590   lower than the paracone, and the preprotocrista and postprotocrista form a broad equilateral

591   triangle around the base of the paracone. The protocone is shifted slightly mesially relative to the

592   paracone. The paracone is ellipsoid in cross-section and the postparacrista tapers to a sectorial

593   blade that connects with the buccolingually compressed metastyle. The metastyle forms a

594   distinct carnassial notch with the postparacrista, and the metastyle rises distally from the notch to

595   approximately one-third the height of the paracone.

596   DPC 17627 represents a subadult individual and provides insight into an earlier

597   ontogenetic stage than that of DPC 11990. The specimen preserves the right P^4, which has fully

598   erupted, and the left dP^4, which still has its roots. The left M^3 was erupting into occlusion. The

599   parastyle of dP^4 is wide and shelf-like, leaving space between the base of the paracone and the

600   cusp of the parastyle. The parastyle connects the wide buccal cingulum to the preprotocrista. A

601   large paraconule forms a distinct crest along the preprotocrista, which slopes to the protocone

602   where the paraconule and protocone form a notch. The protocone is large and triangular and

603   almost rises to the point of divergence between the paracone and metacone. No lingual cingulum

604   is evident along the base of the protocone. The protocone is shifted slightly mesially, as it is on

605   P^4. The postprotocrista slopes to a small metaconule, which is very reduced compared to the

606   paraconule. The postprotocrista terminates at the base of the metacone rather than coursing along

607   the base of the metastyle. The paracone and metacone are heavily worn, though the cross-

608   sections of both indicate that the cusps were buccolingually compressed, especially the

609   postparacrista and the premetacrista, which together form a distinct notch where the cusps

610   diverge. The postmetacrista forms a carnassial notch with the long metastyle. The metastyle is

611   subequal in mesiodistal length to the mesiodistal length of the paracone/metacone base. The

612   buccal face of the metastyle slopes steeply to the thin buccal cingulum, which traces the alveolar

613   margin without forming an ectoflexus. The metastyle of dP^4 contacts the parastyle of M^1 at its

614   mesial-most point. In DPC 11990, the metastyle of P^4 also contacts the mesial-most point of M^1.

615   M^1 is generally similar to dP^4. The parastyle forms a broad shelf between the apex of the

616   parastyle and the base of the paracone. The parastyle is connected to the broad buccal cingulum,

617   which forms a very slight ectoflexus near the base of the paracone. The buccal cingulum rises

618   slightly along the base of the paracone then slopes distally along the base of the metacone and

619   terminates at the base of the metastyle. The preprotocrista terminates at the base of the

620   paraconule, forming a distinct notch between the paraconule and protocone, and a preparaconule

621   crista courses from the apex of the paraconule to the parastyle, forming a broad mesial cingulum.

622   The protocone rises to a prominent cusp that is equal in height to the divergence between the

623   paracone and metacone; it has a more mesial position, relative to the paracone, than the

624   protocone of P^4. There is no lingual cingulum. The postprotocrista slopes steeply to the

625   metaconule, which is not as mesiodistally broad as the paraconule, though still distinct. The

626   metaconule does not have a postmetaconule crista connecting to the metastyle; instead, the

627   postmetaconule crista abuts the lingual face of the metacone. The paracone is buccolingually

628   compressed with a distinctly elliptical cross-section. The apex projects mesially and overhangs

629   the parastylar region. The postparacrista is blade-like and, in buccal view, meets the

630   premetacrista at a right angle. The metacone is more buccolingually compressed than the

631   paracone near its apex, and is mesiodistally longer. The postmetacrista is blade-like and slopes to

632   a deep carnassial notch at the junction with the metastyle. The mesiodistal length of the sectorial

633   metastyle is subequal to the mesiodistal length of the paracone/metacone base. The lingual face

634   of the metastyle is perpendicular to the palate, while the buccal face of the metastyle slopes more

635   gently to the buccal cingulum.

636   M^1 contacts M^2 at the mesial-most point of the parastyle. M^2 is similar in many ways to

637   M^1, with many of the distinctions between dP^4 and M^1 expressed even more extremely between

638   M^1 and M^2. The parastyle of M^2 is shelf-like with a broad region between the parastyle and

639   paracone, but the parastyle is more buccolingually narrow. M^2 has a deeper ectoflexus than M^1

640   though its depth is variable, with the M^2 ectoflexus on DPC 11990 deeper than the M^2 ectoflexus

641   on DPC 17627. The paraconule of M^2 is very pronounced and forms most of the mesial border of

642   a broad talon basin. The protocone projects as far lingually as the protocone of M^1, leaving the

643   protocone buccolingually more elongate than the protocone of M^1. The metaconule of M^2 is more

644   reduced, compared to the size of the paraconule, than that of M^1. On M^2 the metaconule only

645   forms a slight ridge. The postmetaconule crista runs along the base of the metacone and

646   terminates at the base of the metastyle. The paracone and metacone are more buccolingually

647   compressed and the paracone is lower than the metacone, projecting mesially from the metacone.

648   The metacone is relatively wider and its long axis is aligned closer to perpendicular to the palate.

649   As on M^1, the sectorial postmetacrista forms a deep carnassial notch where it meets the

650   metastyle. The metastyle rises distally from the notch before tapering to its distal-most point.

651   M^3 is reduced primarily to a long parastyle and the paracone and protocone cusps. The

652   parastyle contacts the distal-most point of M^2. Mesially, the parastyle connects to the

653   preparacrista, forming a steep mesial face. The protocone projects as far lingually as the

654   protocone of M^2 and it frames a deep trigon basin. The protocone rises close to the height of the

655   paracone. The paracone is more connate than the paracone of M^2, though the postparacrista is

656   buccolingually compressed. The postparacrista terminates at the buccal cingulum, which

657   connects the parastyle to the postprotocrista. The buccal cingulum rises slightly near the distal

658   aspect of the paracone.

659   **Dentary and Lower Dentition**—The holotype of *Brychotherium*, CGM 83750, is a right

660   dentary that preserves lower dental row from the canine to M_3. The cusps of CGM 83750 are

661   worn, particularly the premolars and M_1. Three other dentary specimens are referred to

662   *Brychotherium ephalmos*: DPC 11569A (right dentary), DPC 11569B (left dentary), and DPC

663   17627 (left dentary). CGM 83750 as the only specimen with a complete coronoid process and

664   tooth row distal to the canine. There is variation among the dentary specimens referred to

665   *Brychotherium ephalmos*. This description will first refer to the morphology preserved by CGM

666   83750, then will address the morphological variation present in the referred specimens.

667   The horizontal mandibular symphysis is rugose and was unfused. The symphysis extends

668   distally to the mesial root of P_3. There are multiple mental foramina preserved along the buccal

669   aspect of the horizontal ramus. The most rostral mental foramen is ventral to the mesial root of

670   P_1. The second mental foramen is ventral to the mesial root of P_2 and the third mental foramen is

671   the largest and is ventral to the space between the distal root of P_3 and the mesial root of P_4. The

672   ventral margin of the corpus of the dentary gently curves to the partially preserved angular

673   process then inflects at the midpoint of the coronoid process, forming a convex ventral margin

674   ventral to the dental row. The ventral margin slightly tapers to the canine. The anterior margin of

675   the coronoid process rises at an obtuse angle (~125 degrees) distal to the talonid of M_3. A broad

676   ridge originates on the buccal face of the dentary, ventral to the distal edge of the talonid of M_3.

677   The anterior fibers of the temporalis muscle would have inserted along this margin. The ridge

678   rises to form the anterior margin of the coronoid process. The anterior edge of the masseteric

679   fossa is deeply excavated but the ventral margin of the masseteric fossa is not as well-defined as

680   the anterior portion.

681   The lower incisors are not preserved. The crown of the canine is worn. The buccal face of

682   the canine is traced by multiple longitudinal ridges of enamel. The mesial root of P_1 is very close

683   to the distal edge of the root of the canine and it sweeps distally with the root canine. The distal

684   root of P_1 parallels the distally swept mesial root of P_1. The crown of P_1 is worn, but a portion of

685   the mesiodistally short talonid is preserved. The crown of P_1 is set at an oblique angle relative to

686   the mesiodistal axis of P_2.

687   Like P_1, P_2 has two roots. The roots of P_2 are perpendicular to the alveolar margin. In

688   buccal or lingual view, P_2 is an asymmetrical triangle. There is a small, but pronounced

689   paraconid on the mesial portion of the tooth. The paraconid is mesiodistally aligned with the

690   protoconid. The shorter paraconid is linked to the protoconid by a short preprotocristid that rises

691   steeply from from the paraconid to the apex of the protoconid. The postprotocristid slopes to a

692   mesiodistally short talonid.

693   There is no diastema between P_2 and P_3. Like P_2, P_3 is asymmetrical in buccal and lingual

694   views with a mesiodistally short preprotocristid and mesiodistally long postprotocristid. The

695   paraconid of P_3 is small, but distinct and in a more lingual position than the protoconid. The

696   protoconid of P_3 is at least twice the height of the paraconid. The postprotocristid is

697   buccolingually compressed and slopes to an indistinct talonid basin. A thin lingual cingulum

698   connects the paraconid to the the talonid.

699   The crown of P_4 forms an equilateral triangle in lingual view, and, like each of the

700   premolars, bears striated enamel. P_4 is a stout tooth in occlusal view, its buccolingual width

701   about half its mesiodistal length. The paraconid is a small but distinct cusp, with a postparacristid

702   that forms a small notch with the longer preprotocristid. The paraconid is connected to a weak

703   lingual cingulum that terminates at the base of the protoconid. A distal lingual cingulum begins

704   just posterior to the apex of the protoconid. The cingulum forms the lingual margin of a very

705   shallow talonid basin. The talonid of P_4 has a small hypoconulid that connects to the hypoconid.

706   The hypoconid is buccolingually compressed and rises to half the height of the protoconid. The

707   hypoconid forms a distinct notch with the postprotocristid. The preprotocristid and

708   postprotocristid are sectorial, and the apex of the protoconid curves slightly lingually and

709   inclines very slightly distally.

710   A thin anterior keel on the buccal face of the M_1 paraconid contacts the hypoconulid of

711   P_4. M_1 is heavily worn on CGM 83750, but is well-preserved on DPC 17627. The protoconid is

712   the tallest of the trigonid cusps, followed by the paraconid and the metaconid. The

713   preprotocristid curves slightly mesially as it runs from the apex of the protoconid to the

714   carnassial notch, where the preprotocristid and postparacristid meet at an angle of approximately

715   90 degrees. The shearing surface created by the protoconid and paraconid is set at about an angle

716   of 45 degrees relative to the long axis of the dentary. The apex of the paraconid projects

717   mesially. The metaconid is connate and connects with the base of the paraconid; its apex projects

718   distally and is positioned slightly distal to the apex of the protoconid. A slight depression

719   descends from the junction of the paraconid and metaconid, defining the base of each cusp. The

720   distal face of the trigonid slopes at an obtuse angle (~100 degrees) to the talonid. The talonid

721   basin is about one-third the total mesiodistal length of M_1. The talonid basin is deep, closed

722   buccally by the hypoconid, and closed lingually by the entocristid. The talonid cusps are

723   crestiform. The entoconid is particularly indistinct, effectively submerged into the entocristid,

724   which slopes distally from the base of the metaconid to meet the apex of the hypoconulid. The

725   hypoconulid is a small cusp that is distinguished from the hypoconid by a weak intervening

726   notch or inflection. The hypoconid is the most pronounced of the talonid cusps, and the cristid

727   obliqua slopes ventrally and lingually toward the base of the protoconid from its apex.

728   M_2 is mesiodistally longer, buccolingually broader, and taller than M_1. The contact

729   between M_1 and M_2 is small, with a gap formed between the M_2 paraconid and the distal M_1

730   talonid. M_1 and M_2 are similar in morphology, but differ in relative proportions. The metaconid

731   is relatively low when compared with the paraconid, and the paraconid is relatively broader at its

732   base, forming a stout cusp. The paraconid apex projects mesially and more lingually than the

733   apex of the metaconid. The talonid basin of M_2 makes up ~40% of the mesiodistal length of the

734   entire tooth, and the talonid basin is only about one-third the height of the protoconid. As on M_1,

735   the talonid cusps are crestiform and the entoconid is reduced to an undifferentiated entocristid. In

736   buccal view, the angle formed between the alveolar margin and the distal edge of the protoconid

737   is approximately 100 degrees.

738   M_3 is the tallest tooth in the dentary. It is subequal in mesiodistal length to M_2 though

739   more of its mesiodistal length is occupied by the trigonid. The talonid is ~27% the mesiodistal

740   length of the tooth, and ~25% the height of the protoconid. The paraconid and protoconid on M_3

741   are taller than the same cusps on M_2 but the metaconids on M_3 and M_2 are almost the same

742   height above the alveolar margin, making the M_3 metaconid proportionally smaller compared to

743   the rest of the trigonid. One distinctive feature of M_3 is the morphology of the preprotocristid,

744   which arcs mesially from the apex of the cusp to the deep carnassial notch. The apex of the

745   protoconid projects distally like the metaconid, and both cusps arch somewhat distally toward the

746   talonid basin. The talonid of M_3 is relatively narrow when compared with the talonids of M_1 and

747   M_2. The hypoconid is proportionally smaller, and the hypoconulid forms a more distinct distal

748   point than it does on the more mesial molars.

749   **Dental Variation**—Compared to CGM 83750, which was utilized for most of the

750   description of the lower dentition, DPC 17627 is very similar, though the corpus of the dentary is

751   more gracile than the dentary of CGM 83750. DPC 17627 preserves the two alveoli of P_3 and the

752   distal alveolus of P_2. Like CGM 83750, there is no indication of a diastema between P_2 and P_3.

753   This contrasts with DPC 11569A and DPC 11569B, two specimens that likely represent the right

754   and left dentary of the same individual. Both specimens preserve a diastema between P_2 and P_3

755   that is half the mesiodistal length of P_3. On DPC 11569A and DPC 11569B the paraconids on

756   P_2–P_4 are very small compared to the paraconids on the same premolars on CGM 83750 and

757   DPC 17627. Finally, the talonid basin of M_3 is relatively smaller and narrower, with less clearly

758   defined cusps than are found on the talonids of M_3 on CGM 83750 and DPC 17627. We do not

759   consider these differences significant enough to designate a new taxon based on the current

760   sample. Future work in the L-41 collections will further explore morphological variation in the

761   hyaenodont fauna found at this locality.

762   **Body Mass**—The average mesiodistal length of the lower molars is 9.57 mm, which

763   yields a body mass estimate of 5.24 kg using the equation of Morlo (1999), and 5.96 kg using the

764   equation of Van Valkenburgh (1990). Using only M_2 length yields an estimate of 6.10 kg, and

765   only M_3 length yields an estimate of 6.20 kg. Carnivorans with a comparable body mass include

766   *Vulpes vulpes* (red fox) and *Taxidea taxus* (American badger).

767

768   **Comparisons**

769   **Rostrum**—*Dissopsalis* and *Teratodon*, both Miocene taxa (Barry, 1988; Savage, 1965),

770   are the only demonstrable teratodontines (Solé et al., 2014b; Rana et al., 2015) for which cranial

771   morphology has been described. *Dissopsalis carnifex* is known from the middle to late Miocene

772   of Asia; the holotype was reconstructed and described by Colbert (1933). The fragmentary

773   specimen preserves much of the left and right maxillae as well as the frontal. Colbert (1933)

774   reconstructed the zygomatic arches and much of the posterior skull. As in *Brychotherium*, the

775   palatal margins from P_1 to the anterior root of P_3 of *Dissopsalis* are parallel. P_3 is angled and its

776   buccal margin follows the lateral flare of the maxilla. The infraorbital foramen is positioned

777   dorsal to P_3 in *Dissopsalis*, as it is in *Brychotherium*. Also like *Brychotherium*, the rostral profile

778   of *Dissopsalis*, created by the gently sloping nasals and frontals, is low, and the sagittal crest

779   emerges from the frontal caudal to subtle postorbital "peaks" rather than distinct processes. This

780   differs from late Eocene European taxa like *Hyaenodon* and *Cynohyaenodon*, which have more

781   pronounced postorbital processes and more deeply excavated lineae temporales (Lange-Badré,

782   1979).

783   *Teratodon enigmae*, from the early Miocene of East Africa (Savage, 1965), is also known

784   from the rostrum. KNM-RU 14769 is a fragment of the left maxilla that contains the complete

785   left canine and P^1-P^4. While the premolars are bulbous and very different from those of

786   *Brychotherium*, the alveolus of the buccolingually compressed canine is similar in morphology

787   to that preserved in DPC 11990. The P^1 of *Teratodon* is also set close to, and slightly lingual of,

788   the upper canine, as is suggested by the disposition of the canine and P^1 alveoli of

789   *Brychotherium*. The holotype of *Teratodon* preserves portions of the rostrum from the premaxilla

790   back to the distal aspect of the palate; in this specimen, too, the anterior root of P^1 is lingual to

791   the canine alveolus.

792   Limited comparisons can also be made with *Indohyaenodon* from the early Eocene of

793   India (Rana et al., 2015)*, Tritemnodon from the early Eocene of North America (Gunnell, 1998)*,

794   *Paroxyaena* from the late Eocene of Europe (Lavrov, 2007)*, Apterodon macrognathus* from the

795   early Oligocene of Egypt (Lewis & Morlo, 2010)*, and Pterodon dasyuroides* from the late

796   Eocene of Europe (Lange-Badré, 1979). Each of these taxa has a long, narrow rostrum with a

797   broad nasal aperture. The nasals do not project prominently over the aperture and the nasals

798   widen slightly as they approach the nasal-frontal suture. The frontal in each of these taxa does

799   not exhibit a distinct postorbital process, but instead a postorbital peak (*Pterodon*) or subtle

800   bump (*Apterodon, Paroxyaena*). The linea temporalis (= supraorbital boss in Rana et al., 2015) is

801   demarcated, but not deeply excavated (it is particularly subtle in *Apterodon* and *Paroxyaena* and

802   more distinct in *Indohyaenodon* and *Pterodon*). Along the anterior orbital margin, the lacrimal

803   has a particularly broad facial wing in *Pterodon*, *Apterodon*, and *Paroxyaena*, as it does in

804   *Brychotherium*.

805   The fragmentary palatines of *Brychotherium* indicate that the internal choanae open distal

806   to M^3 and are delimited ventrally by a rugose palatine torus, comparable to the palatine

807   construction of *Paroxyaena* and *Tritemnodon*. The internal choanae of *Pterodon dasyuroides* and

808   *Apterodon macrognathus* open more caudally. In *P. dasyuroides* and *A. macrognathus* the

809   palatines are fused along the midline posterior to the dentition. The palatines of *Apterodon* are

810   fused for more of their length than those of *P. dasyuroides*, forming a palatine tube that extends

811   to the basicranium. Colbert (1933) reconstructed the palatines of *Dissopsalis* as a long, fused

812   palatine tube, likely based on comparisons to the skull of North American *Hyaenodon*, which

813   also has a *Apterodon*-like tube (Mellett, 1977). The palatine morphology of *Dissopsalis* is, in

814   fact, largely unknown.

815   **Upper Dentition**—Like the teratodontines *Dissopsalis* and *Anasinopa*, *Brychotherium*

816   has distinct paracones and metacones on the upper molars that are fused at their bases, but

817   diverge well before their apices. In all three taxa, the paracone and metacone are buccolingually

818   compressed, giving them an elliptical cross section, and the paracone is the smaller of the two

819   cusps. The apex of the metacone projects perpendicular to the plane of the hard palate, while the

820   smaller paracone projects mesially. This differs from hyainailourines (e.g., *Pterodon*

821   *dasyuroides*, *Kerberos*, and *"Pterodon" africanus*), which fuse the paracone and metacone near

822   the apices of the cusps. In hyainailourines, the paracone is the taller of the two cusps and would

823   have been the leading piercing cusp during mastication. The paracone/metacone morphology of

824   Teratodontinae is comparable to the arrangement of these cusps in *Hyaenodon* and *Eurotherium*

825   which, like teratodontines, had metacones that were taller than paracones. However, in

826   *Hyaenodon* and *Eurotherium*, the cusps are not as divergent; rather, in *Hyaenodon*, the paracone

827   projects perpendicular to the plane of the hard palate, like the metacone, and is almost

828   completely fused to the metacone, essentially forming part of the premetacrista (a state evident in

829   unworn upper molars, such as the M^1 of the subadult AMNH 75646). *Apterodon* also has distinct

830   paracones and metacones as in teratodontines, but these cusps are more circular in cross-section

831   and diverge closer to the buccal margin.

832   The molar paracones are more distinct in *Brychotherium* than in *Dissopsalis*, and the

833   molar protocones of *Brychotherium* are more triangular and project lingually, rather than being

834   elongate and shifted far mesially as in *Dissopsalis*. The trigon basins of *Brychotherium* more

835   closely resemble those of *Anasinopa*, though the paraconules and metaconules of *Brychotherium*

836   are relatively well-developed. The deep ectoflexus and large parastyle of the M^{1-2} of

837   *Brychotherium* set the new genus apart from *Anasinopa* and *Dissopsalis*. *Teratodon* has small,

838   tritubercular molars and a distinct ectoflexus on M^2. The M^{1-2} metastyles of *Brychotherium* are

839   mesiodistally longer than the parastyles whereas the para- and metastyles on the M^2 of *Teratodon*

840   are subequal in length. *Indohyaenodon* also has an elongate, arching M^2 metastyle, like

841   *Brychotherium*, but its protocone is more mesiodistally broad. The P^4 paracone of

842   *Indohyaenodon* is more buccolingually compressed than that of *Brychotherium* and its P^4

843   protocone is less distinct. P^4 in *Kyawdawia*, from the middle Eocene of Myanmar (Egi et al.,

844   2005) is also more compressed buccolingually, and the metastyle is taller and more sectorial than

845   that of *Brychotherium*. The M^2 paracone and metacone of *Kyawdawia* are both buccolingually

846   compressed and the mesiodistally elongate metacone is only slightly taller than the paracone.

847   The M^2 ectoflexus of *Kyawdawia* has the same degree of lingual curvature as that of

848   *Brychotherium* and the same well-defined buccal cingulum. The M^1 of middle Eocene *Furodon*

849   shares many features with *Brychotherium*, including an elongate metastyle, buccolingually

850   compressed and apically divergent paracones and metacones, a broad talon basin with a large

851   paraconule, and a prominent and only slightly mesially oriented protocone. *Koholia* is from the

852   late early Eocene and is the oldest Afro-Arabian hyaenodontidan known from its upper dentition.

853   The P^4 protocone of *Brychotherium* is mesiodistally wider than the P^4 protocone of *Koholia*, and

854   the P^4 metastyle of *Brychotherium* is mesiodistally short compared to the elongate metastyle of

855   *Koholia*, which is the same mesiodistal length as the paracone. The M^1 parastyle of *Koholia* is

856   buccolingually wide, with space formed between the apex of the parastyle and the base of the

857   paracone. The M^1 parastyle in *Brychotherium* is buccolingually narrow and cingulum-like. Like

858   in *Brychotherium*, the M^1 paracone and metacone of *Koholia* have distinct apices, but the

859   paracone and metacone are more fully fused in *Koholia* and the paracone is distinctly taller than

860   the metacone. On the M^1 of *Brychotherium* the metacone is slightly taller than the paracone.

861   **Lower Dentition—**Solé et al. (2014b) recovered *Furodon* as a hyainailourine with

862   *Pterodon* and *Akhnatenavus*, with *Furodon* as the only member of this clade with a prominent

863   metaconid. The phylogenetic analyses presented below do not support the Solé et al. (2014b)

864   hypothesis and instead resolve *Furodon* in a close relationship to metaconid-bearing

865   teratodontines. *Brychotherium* and *Furodon* share many features, including their comparable

866   size, relatively tall trigonids, low metaconids, and wide talonid basins with poorly defined

867   talonid cusps. They primarily differ in the morphology of P_4, the protoconid of which projects

868   perpendicular to the alveolar margin in *Brychotherium*, and in occlusal view curves lingually.

869   The lower molar paraconids also project more lingually in *Brychotherium* than they do in

870   *Furodon*, the talonid basins are buccolingually more broad, and the molar hypoconulids are

871   larger.

872   The oldest teratodontine in the analyses of Solé et al. (2014b) and Rana et al. (2015) is

873   *Glibzegdouia*, an early or middle Eocene taxon from Algeria. The M_1 metaconid of *Glibzegdouia*

874   is subequal in height to the paraconid, and the talonid basins of M_{1-2} are lined with distinct

875   entoconids, hypoconulids, and hypoconids, unlike the poorly differentiated talonid cusps of

876   *Brychotherium.* The talonid basin also occupies more than 50% of the total mesiodistal length of

877   the molars of *Glibzegdouia*. The talonid is proportionally smaller and shorter in *Brychotherium*.

878   *Masrasector aegypticum* is a teratodontine from Quarry G (early Oligocene) in the

879   Fayum succession (Simons & Gingerich, 1974). Like *Brychotherium*, *M. aegypticum* has broad

880   talonid basins with indistinct talonid cusps. The smaller *M. aegypticum* is further differentiated

881   from *Brychotherium* in having buccolingually broad premolars and a more tightly packed

882   trigonid, with the paraconid apex perpendicular to the alveolar plane, rather than projecting

883   lingually as it does in *Brychotherium*. The other possible teratodontine from the Fayum,

884   *Metasinopa,* differs from *Brychotherium* in having a much deeper mandibular corpus, a more

885   reduced talonid on M_3, and much smaller M_2-M_3 metaconids, particularly on M_3 where the

886   metaconid barely connects to the paraconid. The reduction of the M_3 metaconid is even more

887   extreme in *Dissopsalis* and *Anasinopa*; the paraconid and protoconid of both taxa are divergent

888   and form an obtuse carnassial notch between the preprotocristid and postparacristid and the

889   metaconid is reduced to a very low or absent cusp (especially in *Dissopsalis*). Both *Dissopsalis*

890   and *Anasinopa* have broad and lingually closed talonids on M_1 and M_2 and reduced talonids on

891   M_3, with the talonid on *Dissopsalis* reduced to a small distal projection from the M_3 trigonid.

892   These features contrast with the connate metaconid, well-developed talonid, and more acute

893   carnassial notch found on the M_3 of *Brychotherium*.

894   *Lahimia*, from the middle Paleocene of Morocco (Solé et al., 2009), and *Boualitomus*,

895   from the early Eocene of Morocco (Gheerbrant et al., 2006), are both small hyaenodontidans that

896   Solé et al. (2014b) and Rana et al. (2015) classified as part of Koholiinae. Like *Brychotherium*,

897   they both retain lower molar metaconids that are slightly lower than the paraconids and distinct

898   talonids with indistinct talonid cusps. They differ from *Brychotherium* in their much smaller size,

899   and by having molars that are mesiodistally subequal in length to each other. *Brychotherium*, like

900   many hyaenodontidans including *Masrasector* and *Pterodon*, but unlike *Lahimia* and

901   *Boualitomus*, has molars that increase in length distally.

902   *Indohyaenodon* and *Kyawdawia*, part of Indohyaenodontinae in Solé et al. (2014b) and

903   Rana et al. (2015), have buccolingually broad talonids that are lingually closed by the entocristid,

904   rather than lingually open as the talonid is in *Brychotherium*. Both taxa also have distinct buccal

905   cingulids on the lower molars that originate from the anterior keel. In *Brychotherium* the anterior

906   keel is small and does not connect to any cingulid. The metaconid is much lower than the

907   paraconid on M_3 in *Indohyaenodon*, *Kyawdawia*, and *Brychotherium,* but the metaconid is

908   subequal to the height of the paraconid on M_1 in the indohyaenodontines and is lower than the

909   paraconid in *Brychotherium*. *Indohyaenodon* and *Brychotherium* also share relatively gracile

910   dentaries that are only a little deeper dorsoventrally than the crown height of M_3.

911

912   HYAENODONTIDA Solé, 2013

913   HYAINAILOURINAE Pilgrim, 1932

914   *AKHNATENAVUS* Holroyd, 1999

915   **Type Species**—*Akhnatenavus leptognathus* Holroyd, 1999.

916   **Emended Generic Diagnosis** (modified from Holroyd, 1999)—Differs from "*Pterodon*"

917   *africanus* and "*Pterodon*" *phiomensis* by being smaller and by having more buccolingually

918   compressed lower premolars; narrow, mesially shifted M^{1-2} protocones; and more buccolingually

919   compressed and elongate M^{1-2} metastyles. Differs from *Metapterodon* by being smaller, retaining

920   a talonid on M_3 rather than having no talonid, having distinct M^{1-2} paracone and metacone cusps

921   rather than being completely fused into a single cusp, having more lingually projecting M^{1-2}

922   protocones rather than having small protocones that are close to the paracone bases, and having

923   distinct M^{1-2} parastyles with spaces between the parastyle and the base of the paracone rather

924   than the parastyles forming only a small projection. Differs from *Pterodon dasyuroides* by

925   having smaller talonids on molars, a reduced M^3 that does not project lingually as far as the M^2

926   protocone, and narrower M^{1-2} protocones with preprotocrista and postprotocrista nearly parallel

927   rather than protocones that are mesiodistally broad and triangular. Differs from *Apterodon* by

928   having fused paracone and metacone cusps on M^{1-2}, molar paraconids that are much shorter than

929   the protoconids, mesiodistally short molar talonids, and M^{1-2} metastyles that are mesiodistally

930   longer than the mesiodistal length of the paracone and metacone bases. Differs from

931   *Brychotherium* by having M^{1-2} paracones that are taller than metacones and narrow, simple M^{1-2}

932   protocones rather than triangular protocones with metaconule and paraconule cusps.

933

934   *AKHNATENAVUS NEFERTITICYON* Borths, Holroyd, and Seiffert, sp. nov.

935   (Figs. 10–15, Table 3)

936   urn:lsid:zoobank.org:act:19CBE178-447C-4182-9AED-C70280CD0673

937   **Etymology**—Meaning "Nefertiti's dog," in reference to Nefertiti, the wife of Akhnaten,

938   who is known from an exceptional cranial specimen.

939   **Holotype**— CGM 83735, cranium with canine, P^2-M^3.

940   **Referred Specimens**—DPC 13518, M^1; DPC 18242, palate with partial canine, alveoli

941   for P^1, and P^2-M^2; DPC 7765, dentary with P_2–M_3 (Described by Holroyd, 1999)

942   **Type Locality**—Jebel Qatrani Locality 41 (L-41), Jebel Qatrani Formation, Fayum

943   Depression, Egypt.

944   **Age**—late Eocene, latest Priabonian, ~34 Ma (Seiffert, 2006)

945   **Geographic Distribution**—Only known from Locality 41.

946   **Diagnosis**—Differs from *Akhnatenavus leptognathus* by being smaller and by having

947   mesiodistally shorter diastemae between the premolars. Rostrum is inferred to be relatively

948   shorter in *A. nefertiticyon* than is implied by the elongate dentary of *A. leptognathus* which has

949   wide diastemae between adjacent premolars. P_3 in *A. nefertiticyon* is distally inclined and

950   relatively buccolingually wider than P_3 in *A. leptognathus*. P_4 in *A. nefertiticyon* is taller than P_4

951   in *A. leptognathus* and P_4 paraconid height is subequal to the mesiodistal length of the tooth

952   rather than shorter than the mesiodistal length. M_1–M_3 have weak to absent ectocingulids and the

953   talonid is reduced in *A. nefertiticyon* compared to the slight ectocingulids and better developed

954   cusp-bearing talonids of *A. leptognathus*.

955

956   **Description**

957   **Cranium**—CGM 83735 is a complete cranium that was dorsoventrally crushed, with the

958   left portion of the skull folded medially. The best preserved portions of the cranium are the right

959   palate and dentition, the right squamosal, the nuchal crest, the posterior aspect of the sagittal

960   crest, portions of the parietals, and the anterior portion of the frontal. A complete atlas is

961   preserved on the right basicranial region and a rib is preserved attached to the right parietal.

962   The atlas is preserved in dorsal view with deep facets for articulation with the occipital

963   condyles visible in ventral view, along with the vertebral foramina and the articular facets for the

964   axis. The left articular facet for the axis, visible in Fig. 10A and Fig. 11A, is broad and not as

965   concave as the facets for the occipital condyles. The rugose dorsal tubercle is preserved along the

966   dorsal arch, which is craniocaudally wide, approximating the dorsoventral diameter of the

967   vertebral foramen. Fragments of the right transverse process suggest that the structure swept

968   laterally before curving caudally. The proximal portion of a rib is preserved in caudal view with

969   a deep costal groove along its body. It is mediolaterally broad, likely a first or second rib.

970   The nasals are relatively well-preserved, though the nasal aperture is not. Originating

971   rostrally from a slight lateral expansion, the nasals narrow posteriorly and then expand laterally

972   superior to the infraorbital foramen. The nasal-frontal suture reaches its posterior-most point at

973   the midline of the cranium, and the suture trends at a 45-degree angle to the nasal-maxilla suture

974   along the lateral border of the nasal. The facial portion of the maxilla is rostrally elongate. The

975   maxilla is perforated by the infraorbital foramen, which is dorsal to the distal root of P^3. The

976   maxilla flares laterally posterior to the infraorbital foramen. The rugose maxillary portion of the

977   maxilla-jugal suture indicates that the jugal formed the inferior margin of the orbit. The large

978   lacrimal formed the anterior portion of the orbital rim. The orbital margin of the lacrimal has a

979   dorsoventrally elongate lacrimal tubercle. The facial wing of the lacrimal is extensive, reaching

980   from the anterior orbital margin, which is superior to the mesial root of M^2, anteriorly to the

981   distal root of P^4. The frontal forms the superior margin of the orbit and preserves the deeply

982   excised linea temporalis, which leads to the sagittal crest. The sagittal crest tracks the

983   interparietal suture to the nuchal crest. The sutures of the bones that form the nuchal crest are not

984   clear, though the occipital forms the lateral portions of the nuchal crest in *Pterodon dasyuroides*

985   and *Apterodon macrognathus*, and the parietals form the medial portions of the crest near the

986   sagittal crest. There are suggestions of a suture in these regions of the skull of *Akhnatenavus,*

987   which are indicated in Fig. 11. The entire nuchal crest stands prominently above the cranial vault

988   with the tallest portion of the sagittal crest bridging the space between the posterior aspect of the

989   cranial portion of the parietal and the apex of the nuchal crest. The crest curves laterally, then

990   recurves medially towards the foramen magnum, with the supraoccipital forming a clover-leaf-

991   shape in caudal view. The exoccipital curves laterally from the ventral extension of the nuchal

992   crest and supraoccipital. The occipital condyle is dorsoventrally elongate, though its relationship

993   to the foramen magnum is difficult to interpret.

994   The left mandibular (or glenoid) fossa indicates that the mandibular condyle was

995   mediolaterally wide and dorsoventrally short, with the width of the condyle about three times the

996   height. A large postglenoid foramen is preserved posterior to the mandibular fossa. The right

997   zygomatic process of the squamosal has an anteroposteriorly broad origin. The zygomatic

998   process is dorsoventrally tall and robust near the mandibular condyle and it tapers as it trends

999   rostrally. The fragmentary jugal would have formed a short contact with the inferior margin of

1000   the squamosal and continued the zygomatic arch to the inferior orbit and the contact of the jugal

1001   with the maxilla. The palatal portion of the maxilla is rugose and deeply embayed between the

1002   protocones. The maxilla-palatine suture is not easily traced, but the posterior margin of the palate

1003   is marked by a torus between the distal-most molars. The palatines extend posterior to the torus;

1004   though they are broken and the morphology of the internal choanae is obscured. The ventral face

1005   of the left palatine preserves a broken suture, evidence that the right and left palatine formed a

1006   suture posterior to the last upper molar, and diverged approximately mid-cranium.

1007   **Upper Dentition**—The upper right canine is preserved in CGM 83735. The root is ~1.5

1008   times the length of the crown and is widest just dorsal to the enamel-dentine junction. The

1009   enamel is longitudinally striated and the crown is round in cross-section rather than

1010   dorsoventrally depressed. The two roots of P^1 are preserved in DPC 18242 and the tooth is

1011   crowded close to the mesial margin of the alveolus of the canine. P^2 also has two roots and there

1012   is a small gap between P^1 and P^2. P^2 is mesiodistally longer than P^1. The buccolingual width of

1013 P^2 is about half its mesiodistal length. The tooth has no parastyle or buccal cingulum. The

1014   paracone is recurved, and a convex curve is formed between the metastyle and the apex of the

1015   paracone. The metastyle is short, <25% the mesiodistal length of the tooth, and buccolingually

1016   compressed. The mesiodistal length of P^3 is subequal to the length of P^2. A small gap separates

1017   the two premolars. A very small parastyle is present on P^3. Like P^2, the paracone sweeps distally

1018   and a buccolingually compressed metastyle protrudes from P^3. The metastyle is offset from the

1019   mesiodistal axis of the paracone where the palate widens laterally, posterior to the infraorbital

1020   foramen. A slight lingual shelf is present, though it is not developed into a distinct protocone as

1021   is present on P^4. P^4 is mesiodistally longer than P^3. The parastyle forms a prominent mesial cusp

1022   and the metastyle is an elongate, buccolingually compressed blade that is more than half the

1023   mesiodistal length of the base of the paracone. The buccolingually compressed paracone sweeps

1024   distally and the postparacrista forms a deep carnassial notch with the arching metastyle. The

1025   protocone cusp is buccolingually shorter than its mesiodistal width and is lined mesially by a

1026   cingulum-like preprotocrista and lined distally by the postprotocrista, which runs along the base

1027   of the paracone and metastyle.

1028   The metastyle of P^4 is braced buccally by the parastyle of M^1 where the teeth are in

1029   contact. The parastyle of M^1 is a broad cingulum-like shelf with a small and distinct apex, and

1030   there is no space between the apex of the parastyle and the base of the paracone. A thin buccal

1031   cingulum traces the base of the paracone and metastyle. The ectoflexus is very slightly distal to

1032   the metacone. The parastyle cusp is in line with the preparacrista, which is a buccolingually

1033   compressed, sectorial blade. The apex of the paracone is slightly taller than the metacone. The

1034   metacone is also buccolingually compressed but its base is mesiodistally elongate compared to

1035   the base of the paracone. The groove that distinguishes the fused paracone and metacone is

1036   visible in buccal and lingual view. The postmetacrista is thinner and mesiodistally longer than

1037   the preparacrista. The sectorial blade on the metacone forms a deep carnassial notch with the

1038   metastyle. The elongate metastyle is half the mesiodistal length of the tooth. From the carnassial

1039   notch the metastyle traces a convex, then concave, line to the distal-most point of the tooth. The

1040   protocone is broad with a distinct preprotocrista, a small paraconule, and no metaconule. The

1041   protocone is buccolingually as broad as it is mesiodistally wide and it has a strong mesial

1042   deviation relative to the paracone. The protocone is shifted so far mesially that it is lingual to the

1043   metastyle of P^4. M^1 contacts M^2 lingual to the parastylar apex. M^2 is mesiodistally longer than

1044 M^1. Compared with M^1, M^2 has a larger parastyle that projects buccally. This gives M^2 a deeper

1045   ectoflexus than M^1. M^2 is taller than M^1 and the cleft between the paracone and metacone is

1046   more faint, though the apex of the paracone and metacone are both distinct, with the paracone

1047   slightly taller than the metacone. The protocone is buccolingually longer than its mesiodistal

1048   width, making the protocone on M^2 appear slenderer than the protocone on M^1. The protocones

1049   on both molars are subequal in width, though the protocone of M^2 does not angle as far mesially

1050   as the protocone of M^1. M^3 contacts the lingual face of the metastyle of M^2. The tooth is not

1051   buccolingually wide, only reaching the lingual-most point of the metacone of M^2. The paracone

1052   is very small and the entire tooth is mesially angled. This does not appear to be postmortem

1053   distortion, but the natural orientation of the small terminal molar.

1054   **Body Mass**—The mesiodistal length of the lower molars was measured between the

1055   postprotocrista of adjacent molars, which yielded an average molar length of 12.45 mm for DPC

1056   18241 and 12.0 for CGM 83735. Using Morlo (1999), the body mass estimate for DPC 18241 is

1057 ~15.8 kg and for CGM 83735 is ~13.86 kg. Using Van Valkenburgh (1990), M_2 length ($M_2 =$

1058 13.1 mm) yields estimates of 17.6 kg and 17.2 kg and only M_3 length ($M_3 = 13.4$ mm) yields an

1059 estimate of 17.4 kg and 18.3 kg. The average estimated body mass is ~16.7 kg, within range of

1060 *Gulo gulo* (wolverine), *Lynx lynx* (Eurasian lynx), and *Canis simensis* (Ethiopian wolf) (body

1061 mass estimates from Finarelli & Flynn, 2009).

1062

1063 **Comparisons**

1064   *Akhnatenavus nefertiticyon* shares many cranial and dental features with species placed in

1065 Hyainailourinae by Polly (1996), Solé et al. (2014b) and Solé et al. (2015). Most notably,

1066 *Pterodon dasyuroides*, *Hemipsalodon*, and *Megistotherium* each also have distinctive, wedge-

1067 shaped nuchal crests that trend medially toward the foramen magnum, a feature also preserved in

1068 *A. nefertiticyon*, the oldest Afro-Arabian hyainailourine known from cranial material. *Apterodon*

1069 *macrognathus* also has this narrowed nuchal crest, which inclines caudally like the nuchal crest

1070 of *Akhnatenavus nefertiticyon*. This morphology contrasts with the broad nuchal crest of

1071 *Hyaenodon* and *Eurotherium*, which trends laterally toward the mastoid process (see Solé et al.,

1072 2015:Fig. 5). Another cranial feature shared by *A. nefertiticyon* and the other hyainailourines is

1073 the extensive facial wing of the lacrimal, which reaches from the anterior margin of the orbit to

1074 the distal root of P^4. A rostrally extensive lacrimal is also shared with *Brychotherium*. More

1075 difficult to determine is the extent of palatine fusion in *A. nefertiticyon*, a feature that differs

1076 between *Pterodon dasyuroides*, which has palatines that diverge closer to the M^3 than the

1077 mandibular fossa, and *Megistotherium*, which has palatines that are fused through the middle

1078 section of the cranium and only diverge close to basicranium. *A. nefertiticyon* does share the

1079 dorsoventrally deep zygomatic process of the squamosal with *Megistotherium*. The zygomatic

1080   arch is not completely preserved in *Pterodon dasyuroides*, but is preserved in *Apterodon*

1081   *macrognathus* and *Kerberos langebadreae*, both of which have dorsoventrally deep zygomatic

1082   arches that form robust attachment sites for the masseter muscle. Unlike *Apterodon* but like

1083   *Kerberos*, *Akhnatenavus* has distinct temporal lines leading to the origin of the sagittal crest.

1084   These deep lines, which indicate the anterior origin of the temporalis muscle, are comparable in

1085   depth to the lines preserved on the frontals of *Pterodon dasyuroides*. "*Pterodon*" *africanus* is

1086   known from a rostral specimen (SMNS 11575) that was sculpted into a complete cranium

1087   (Schlosser, 1911). The anterior portion of the skull preserves the broad nasal aperture and gently

1088   sloping nasals that are shared with *Pterodon dasyuroides*, *Kerberos*, and *Akhnatenavus*. It also

1089   preserves the slight postorbital eminence or subtle peak noted in *Brychotherium*. There is no

1090   indication of distinct, *Hyaenodon*-like postorbital processes in *Akhnatenavus*. Instead, the

1091   neurocranium is elongate along the anteroposterior axis with very slight waisting in the middle

1092   region of the skull as it is in *Apterodon* and *Pterodon dasyuroides*. The neurocranium of

1093   *Hyaenodon* and *Eurotherium* is hourglass-shaped in dorsal view, going from an expanded

1094   postorbital frontal to a narrow parietal around the sagittal crest, to a posteriorly expanded

1095   squamosal-parietal region.

1096   Compared to the atlas preserved with CGM 83735, the atlas of *Megistotherium* (NHM

1097   M21902) has much broader transverse processes than *A. nefertiticyon* would have had, based on

1098   what is preserved along the fractured lateral margin of the *A. nefertiticyon* atlas. NHM M9472 is

1099   an atlas attributed to *"Pterodon" africanus*, which shares with *Akhnatenavus* transverse

1100   processes that are less robust than those of *Megistotherium*. The transverse processes of

1101   *"Pterodon" africanus* and *Akhnatenavus* sweep laterally, perpendicular to the vertebral foramen,

1102   and then caudally, rather than sweeping cranially before trending laterally as they do in

1103   *Megistotherium*. The dorsal arch of each hyainailourine atlas is craniocaudally long and thick

1104   compared to the much narrower dorsal arch of *Hyaenodon* (AMNH 8775; BSPG 1898 IV 32).

1105   Dentally, *Akhnatenavus* shares with other hyainailourines a fused, buccolingually

1106   compressed upper molar paracone and metacone, with the paracone taller than the metacone.

1107   This arrangement differs from the partially fused paracone and metacone of Teratodontinae,

1108   which have taller metacones than paracones, and Hyaenodontinae, which have fused paracones

1109   and metacones, but the metacone is the taller of the two cusps and the paracone is fused to the

1110   mesial aspect of the metacone. *Akhnatenavus* differs from *"Pterodon" africanus* and

1111   *"Pterodon" phiomensis* primarily in size, but there are dental distinctions, particularly in the

1112   overall robusticity of the dentition of *"Pterodon" africanus*. P^4 in *"Pterodon" africanus* (NHM

1113   M21897) has a short, shelf-like protocone compared to the lingually projecting P^4 protocone of

1114   *Akhnatenavus*. Like *Akhnatenavus*, the parastyle of M^2 is better developed than the parastyle of

1115 M^1 and the ectoflexus is slightly deeper, though not as lingually excavated as that of

1116   *Akhnatenavus*. The paracones of each preserved premolar and molar of *"Pterodon" africanus*

1117   sweep distally at stronger angles than the paracones of *Akhnatenavus*. *"Pterodon" syrtos* from

1118   Quarry M, an early Oligocene locality in the Fayum (Holroyd, 1999), differs from the other

1119   Afro-Arabian *"Pterodon"* species and *Akhnatenavus* by reducing the parastyles to thin mesial

1120   cingula.

1121   Even greater differences in robusticity are evident between *Akhnatenavus* and the large

1122   early Miocene *Hyainailouros napakensis* (NHM M19090) and *Megistotherium*. In the early

1123   Miocene taxa, the buccolingual width of the molars and mesiodistal length of the molars are

1124   closer to subequal. Like *Akhnatenavus*, the protocone of M^1 in *Hyainailouros* crosses the

1125   transverse plane of the P^4 metastyle and the protocone of M^2 is narrower and more lingually

1126   oriented than the protocone of M^1. The upper dentition of *Megistotherium* is not well-preserved,

1127   but the skull does preserve the alveoli, which indicate that small gaps were present between P^1

1128   and P^2, and between P^2 and P^3. These short diastemata are also present between these teeth in

1129   *Akhnatenavus*. In all hyainailourines discussed so far, including *Pterodon dasyuroides*, the upper

1130   molar paracone and metacone are distinguishable by a shallow buccal and lingual groove that

1131   runs between them. This differs from the condition in *Metapterodon*, a genus known from the

1132   early Oligocene (Holroyd, 1999) through the Miocene (Lewis & Morlo, 2010), which has

1133   completely fused the paracone and metacone and it is very difficult to distinguish the two cusps

1134   from one another. The metastyle, paracone, and metacone of *Metapterodon* are buccolingually

1135   compressed into delicate, blade-like structures. The protocone and parastyle are much more

1136   reduced than they are in *Akhnatenavus*, "*Pterodon*" *africanus*, and *Pterodon dasyuroides*.

1137   *Akhnatenavus* differs from the European hyainailourines *Pterodon dasyuroides* and

1138   *Kerberos* in the reduction of M^3, which, in the European taxa, retains a distinct protocone that

1139   projects as far lingually as the protocone of M^2. *Kerberos* and *P. dasyuroides* also have

1140   prominent paracones on M^3, and a sectorial parastyle. The distinction between M^1 and M^2 in *P.*

1141   *dasyuroides* is not as clear as it is in *Akhnatenavus*. In *P. dasyuroides*, the parastyle of M^1 is a

1142   distinct cusp and it forms a slight ectoflexus and the protocones of the two molars are shifted

1143   mesially at similar angles. The contact between M^1 and M^2 in *P. dasyuroides* is small, with the

1144   distal-most point of the metastyle of M^1 touching the mesial-most point of the parastyle of M^2,

1145   where the buccolingually more broad parastyle of the M^2 in *Akhnatenavus* buccally embraces the

1146   metastyle of M^1.

1147

1148   PHYLOGENETIC RESULTS

1149

1150   **Maximum Parsimony**

1151   The maximum parsimony analysis recovered ~~650~~ most parsimonious trees (MPT) each

1152   with a length of 1029 steps, a consistency index (CI) of 0.187, and a retention index (RI) of

1153   0.613 with three parsimony uninformative characters. The character-taxon matrix contains

1154   41.5% missing data with individual OTUs ranging from a minimum of 0% missing data

1155   (*Hyaenodon horridus*) to 84% missing data (*Koholia*) with a median of 40% of missing data

1156   across all OTUs. Synapomorphies for the clades in the strict consensus are listed in Table S3

1157   with a single lined arrow indicating an ambiguous synapomorphy and double lined arrow

1158   indicating an unambiguous synapomorphy. With regard to the species described here, the strict

1159   consensus tree (Fig. 16) does not uphold a monophyletic Teratodontinae (leaving the lower-level

1160   position of *Brychotherium* uncertain), and relationships among African and Asian species are

1161   largely unresolved; only some hyainailourines (i.e., a strictly African clade including

1162   "*Pterodon*," *Akhnatenavus*, and Miocene *Isohyaenodon*, *Leakitherium*, and *Megistotherium*,

1163   forming one branch of a trichotomy that also includes North American *Hemipsalodon* and

1164   European *Kerberos*) and Apterodontinae (*Apterodon* + *Quasiapterodon*) are retained as clades

1165   within a large polytomy that includes all other hyainailourines, teratodontines,

1166   indohyaenodontines, koholiines, North American *Tritemnodon* and *Pyrocyon*, and European

1167   *Paroxyaena*.

1168   We also show the Adams consensus of the 650 MPTs in Fig. 16, with alphanumeric

1169   codes listed to the left of the relevant node, Bremer values indicated to the right of the node, and

1170   bootstrap support for the node (if >50%) in italics below the Bremer support value. The

1171   agreement subtree is shown next to the Adams consensus tree in Fig. 17 with OTUs recovered

1172   consistently in the same phylogenetic position indicated with black text and connecting branches.

1173   The Adam's consensus suggests that the species that break down into a polytomy at the

1174   base of node P31 (koholiines, *Masrasector aegypticum*, *Pyrocyon*, and *Tritemnodon*) contribute

1175   to irresolution within P31. This is further corroborated by the structure of the agreement subtree

1176   which does not recover these OTUs at P31 in a consistent phylogenetic position. In the Adams

1177   consensus and agreement subtree, Apterodontinae joins an expanded Hyainailourinae that

1178   includes the aforementioned taxa as well as European *Pterodon dasyuroides*, African

1179   *Metapterodon*, and Asian *Orienspterodon*. In the Adams consensus the most basal position ever

1180   occupied by *Brychotherium* in the MPTs is as at the same level as *Anasinopa*, *Dissopsalis* and

1181   *Furodon*. The remaining teratodontines (*Glibzegdouia*, *Masrasector ligabuei*, and *Teratodon*)

1182   form another clade in the Adams consensus (P33). *Akhnatenavus nefertiticyon* is the sister taxon

1183   of *Akhnatenavus leptognathus* in all MPTs (P45)*;* the monophyly of the genus is supported by

1184   four unambiguous synapomorphies and a Bremer value of 2, and is consistently nested within

1185   Hyainailourinae in a polytomy with "*Pterodon*" *africanus*, "*Pterodon*" *phiomensis*, and Miocene

1186   hyainailourines (P44).

1187   Apterodontinae (P39; Bremer = 4) is unambiguously supported by 13 synapomorphies,

1188   and *Apterodon* (P40; Bremer = 5) is unambiguously supported by four synapomorphies (Table

1189   S3). Hyainailourinae (P43; Bremer = 1) is unambiguously supported by 23 synapomorphies

1190   (Table S3). A clade that contains exclusively Afro-Arabian hyainailourines (P44; Bremer = 1;

1191   i.e., excluding North American *Hemipsalodon*, European *Kerberos*, and more basal taxa) is

1192   united by four unambiguous synapomorphies (Table S3), the clade formed by the Miocene

1193   hyainailourines *Isohyaenodon*, *Leakitherium*, and *Megistotherium* (P47; Bremer = 4) is

1194   unambiguously supported by five synapomorphies, and *Megistotherium* and *Leakitherium* (P48;

1195   Bremer = 2) are united by one unambiguous synapomorphy.

1196   The closest sister taxa of P31 are *Prototomus*, *Sinopa*, Limnocyoninae, and a *Galecyon-*

1197   *Gazinocyon* clade, all of which break down into a polytomy with P31 at the base of node P22 in

1198   the strict consensus; on the Adams consensus tree, *Prototomus phobos* and *Sinopa* are sister taxa

1199   of P31. The sister taxon of P21 is *Arfia*, a North American genus from the early Eocene whose

1200   monophyly is well-supported (Bremer = 8; Bootstrap = 90%). Limnocyoninae (P23; Bremer = 1)

1201   is unambiguously supported by eight synapomorphies, and, within that subfamily, the genus

1202   *Prolimnocyon* (P24), which includes late Paleocene *Prolimnocyon chowi* from Asia and early

1203   Eocene *Prolimnocyon atavus* from North America, is supported by a Bremer value of 3. *Sinopa*

1204   (P30), like *Prolimnocyon*, is known from species in North America (*Sinopa grangeri*) and Asia

1205   (*Sinopa jilinia*), and is unambiguously supported by four synapomorphies. Node P20, which

1206   joins *Arfia* with P22, is supported by a Bremer value of 1 and seven unambiguous

1207   synapomorphies (Table S3).

1208   The sister taxa of P20 are almost entirely European, including early Eocene *Lesmesodon*

1209   and *Morlodon* and a large clade of "proviverrines" and hyaenodontines (P4) whose relationships

1210   are well-resolved in the strict consensus. As this is the first phylogenetic analysis of

1211   Hyaenodontida to sample extensively from Hyaenodontinae as well as other African and Asian

1212   hyaenodontidan subfamilies, the relationships within clade P4 are worthy of additional

1213   discussion. Clade P4 is supported by a Bremer value of 1 and nine unambiguous synapomorphies

1214   (Table S3) and includes *Proviverra* as its basal-most taxon. The placements of each consecutive

1215   "proviverrine" sister taxon of hyaenodontines are supported by a Bremer value of 1, and include,

1216   from the basal node P5 (supported by seven unambiguous synapomorphies, see Table S3),

1217   *Allopterodon*; a *Eurotherium* + *Leonhardtina* clade (clade P7, branching off at node P6, which is

1218   supported by four unambiguous synapomorphies); a *Boritia-Parvagula* clade (P10, supported by

1219   three unambiguous synapomorphies, branching off at node P9); *Quercytherium* (P12, supported

1220   by a Bremer value of 6, bootstrap of 60, and eight unambiguous synapomorphies; branching off

1221   at node P11); *Cynohyaenodon* (branching off at node P13; supported by three synapomorphies);

1222   *Preregidens* (branching off at node P14, supported by seven unambiguous synapomorphies);

1223   *Matthodon* (branching off at node P15, supported by eight unambiguous synapomorphies); and

1224   *Oxyaenoides* (branching off at P16, nine unambiguous synapomorphies). The placement of

1225   *Oxyaenoides* close to hyaenodontines is strikingly different from the placement found by Rana et

1226   al. (2015) in which it was placed on the other side of the hyaenodontidan tree, closer to

1227   hyainailourines than apterodontines. Hyaenodontinae (P17) is a relatively well-supported clade

1228   (Bremer = 8; Bootstrap = 63) in which middle Eocene *Propterodon* species fall into a polytomy

1229   as the sister taxon of late Eocene/early Oligocene *Hyaenodon* (P18). Hyaenodontinae is

1230   unambiguously supported by 12 synapomorphies. *Hyaenodon* is well-supported as a clade (P18;

1231   Bremer = 6; Bootstrap = 79%) and is unambiguously supported eight synapomorphies.

1232   The sister group of all other hyaenodontidans is early Eocene European *Eoproviverra*

1233   (P1). Hyaenodontida (P1) has a Bremer support of 2 and Bootstrap support of 50% and is

1234   unambiguously supported by six synapomorphies. Outside of Hyaenodontida, the closest

1235   relatives among the non-hyaenodontidan species sampled is a *Cimolestes-Tinerhodon* clade

1236   (P56), which is supported by a Bremer value of 2 and three unambiguous synapomorphies.

1237

1238   **Bayesian Phylogenetic Inference**

1239   The "allcompat" (majority-rule plus compatible groups) topology recovered through

1240   standard Bayesian analysis is shown in Fig. 18 with posterior probabilities (PP) indicated to the

1241   right of the relevant node and the alphanumeric code used in this discussion to the left of the

1242   relevant node. The results of the parsimony character optimization onto the "allcompat" tree are

1243   listed in Table S3.

1244   Teratodontinae (B47) is recovered as a moderately supported clade (PP = 0.70), unlike

1245   the parsimony analysis, which collapsed all teratodontines into an unresolved polytomy.

1246   *Brychotherium* is placed as the sister taxon of *Dissopsalis* (B53; PP = 0.35) as part of a larger,

1247   very weakly supported clade (B51; PP = 0.16) with *Furodon* and *Anasinopa* (as in clade P37 on

1248   the Adams consensus derived from the parsimony analysis). The sister taxon of B51 (B48; PP =

1249   0.39) includes *Masrasector*, *Glibzegdouia*, and *Teratodon* and resembles clade P39 in the

1250   parsimony Adams consensus, but in the Bayesian analysis both species of *Masrasector* are

1251   included in Teratodontinae, though the genus is not monophyletic; instead, *Masrasector ligabuei*

1252   is the sister taxon to a clade B49 (PP = 0.40) that includes *Masrasector aegypticum* from Egypt

1253   and *Teratodon + Glibzegdouia* (B50; PP = 0.16).

1254   *Akhnatenavus nefertiticyon* is strongly supported (B67; PP = 0.93) as the sister taxon of

1255   *Akhnatenavus leptognathus*. *Akhnatenavus* is placed as the sister clade to the more deeply nested

1256   Afro-Arabian hyainailourines, including African "*Pterodon*" species and Miocene

1257   hyainailourines (B68; PP = 0.42). *Akhnatenavus* + B68 (B66) is only moderately supported (PP

1258   = 0.44), and is followed by the successive non-African sister taxa *Hemipsalodon* (branching off

1259   at B65, PP = 0.50) and *Kerberos* (branching off at B64, PP = 0.50). Successively more inclusive

1260   clades subsume African *Metapterodon* (at node B63, PP = 0.38), European *Pterodon*

1261   *dasyuroides* (at node B62, PP = 0.42), African *Koholia* (at node B61, PP = 0.36), Asian

1262   *Orienspterodon* (at node B60, PP = 0. 32), and European *Paroxyaena* (at node B58, PP = 0.29).

1263   The weakly supported clade formed by Apterodontinae and Hyainailourinae (B54, PP =

1264   0.28) was called Hyainailouridae by Solé et al. (2015). Apterodontinae (B55) is strongly

1265   supported as a clade (PP = 0.79) with *Quasiapterodon* as the sister taxon of *Apterodon*, a

1266   strongly supported genus (PP = 0.94) with *Apterodon macrognathus* recovered as the basal-most

1267   species, and *Apterodon gaudryi*, from the early Oligocene of Europe being the sister taxon of

1268   *Apterodon langebadreae*, from the early Oligocene of Afro-Arabia (at node B57; PP = 0.92).

1269   The oldest African hyaenodontidans, *Lahimia* and *Boualitomus*, form a strongly

1270   supported clade (B40; PP = 0.89) as they did in the parsimony analysis, but have no special

1271   relationship to teratodontines or hyainailourines to the exclusion of various other species from

1272   the Eocene of Asia, Europe, and North America. For instance, *Tritemnodon*, from the early

1273   Eocene of North America, is placed closer to teratodontines and hyainailourids, and with

1274   moderate support (B41; PP = 0.56), followed by successive taxa referred to Indohyaenodontinae

1275   by Solé et al. (2014b) and Rana et al. (2015). The clades that successively include the

1276   paraphyletic "indohyaenodontines" *Indohyaenodon* (B42; PP = 0.37), *Kyawdawia* (B43; PP =

1277   0.32), and *Paratritemnodon* (B44; PP = 0.33) are weakly supported, as is the more deeply nested

1278   clade that includes early Oligocene African *Metasinopa fraasi* (B45; PP = 0.31) as the sister

1279   taxon of the weakly supported (PP = 0.21) clade that contains Teratodontinae, Apterodontinae,

1280   and Hyainailourinae (B46).

1281   The composition of the clade that contains *Arfia*, *Sinopa*, Limnocyoninae,

1282   Indohyaenodontinae, Teratodontinae, Apterodontinae, and Hyainailourinae (B23; PP = 0.42) is

1283   identical in taxonomic composition to clade P20 except for the inclusion of *Preregidens*. The

1284   earliest divergences are among predominantly North American taxa. The sister group of all other

1285   members of B23 (B24) contains the two species of *Prototomus*, *Sinopa* (B27; PP = 0.85), and

1286   *Arfia* (B28; PP = 1.0). In the parsimony analysis, *Prototomus minimus*, an earliest Eocene

1287   species from Europe (Smith & Smith, 2001), was recovered in a more basal position in

1288   Hyaenodontida than *Prototomus phobos*, an early Eocene species from North America ~~(Zack,~~

1289   ~~2011)~~, but the Bayesian analysis places both *Prototomus* species as sister taxa of an *Arfia-Sinopa*

1290   but with weak support (B24; PP = 0.24 and B25; PP = 0.26). Successively more exclusive clades

1291   leading to the common node of the clade containing hyainailourids, teratodontines, and

1292   koholiines (B39) first exclude Limnocyoninae (node B33, PP = 0.22), followed by a *Galecyon-*

1293   *Gazinocyon* clade (node B37, PP = 0.27), *Preregidens* (node B38, PP = 0.36) and *Pyrocyon*.

1294   As in the parsimony analysis, *Tinerhodon* is recovered as the sister taxon of *Cimolestes*

1295   (B74; PP = 0.59) outside of Hyaenodontida. The Hyaenodontida + *Tinerhodon* + *Cimolestes*

1296   clade (B73) is strongly supported (PP = 0.95), as is Hyaenodontida (B1, PP = 1.0). The basal

1297   nodes of Hyaenodontida are different from the basal polytomy recovered using parsimony

1298   analysis (P1) with several early Eocene taxa from Europe (*Eoproviverra*, *Lesmesodon* +

1299   *Parvagula*, and *Morlodon*) representing successive sister taxa of more deeply nested

1300   hyaenodontidans. As in the parsimony analysis, *Eoproviverra* is the sister taxon of all other

1301   hyaenodontidans (B1) but, in contrast, the Bayesian analysis recovers successively more

1302   exclusive clades that first subsume *Lesmesodon* + *Parvagula* (B2, PP = 0.75) and then *Morlodon*

1303   (B4, PP = 0.15). The sister group of *Morlodon* is a weakly supported clade (B5, PP = 0.13) that

1304   diverges into Proviverrinae/Hyaenodontinae (B6, PP = 0.13) and the clade already discussed

1305   above (B23) of predominantly North American, Asian, and Afro-Arabian taxa.

1306   The basal nodes in the Proviverrinae/Hyaenodontinae clade (B6) are weakly supported

1307   (B7, PP = 0.15; B8, PP = 0.26; B9, PP = 0.33; B11, PP = 0.38) and the branching order differs

1308   from that in the parsimony analysis. In the Bayesian analysis, *Quercytherium* is more basal than

1309   *Eurotherium* and *Leonhardtina* (the latter of which also do not form a clade as in the parsimony

1310   analysis), and *Preregidens* is not recovered in Proviverrinae + Hyaenodontinae. *Cynohyaenodon*

1311   is the sister taxon to several strongly supported and successively more nested clades containing

1312   derived hyaenodontines and derived "proviverrines," including clades with *Leonhardtina* (B12 =

1313   0.87), *Eurotherium* (B13 = 0.92), *Matthodon* (B15, PP = 0.94), and *Oxyaenoides* (B16, PP =

1314   0.96) as successive sister taxa of Hyaenodontinae. As in the parsimony analysis, *Propterodon* is

1315   not monophyletic, with *Propterodon morrisi* being the sister group of all other hyaenodontines

1316   including *Propterodon tongi*; the *P. tongi* + *Hyaenodon* clade (B19) is moderately supported (PP

1317   = 0.53). *Hyaenodon* (B20) is strongly supported (PP = 1.0) and the two early Oligocene species

1318   from Asia, *Hyaenodon neimongoliensis* and an undescribed *Hyaenodon* species from Ergiliyn

1319   Dzo, are successive sister taxa to latest Eocene *Hyaenodon minor* from Europe and the late

1320   Eocene/early Oligocene *Hyaenodon horridus* from North America.

1321

1322   **Tip-Dating Bayesian Inference**

1323   The "allcompat" topology recovered using the Bayesian tip-dating method is shown in

1324   Fig. 19 with branches color-coded to indicate relative percent change per million years (%

1325   change/Ma). The alphanumeric code to the left of the relevant node corresponds with this

1326   discussion and posterior probabilities (PP) are italicized and placed to the right or below the

1327   relevant node. Table S4 contains the statistics generated by the tip-dating analysis most relevant

1328   to this study: median and mean age, median and mean relative rates, posterior probabilities, and

1329   the 95% confidence interval for the youngest and oldest age estimates for each node. Each taxon

1330   is shown with the full estimated age range drawn from the literature (Table S2) and the mean age

1331   for each taxon, as recovered with tip-dating Bayesian analysis, is indicated in the Fig. 19. Some

1332   taxa are reconstructed with a median divergence date that postdates the earliest possible age for

1333   the taxon (see *Eurotherium* in Fig. 19), but the mean estimated age for each taxon always

1334   postdates the median estimated divergence date. Divergence dates discussed below are mean age

1335   estimates. The results of the parsimony character optimization onto the "allcompat" tip-dating

1336   tree are listed in Table S3.

1337   In order to perform the tip-dating analysis and place a prior on the age of Hyaenodontida,

1338   that clade had to be explicitly defined. Because *Tinerhodon* was recovered as the sister taxon of

1339   *Cimolestes* using both parsimony and standard Bayesian analysis, *Tinerhodon* was excluded

1340   from Hyaenodontida in the tip-dating analysis. *Tinerhodon*, *Cimolestes*, and *Maelestes* were

1341   recovered as the sister group of Hyaenodontida (T73; PP = 0.63). *Tinerhodon* and *Cimolestes* are

1342   estimated to have split from each other during the Late Cretaceous (~73 Ma). Hyaenodontida is

1343   estimated to have originated in the Late Cretaceous at ~68.5 Ma.

1344   As in the parsimony and standard Bayesian analyses, the monophyly of *Akhnatenavus* is

1345   strongly supported (T67; PP = 0.95), and the divergence between the two species is reconstructed

1346   as having occurred ~37 Ma (late Eocene). Also like the parsimony and standard Bayesian

1347   analyses, *Akhnatenavus* is the sister clade to the rest of the Afro-Arabian hyainailourines (T66;

1348   PP = 0.44), a clade that is estimated to have originated in the late middle Eocene (~42 Ma).

1349   Evolutionary rates in the hyainailourine clade are relatively slow (<1.0% change/Ma) and the

1350   branch supporting *Akhnatenavus* (T67) is only moderately faster (~1.37% change/Ma) than the

1351   evolutionary rates of neighboring branches. Hyainailourinae as a whole (T62) is strongly

1352   supported (PP = 0.72) and is estimated to have originated in the middle Eocene (~47 Ma); it is

1353   taxonomically identical to Hyainailourinae as recovered by the standard Bayesian analysis (B62).

1354   A *Pterodon dasyuroides* + *Metapterodon* clade (T63; PP = 0.44) is the sister group of all other

1355   hyainailourines. Successively more nested clades include *Kerberos* (T64; PP = 0.23) and

1356   *Hemipsalodon* (T65; PP = 0.28) as sister taxa of Afro-Arabian hyainailourines. There is weak

1357   support for the placement of *Akhnatenavus* as the sister clade of the rest of Hyainailourinae (T66;

1358   PP = 0.44). As in the Bayesian analysis, African "*Pterodon*" is paraphyletic with respect to the

1359   Miocene hyainailourines *Isohyaenodon*, *Leakitherium*, and *Megistotherium*, the monophyly of

1360   which is strongly supported (T70, PP = 0.99); this result is consistent with both the parsimony

1361   (node P51) and standard Bayesian analyses (node B70).

1362   As in the standard Bayesian analysis, *Brychotherium* is nested within Teratodontinae

1363   (T48; PP = 0.50), but in contrast to the results from the parsimony and standard Bayesian

1364   analyses, *Brychotherium* is the sister taxon of a (*Teratodon*, (*Masrasector*, (*Anasinopa*,

1365   *Dissopsalis*))) clade (T49, PP = 0.38) that is estimated to have diverged at ~45 Ma. *Anasinopa*

1366   and *Dissopsalis* are strongly supported as sister taxa (T52; PP = 0.79) in a clade that is estimated

1367   to have originated ~27 Ma (middle Oligocene). Teratodontinae as a whole is estimated to have

1368   appeared ~58 Ma (late Paleocene), with *Glibzegdouia* and *Furodon* as its most basal members.

1369   The stem leading to the clade *Glibzegdouia* + T48 (T47) has a moderate rate of evolutionary

1370   change (1.04% change/Ma) and is the last of the basal teratodontine branches to change at a

1371   moderate rate. All more derived teratodontine branches show slower rates except for the

1372   *Brychotherium* (1.4% change/Ma) and *Dissopsalis* branches (1.34% change/Ma).

1373   The clade that includes Apterodontinae and Hyainailourinae plus *Koholia*, *Tritemnodon*,

1374   and *Paroxyaena* (T53) is weakly supported (PP = 0.29) and is estimated to have originated

1375   during the Paleocene (~59 Ma) along a branch that was marked by rapid evolutionary change

1376   (2.71% change/Ma). The clade *Tritemnodon + Koholia* (T54) is weakly supported (PP = 0.39)

1377   and is the sister group of the larger Apterodontinae + Hyainailourinae + *Paroxyaena* clade (T55,

1378   which is supported by a PP of 0.35). *Paroxyaena* is robustly supported (T56; PP = 0.98) as a

1379   clade. *Paroxyaena* is estimated to have diverged from Apterodontinae + Hyainailourinae during

1380   the Ypresian (T55; ~54.5 Ma). The clade Apterodontinae + Hyainailourinae (T57) is estimated to

1381   have diverged during the Ypresian (~53 Ma); the stem leading to this clade is reconstructed as

1382   having had a relatively fast evolutionary rate (2.81% change/Ma).

1383   Apterodontinae (T59) has robust support (PP = 0.99) and is estimated to have originated

1384   during the Lutetian (middle Eocene, ~43 Ma). *Quasiapterodon* is recovered as the sister taxon to

1385   the genus *Apterodon* on a branch characterized by a moderate relative evolutionary rate (~1.54%

1386   change/Ma). The monophyly of *Apterodon* is weakly supported (T59; PP = 0.47) and the three

1387   species sampled here are estimated to have first diverged during the Bartonian (late middle

1388   Eocene, ~40.6 Ma).

1389   Hyainailourinae, Apterodontinae, Indohyaenodontinae, and Teratodontinae form a very

1390   weakly supported Hyainailouroidea clade (T41; PP = 0.09) that is estimated to have originated

1391   during the early Paleocene (~65 Ma). The common stem shows a fast relative evolutionary rate

1392   (2.94% change/Ma). This large clade (T41) includes two major sub-clades with early

1393   divergences: Indohyaenodontinae + Teratodontinae (T42) and Hyainailourinae + Apterodontinae

1394   (T53). The indohyaenodontine/teratodontine clade (T42; PP = 0.15) is estimated to have

1395   originated in the early Paleocene (~63 Ma). Unlike in the standard Bayesian analysis,

1396   Indohyaenodontinae (T43; PP = 0.30) is monophyletic and its origin is placed in the middle

1397   Paleocene (~60 Ma).

1398 A major difference between the standard Bayesian and tip-dating Bayesian allcompat

1399 topologies is the structure of relationships near the origin of Hyaenodontida. In the tip-dating

1400 analysis, *Eoproviverra* is not recovered as the sister taxon to all other hyaenodontidan clades.

1401 Instead, *Eoproviverra* is nested within the very weakly supported clade Hyaenodontidae (T8; PP

1402 = 0.11) as the sister taxon of *Proviverra* (T14; PP = 0.54). Based on the tip-dating results, the

1403 earliest split in Hyaenodontida gave rise to two large clades: one originated ~68 Ma (T2) and

1404 includes the *Sinopa* clade (T3) and Hyaenodontidae, and the other originated ~68 Ma (T29) and

1405 includes Limnocyoninae, the *Galecyon* clade, the *Lahimia* clade, and Hyainailouroidea. In each

1406 of these major hyaenodontidan clades, the earliest diverging clades are predominantly composed

1407 of North American taxa once classified as "proviverrines" though these early-diverging

1408 relationships have very weak support (T2; PP = 0.06 and T29; PP = 0.17).

1409 The *Sinopa* clade (T3) includes *Arfia* (T5; PP = 1.0), *Prototomus*, and *Sinopa* (T7; 0.97)

1410 and is sister clade to the predominantly European clade Hyaenodontidae (T8; PP = 0.11), which

1411 includes European "Proviverrinae" and Hyaenodontinae. The branch supporting Hyaenodontinae

1412 has a rapid relative evolutionary rate (3.21% change/Ma) and an estimated origin of ~66.7 Ma.

1413 The oldest taxa in Hyaenodontinae are from the earliest Eocene, and multiple, unsampled,

1414 rapidly diverging lineages are reconstructed as originating during the Paleocene.

1415 In the tip-dating analysis topology *Parvagula*, *Lesmesodon*, and *Morlodon* are recovered

1416 within Hyaenodontidae, though all PP support for these early-diverging relationships is very

1417 weak (T9; PP = 0.12, T11; PP = 0.06; T12; PP = 0.10). The composition of the clade defined by

1418 the divergence of *Cynohyaenodon* (T15; PP = 0.26) at ~62 Ma is identical in taxonomic

1419 composition to clade B9 in the standard Bayesian analysis, and only differs in topology in the

1420 placement of *Quercytherium* (T17; PP = 1.0) and *Leonhardtina* (T19; PP = 0.37). During the late

1421 Paleocene and early Eocene, along the branch that includes *Matthodon* (T21) and the branch that

1422 includes *Oxyaenoides* (T22), relatively rapid evolutionary changes took place (T21; 5.22%

1423 change/Ma, T22; 5.27% change/Ma) before the origin of the clade that includes Hyaenodontinae

1424 (T24; PP = 0.98) in the early Eocene (~49.4 Ma). The stem supporting Hyaenodontinae (T24)

1425 has a fast relative evolutionary rate (3.49% change/Ma). The relationships within

1426 Hyaenodontinae are the same as in the standard Bayesian analysis. The results of this analysis

1427 place the origins of *Hyaenodon* (T26) in the late middle Eocene (~40.9 Ma).

1428   The most rapid median evolutionary rate in the tip-dating analysis is reconstructed along

1429 the branch supporting the clade that includes all Afro-Arabian hyaenodontidans, the *Galecyon*

1430 clade and Limnocyoninae (T29; PP = 0.17; 8.45% change/Ma). The clade composed of

1431 predominately North American taxa (*Galecyon* clade and Limnocyoninae; T30; PP = 0.10) that

1432 originated in the earliest Paleocene (~65.4 Ma) and is sister to the larger, very weakly supported

1433 clade that includes all Afro-Arabian taxa (T37; PP = 0.03). Within the Afro-Arabian clade (T37)

1434 the oldest hyaenodontidan in the analysis, *Lahimia*, is recovered as the sister taxon of

1435 *Boualitomus* (T39; PP = 0.96), a relationship supported by a branch with a very rapid

1436 evolutionary rate (4.75% change/Ma). *Lahimia + Boualitomus* (T39), is not closely related to

1437 *Koholia* and thus Koholiinae is not recovered by tip-dating analysis. Instead *Lahimia +*

1438 *Boualitomus* is the sister clade to *Preregidens + Pyrocyon* (T40; PP = 0.12) and these four taxa

1439 form the sister clade of the very weakly supported Hyainailouroidea (T41; PP = 0.09).

1440

1441   BIOGEOGRAPHIC RESULTS

1442

1443 **Biogeographic reconstructions on the maximum parsimony topology**

1444   As described above, three methods of biogeographic analysis were applied to the

1445   maximum parsimony strict consensus tree: parsimony optimization of geographic areas (PO),

1446   likelihood optimization of geographic areas (LO), and Bayesian Binary MCMC (BBM). The

1447   biogeographic reconstruction for each node in the strict consensus parsimony topology is

1448   presented in Table S5 and the continental area designated for each OTU and the results of the

1449   BBM analysis are shown in Fig. 20. The pie chart over each node represents the probability that

1450   the clade originated from each continental area.

1451   The root node of Hyaenodontida (P1) is unambiguously reconstructed with Europe as the

1452   origin for the entire clade using parsimony optimization (PO). A European origin for

1453   Hyaenodontida is strongly supported by likelihood optimization (LO = 93.92%) and Bayesian

1454   Binary MCMC analysis (BBM = 99.68%). Node P2 supports a polytomy comprised of

1455   *Morlodon*, *Lesmesodon*, a clade of "Proviverrinae" and Hyaenodontinae (P4), and the clade

1456   (P20) that includes *Arfia* (P21), Limnocyoninae (P23), *Galecyon + Gazinocyon* (P26), *Sinopa*

1457   (P30), *Prototomus*, "Koholiinae," "Indohyaenodontinae," "Teratodontinae," Apterodontinae, and

1458   "Hyainailourinae" (P31) is reconstructed, like the root of Hyaenodontida, with an unambiguous

1459   origin in Europe (PO) with strong support from the other biogeographic methods (LO = 99.73%;

1460   BBM = 99.79%). Within the "Proviverrinae"/Hyaenodontinae clade (P4), all stem nodes and

1461   constituent clades [*Leonhardtina* and *Eurotherium* (P7), *Boritia* and *Parvagula* (P10),

1462   *Quercytherium* (P12)] are unambiguously reconstructed as originating in Europe with strong

1463   support from all biogeographic methods. A dispersal to Asia is implied at the basal node of

1464   Hyaenodontinae (P17), with the node shared by *Propterodon* and *Hyaenodon* unambiguously

1465   reconstructed in Asia, which is highly likely using LO (98.31%) and BBM (96.77%). *Hyaenodon*

1466   is also unambiguously Asian in origin (LO = 97.51%, BBM = 99.9%) with subsequent dispersals

1467   to North America (*Hyaenodon horridus*) and Europe (*Hyaenodon minor*).

1468   The common node (P20) that unites *Arfia* (P21) as the sister clade to P22 (a clade that

1469   includes Limnocyoninae, *Galecyon + Gazinocyon,* "Koholiinae," "Teratodontinae,"

1470   Apterodontinae, and "Hyainailourinae") is unambiguously resolved with a North American

1471   origin (LO = 89.89%; BBM = 82.38%) and a small likelihood of an origin in Europe (LO =

1472   8.63%; BBM = 17.53%). This reconstruction implies a dispersal of hyaenodontidans from

1473   Europe to North America. Node P22 unites a polytomy comprised of the unambiguously North

1474   American Limnocyoninae (P23; LO = 99.90%; BBM = 99.99), the unambiguously North

1475   American *Galecyon* clade (P26; LO = 99.76%; BBM = 99.99%), North American *Prototomus*

1476   *phobos*, European *Prototomus minimus*, and clade P31 ("Koholiinae," "Indohyaenodontinae,"

1477   Apterodontinae, "Hyainailourinae"). P22 is unambiguously North American in origin with a high

1478   likelihood of this origin using the other biogeographic methods (LO = 99.72%; BBM = 92.47%).

1479   Multiple dispersals to Afro-Arabia, North America, and Europe are implied at node P31, which

1480   supports a large polytomy that includes taxa categorized as "Teratodontinae" (*Brychotherium*,

1481   *Dissopsalis, Anasinopa, Glibzegdouia, Metasinopa,* and *Teratodon*) in Solé et al. (2014b) and

1482   Rana et al. (2015); as "Koholiinae" (*Koholia, Lahimia, Boualitomus,* and *Metapterodon*) in Solé

1483   et al. (2014b); as "Indohyaenodontinae" (*Indohyaenodon, Kyawdawia, Paratritemnodon*) in Solé

1484   et al. (2014b); as "Hyainailourinae" (*Paroxyaena, Pterodon dasyuroides,* and *Orienspterodon*) in

1485   Solé et al. (2015); and as "Sinopaninae" (*Pyrocyon* and *Tritemnodon*) in Rana et al. (2015). The

1486   polytomy at node P31 also includes Apterodontinae (P39), a clade unambiguously resolved with

1487   an Afro-Arabian origin (LO = 99.81%; BBM = 99.99%) and a clade of hyainailourines (P43)

1488   that includes *Akhnatenavus* that is unambiguously Afro-Arabian in origin (LO = 84.85%; BBM

1489   = 86.65%). This large polytomy, P31, has a contradictory biogeographic reconstruction.

1490   Parsimony optimization unambiguously recovers an Afro-Arabian origin for the clade, implying

1491   a dispersal from North America to Afro-Arabia between node P22 and node P31. Likelihood

1492   optimization also supports Afro-Arabia as the most likely continent of origin for P31. However,

1493   BBM analysis only resolves an Afro-Arabian origin for P31 as 9.83% likely. More likely,

1494   according to the BBM analysis, is a North American origin (75.85%) or European origin

1495   (11.84%) with multiple dispersals between each of the continents. What is certain, according to

1496   the maximum parsimony topology, is at least two lineages dispersed to Afro-Arabia —

1497   Apterodontinae (P39) and a subset of hyainailourines (P43)— and radiated there with the lineage

1498   leading to *Apterodon gaudryi* (P40) dispersing from Afro-Arabia to Europe, the lineage leading

1499   to *Kerberos* (P43) dispersing from Afro-Arabia to Europe, and the lineage leading to

1500   *Hemipsalodon* (P43) dispersing from Afro-Arabia to North America. Direct dispersal between

1501   Afro-Arabia and North America, as implied at multiple nodes in the P31 clade, is unlikely and

1502   these dispersals likely passed through Europe or Asia but this strict consensus topology is not

1503   well-resolved enough to offer insight into which dispersal routes were most likely followed by

1504   hyaenodontidans between North America and Afro-Arabia.

1505

1506   **Biogeographic reconstructions on the "allcompat" Bayesian topology**

1507   The results of each method for reconstructing biogeography on the Bayesian "allcompat"

1508   topology [parsimony optimization (PO), likelihood optimization (LO), and Bayesian Binary

1509   MCMC (BBM)] are listed in Table S6 and the results of BBM are shown in Fig. 21 imposed on

1510   the standard Bayesian topology. The root node of Hyaenodontida (B1) is unambiguously

1511   resolved as European using parsimony optimization and is strongly supported as such by the

1512   other methods (LO = 96.36%; BBM = 99.86%). The clade *Parvagula + Lesmesodon* (B3) is

1513   unambiguously European in origin (LO = 99.74%; BBM = 99.86%), as is the common node of

1514   *Parvagula + Lesmesodon* and the rest of Hyaenodontida (B2; LO = 99.74%; BBM = 99.99%),

1515   and the clade that unites Proviverrinae/Hyaenodontinae, *Sinopa*, *Arfia*, Limnocyoninae, *Lahimia*

1516   + *Boualitomus*, "Indohyaenodontinae," Teratodontinae, Apterodontinae, and Hyainailourinae

1517   (B5; LO = 97.55%; BBM = 99.89%). Proviverrinae/Hyaenodontinae (B6) is also unambiguously

1518   European (LO = 99.84%; BBM = 100%) and every node more deeply nested in the clade is as

1519   strongly supported with a European origin until node B16, which supports *Oxyaenoides* as the

1520   sister clade to Hyaenodontinae. *Oxyaenoides* + Hyaenodontinae (B16) is unambiguously

1521   reconstructed as having originated in Europe (LO = 75.25%; BBM = 99.58%) though LO also

1522   recovers a 19.26% probability of an Asian origin for the clade. Hyaenodontinae (B18;

1523   *Propterodon + Hyaenodon*) is unambiguously resolved with an Asian origin (LO = 98.63%;

1524   BBM = 97.61%). *Hyaenodon* (B20) is also unambiguously reconstructed with an Asian origin

1525   and the clade *H. horridus + H. minor* (B22) is ambiguously resolved as having originated either

1526   in Asia [the most likely result using LO (39.71%) and BBM (60.24%)], Europe (LO = 26.69%;

1527   BBM = 20.62%), or North America (LO = 32.87%; BBM = 18.85%).

1528   The clade that contains *Sinopa*, *Arfia*, Limnocyoninae, *Lahimia + Boualitomus*,

1529   "Indohyaenodontinae," Teratodontinae, and Hyainailouridae (B23) is ambiguously reconstructed

1530   as having originating in either Europe (LO = 53.19%; BBM = 45.35%) or North America (LO =

1531   76.72%; BBM 23.18%). The *Sinopa-Arfia-Prototomus* clade (B24) is ambiguously reconstructed

1532   with either a European (LO = 54.25%; BBM = 73.51%) or North American (LO = 44.83%;

1533   BBM = 26.32%) origin, with its more deeply nested clade (B25) being unambiguously of North

1534   American origin (LO = 88.53%; BBM = 98.11%). The clade containing Limnocyoninae (B30) is

1535 the sister clade to "Indohyaenodontinae," Teratodontinae, Apterodontinae, and Hyainailourinae

1536 (B29) and is unambiguously North American in origin (LO = 89.74%; BBM = 96.25%), as is

1537 Limnocyoninae (B30; LO = 97.61%; BBM = 99.83%) and *Gazinocyon + Galecyon* (B34; LO =

1538 98.99%; BBM = 99.96%). *Preregidens* is reconstructed as having dispersed from North America

1539 to Europe. The common ancestor of *Lahimia + Boualitomus* is unambiguously Afro-Arabian

1540 (B40; LO = 98.57%; BBM = 99.42%), but a dispersal from North America to Afro-Arabia is

1541 reconstructed along their common stem.

1542 A dispersal from North America to Asia is reconstructed at the node uniting

1543 *Indohyaenodon* with other indohyaenodontines, Teratodontinae, Apterodontinae, and

1544 Hyainailourinae; their common node is unambiguously reconstructed as Asian (LO = 91.23%;

1545 BBM = 98.69%). A subsequent dispersal from Asia to Afro-Arabia is reconstructed between

1546 nodes B44 and B45, the latter of which joins African *Metasinopa* to Teratodontinae,

1547 Apterodontinae, and Hyainailourinae; B45 is unambiguously reconstructed as being of Afro-

1548 Arabian origin (LO = 94.54%; BBM = 98.04%).

1549 Teratodontinae (B47) and all of its internal nodes are unambiguously Afro-Arabian (B47

1550 LO = 99.90%; BBM = 100%), as is the common node that Teratodontinae shares with

1551 Apterodontinae and Hyainailourinae (B46; LO = 97.81%; BBM = 99.95%). Apterodontinae

1552 (B55) and all internal nodes are also unambiguously Afro-Arabian in origin (LO = 99.14%;

1553 BBM = 100%), supporting trans-Tethyan dispersal to Europe to account for the presence of

1554 *Apterodon gaudryi* on that landmass.

1555 The biogeographic history of Hyainailourinae and its possible relatives is particularly

1556 complex. The node that unites *Paroxyaena* and more deeply nested hyainailourines (B58) is

1557 unambiguously Afro-Arabian (LO = 44.01%; BBM = 91.74%) though LO also resolves high

1558   probabilities for a European origin (29.79%) and an Asian origin (23.04%); the most probable

1559   reconstructions on the Bayesian topology imply that *Paroxyaena* dispersed from Afro-Arabia to

1560   Europe. *Orienspterodon* is the next most deeply nested hyainailourine relative and the common

1561   node it shares with other hyainailourines (B60) is unambiguously Afro-Arabian in origin using

1562   PO, an origin supported by BBM (90.63%), but LO analysis recovers Asia as a more likely

1563   center of origin (54.14%) with Afro-Arabia as the second-most probable continent of origin for

1564   the clade (30.70%). *Koholia* is the sister group of definitive hyainailourines, and their common

1565   node (B61) is unambiguously Afro-Arabian (LO = 62.78%; BBM = 98.07%) with LO recovering

1566   a 21.77% probability that this clade originated in Europe. *Pterodon dasyuroides*, a European

1567   taxon, is part of the next most deeply nested clade (B62), which has an unambiguous origin in

1568   Afro-Arabia, a reconstruction strongly supported by BBM (85.25%), but less probable using LO

1569   (17.89%) than a European origin for B62 (81.10%). *Metapterodon*, nested between European

1570   *Pterodon dasyuroides* and *Kerberos*, is an Afro-Arabian taxon whose common node with more

1571   derived hyainailourines (B63) is unambiguously Afro-Arabian using PO, an origin supported by

1572   BBM (94.26%) but, again, LO recovers Europe as the more likely continent of origin for the

1573   clade (64.17%) followed by Afro-Arabia (33.47%). The common node for *Kerberos* and all more

1574   deeply nested hyainailourines (B64) is unambiguously Afro-Arabian in origin (LO = 33.32%;

1575   BBM = 79.06%) but LO resolves the most probable area of origin as Europe (LO = 63.56; BBM

1576   = 19.3%). *Hemipsalodon* is sister taxon to an entirely Afro-Arabian clade of hyainailourines and

1577   their common node (B65) is unambiguously resolved with an Afro-Arabian origin (LO =

1578   57.79%; BBM = 81.24%). *Akhnatenavus* (B67) is unambiguously Afro-Arabian (LO = 99.93%;

1579   BBM = 99.94%) and the node shared with more deeply nested Afro-Arabian hyainailourines

1580   (B66) is also unambiguously Afro-Arabian (LO = 97.84%; BBM = 99.94%), as are all nodes in

1581   the Afro-Arabian hyainailourine clade.

1582

1583   **Biogeographic reconstructions on the tip-dating topology**

1584   The tip-dating topology differs from the standard Bayesian topology in a number of ways

1585   that change the biogeographic reconstructions of ancestral nodes within Hyaenodontida when

1586   parsimony optimization (PO), likelihood optimization (LO), and Bayesian Binary MCMC

1587   (BBM) methods are applied to the tree. The inclusion of specific divergence dates and branch

1588   lengths from tip-dating analysis also alter some biogeographic hypotheses based on the

1589   parsimony and standard Bayesian topologies. The results of each method are listed in Table S7

1590   and the results of BBM analysis are shown over the corresponding nodes in Fig. 22.

1591   Unlike in the standard Bayesian topology, Hyaenodontida (T1) is unambiguously

1592   resolved with an origin in North America (LO = 69.57%; BBM = 83.96%). Hyaenodontida is

1593   split into two major clades, one that includes Hyaenodontidae (T2) and one that includes

1594   Hyainailouroidea (T29). Node T2 is unambiguously North American in origin (LO = 76.46%;

1595   BBM = 62.24%) though there is a high probability of a European origin for T2 (LO = 26.97%;

1596   BBM = 36.85%). Node T29 is also unambiguously North American (LO = 72.05%; BBM =

1597   87.75%) with the next-most likely origin for the node that includes Hyainailouroidea in Afro-

1598   Arabia (LO = 15.54%; BBM = 8.17%).

1599   The larger clade that contains Hyaenodontidae (T2) includes a predominately North

1600   American *Sinopa* clade (T3) that is unambiguously North American in origin (LO = 84.88%;

1601   BBM = 87.7%) and a predominately European clade with "Proviverrinae" and Hyaenodontinae

1602   (T8) that is unambiguously European in origin (LO = 92.05%; BBM = 99.67%). Despite the

1603   inclusion of *Prototomus minimus* from Europe and *Sinopa jilinia* from Asia, every node within

1604   the *Sinopa* clade (T3) is unambiguously North American in origin (T4; LO = 85.71%; BBM =

1605   70.6%, T5, *Arfia*; LO = 99.79%; BBM = 99.84%, T6; LO = 93.46%; BBM = 98.56%, T7,

1606   *Sinopa*; LO = 91.89%; BBM = 97.51%) implying dispersal from North America to Europe in the

1607   lineage that includes *Prototomus minimus*, and dispersal from North America to Asia in the

1608   lineage that includes *Sinopa jilinia*.

1609   The sister clade of the *Sinopa* clade, Hyaenodontidae (T8), is unambiguously European in

1610   origin (LO = 92.05%; BBM = 99.67) and all of the nodes and clades contained within

1611   Hyaenodontidae are unambiguously European in origin (T8–T22; LO >92%; BBM >99%)

1612   except for the nodes defined as part of Hyaenodontinae (T24). During the early Eocene, the

1613   ancestor of Hyaenodontinae (T24) dispersed from Europe to Asia and the origin of

1614   Hyaenodontinae (T24) is unambiguously in Asia (LO = 96.32%; BBM = 97.72%). The

1615   taxonomically diverse genus *Hyaenodon* (T26) is also unambiguously Asian in origin (LO =

1616   96.59%; BBM = 99.99%). The biogeographic scenario surrounding the dispersal of *Hyaenodon*

1617   to North America (represented in this analysis by *H. horridus*) and to Europe (*H. minor*) is

1618   ambiguous with the common ancestor of these species most likely originating in Asia (LO =

1619   52.32%; BBM = 59.83%) before dispersal to North America and Europe, though there is support

1620   for this common ancestor originating in Europe (LO = 24.92%; BBM = 21.82%) or North

1621   America (LO = 22.02%; BBM = 18.06%).

1622   As stated above, the large clade that includes Limnocyoninae, the *Galecyon* clade, and

1623   Hyainailouroidea (T29) is unambiguously North American in origin. The clade composed largely

1624   of North American taxa, *Galecyon* clade + Limnocyoninae (T30), is unambiguously North

1625   America in origin (LO = 95.99%; BBM = 99.88%) and all nodes contained within the *Galecyon*

1626   clade and Limnocyoninae (T31–T36) unambiguously originate in North America (LO >95%;

1627   BBM >99%). This reconstruction indicates Asian *Prolimnocyon chowi* is the result of a dispersal

1628   event from North America to Asia during the late Paleocene.

1629   The *Galecyon* clade + Limnocyoninae clade (T30) is sister to the large clade that includes

1630   all Afro-Arabian taxa (T37). This node is ambiguously reconstructed as either Afro-Arabian or

1631   North American in origin, though an Afro-Arabian origin is more likely (LO = 48.27%; BBM =

1632   73.37%) than a North American origin (LO = 43.31%; BBM = 24.21%). This reconstruction

1633   indicates the ancestor of *Lahimia*, Indohyaenodontinae, Teratodontinae, Apterodontinae, and

1634   Hyainailourinae likely dispersed to Afro-Arabia from North America in the Late Cretaceous.

1635   Direct dispersal between these continents seems unlikely and the implications of this dispersal

1636   are discussed below.

1637   The clade that contains the oldest known hyaenodontidan, *Lahimia*, along with

1638   *Preregidens*, *Pyrocyon*, and *Boualitomus* (T38) has an ambiguous origin in Afro-Arabia (LO =

1639   51.97%; BBM = 79.77%) or North America (LO = 39.72%; BBM = 16.66%), though an Afro-

1640   Arabian origin is more likely. This result implies the ancestors of North American *Pyrocyon* and

1641   European *Preregidens* (T40) independently dispersed from Afro-Arabia (LO = 29.76%; BBM =

1642   49.78%) or the common ancestor of these taxa dispersed from Afro-Arabia to North America

1643   (LO = 49.78%; BBM = 48.95%) or from Afro-Arabia to Europe (LO = 18.56%; 37.57%). The

1644   clade that includes *Lahimia* and *Preregidens* (T38) is the sister clade of Hyainailouroidea (T41).

1645   Hyainailouroidea is unambiguously Afro-Arabian in origin (LO = 66.14%; BBM = 94.99%). The

1646   clade that includes Indohyaenodontinae and Teratodontinae (T42) also unambiguously originated

1647   in Afro-Arabia (LO = 68.48%; BBM = 94.1%). Indohyaenodontinae (T43) is unambiguously

1648   Asian in origin (LO = 82.18%; BBM = 96.4%) implying the ancestor of indohyaenodontines

1649   dispersed from Afro-Arabia to Asia during the Paleocene or early Eocene. Afro-Arabian

1650   *Metasinopa fraasi* is nested within Indohyaenodontinae as the sister taxon of *Paratritemnodon*.

1651   *Paratritemnodon* + *Metasinopa* (T45) is unambiguously Asian in origin (LO = 96.36%; BBM =

1652   96.83%), indicating the ancestor of *Metasinopa* dispersed from Asia to Afro-Arabia during the

1653   Eocene. The sister clade of Indohyaenodontinae (T43) is Teratodontinae, a clade that includes

1654   *Brychotherium* and is entirely composed of Afro-Arabian taxa. Every node in Teratodontinae is

1655   unambiguously Afro-Arabian in origin (T46–T52; LO > 95%; BBM > 99%).

1656   The sister clade of Indohyaenodontinae + Teratodontinae that includes *Koholia*,

1657   *Tritemnodon*, *Paroxyaena*, Apterodontinae, and Hyainailourinae (T53) is unambiguously Afro-

1658   Arabian in origin (LO = 74.41%; BBM = 94.75%). This clade contains taxa from North America

1659   (*Tritemnodon*, *Hemipsalodon*), Europe (*Paroxyaena*, *Apterodon gaudryi*, *Pterodon dasyuroides*,

1660   and *Kerberos*), and Asia (*Orienspterodon*) but all nodes within the clade are unambiguously

1661   reconstructed with an Afro-Arabian origin (T53–T71) using parsimony optimization except T56,

1662   the node that supports the monophyly of *Paroxyaena*. This is evidence that most of the dispersal

1663   scenarios that concern apterodontines and hyainailourines involve dispersal events from Afro-

1664   Arabia to the northern continents. *Koholia* + *Tritemnodon* (T54) is likely Afro-Arabian in origin

1665   (LO = 76.29%; BBM = 89.02%) and the ancestor of *Tritemnodon* dispersed from Afro-Arabia to

1666   North America during the early Eocene. The ancestor of *Paroxyaena* dispersed from Afro-

1667   Arabia (T55; LO = 68.57%; BBM = 83.19%) to Europe (T56; LO = 98.48%; BBM = 99.62%)

1668   during the early Eocene. Apterodontinae (T58) originated in Afro-Arabia (LO = 96.49%; BBM =

1669   99.94%), indicating the ancestor of European *Apterodon gaudryi* (T60) dispersed from Afro-

1670   Arabia to Europe during the late Eocene or early Oligocene.

1671   The common node for Hyainailourinae and *Orienspterodon* (T61) is unambiguously

1672   Afro-Arabian in origin (LO = 62.37%; BBM = 80.23%), implying the lineage that includes

1673   *Orienspterodon* dispersed from Afro-Arabia to Asia during the middle Eocene. Hyainailourinae

1674   (T62) is unambiguously Afro-Arabian (LO = 58.70%; BBM = 63.42%) though there some

1675   support for a European origin for Hyainailourinae (LO = 34.95%; BBM = 34.61%). The

1676   common node shared by European *Pterodon dasyuroides* and Afro-Arabian *Metapterodon*

1677   *kaiseri* (T63) is unambiguously Afro-Arabian, a result supported by BBM (59.9%). The LO

1678   analysis resolves this node as more likely European in origin (63.02%) and an Afro-Arabian

1679   origin for *Pterodon dasyuroides* + *Metapterodon* is resolved by LO as less likely (33.07%). This

1680   result complicates the dispersal of *Pterodon dasyuroides*, but it does not eliminate the possibility

1681   that the common ancestor of *P. dasyuroides* dispersed from Afro-Arabia to Europe during the

1682   middle Eocene. *Kerberos*, a European hyainailourine, is the sister taxon of the clade that includes

1683   North American *Hemipsalodon* and Afro-Arabian hyainailourines, and the common node (T64)

1684   is unambiguously Afro-Arabian in origin. The Afro-Arabian origin of T64 is supported by LO

1685   (59.2%) but not BBM (41.5%), which resolves Europe as a slightly more likely origin (55.85%)

1686   of the clade. This further supports the hypothesis that there were hyainailourines dispersing

1687   between Afro-Arabia and Europe in the middle Eocene, though the direction of this dispersal is

1688   ambiguous when all three biogeographic methods are applied to the tip-dating topology. Node

1689   T65 supports *Hemipsalodon* as the sister taxon of a clade of Afro-Arabian hyainailourines. The

1690   origin of T65 is unambiguously Afro-Arabian (LO = 66.97%; BBM = 61.13%), though there is

1691   also support for a European (LO = 22.34%; BBM = 17.88%) or North American (LO = 9.65%;

1692   BBM = 20.61%) origin for the clade.

1693   *Akhnatenavus* (T67) is unambiguously Afro-Arabian in origin (LO = 99.9%; BBM =

1694   100%) as is the common node (T66) shared with more deeply nested Afro-Arabian

1695   hyainailourines (LO = 97.58%; BBM = 99.92%). All Afro-Arabian hyainailourine clades more

1696   deeply nested than clade T66 are unambiguously resolved with an origin in Afro-Arabia with LO

1697   probabilities greater than 99% and BBM probabilities equal to 100%. Ultimately, according to

1698   the tip-dating analysis, Afro-Arabia is the center of hyainailouroidean radiation beginning in the

1699   Paleocene and is most likely the continent of origin for the ancestors of Indohyaenodontinae,

1700   Teratodontinae, Apterodontinae, and Hyainailourinae.

1701

1702   DISCUSSION

1703

1704   **Phylogenetic position of *Brychotherium* and Teratodontinae**

1705   In both the standard Bayesian analysis and the Adams consensus derived from the

1706   parsimony analysis, *Brychotherium* was placed in the same clade as *Dissopsalis*, *Anasinopa*, and

1707   *Furodon* (P37, B51) to the exclusion of other teratodontines (Figs. 18, 16). The close relationship

1708   of *Brychotherium* with *Dissopsalis* and *Anasinopa* is not particularly surprising, because Solé et

1709   al. (2014b) also included *Brychotherium* in their analysis based on the descriptions and images of

1710   more fragmentary specimens provided by Holroyd (1994) in her doctoral dissertation, and found

1711   a well-supported (Bremer = 4) *Anasinopa-Brychotherium-Dissopsalis* clade as part of a similarly

1712   robust Teratodontinae (Bremer = 4) that also included *Masrasector*, *Teratodon*, and

1713   *Glibzegdouia*. The placement of early or middle Eocene *Furodon* as a derived teratodontine in

1714   the analyses presented here is more surprising, as this result differs from the parsimony-based

1715   results of Solé et al. (2014b) and Rana et al. (2015), both of which found *Furodon* to be a basal

1716   hyainailourine. It is particularly noteworthy that the standard Bayesian analysis places *Furodon*

1717   deep within Teratodontinae as the sister taxon of Miocene *Anasinopa*, requiring an extensive

1718   ghost lineage for the *Anasinopa* branch through most of the Eocene and Oligocene. Similarly

1719   extensive ghost lineages are also required by the topology recovered by Rana et al. (2015), who

1720   found Miocene *Anasinopa* and *Dissopsalis* to be paraphyletic with respect to Paleogene

1721   teratodontines, and with the oldest teratodontine in their analysis (*Glibzegdouia*) being the most

1722   deeply nested. Such long ghost lineages, and near-inversions of the expected relationship

1723   between node age and stratigraphic succession, hints at the possibility of a misplaced root for

1724   teratodontines in those analyses.

1725   The tip-dating analysis presented here (Fig. 19) instead places *Furodon* as the sister taxon

1726   of all other teratodontines, diverging from the other species in the late Paleocene or early

1727   Eocene, a result that is more consistent with the stratigraphic succession of species. In the tip-

1728   dating topology, Miocene *Anasinopa* and *Dissopsalis* are strongly supported (PP = 0.79) as sister

1729   taxa, with Oligocene species of *Masrasector* weakly situated as the clade's sister group, again

1730   significantly reducing the lengths of the ghost lineages implied by the other methods and

1731   previous studies. Tip-dating analysis also resolves *Glibzegdouia* and *Brychotherium* as tips of

1732   lineages that diverged from other teratodontines during the early and middle Eocene,

1733   respectively. This more basal position for *Brychotherium* is comparable to the position occupied

1734   by *Brychotherium* among "Afroasian proviverrines" in the study of Egi et al. (2005, in which

1735   *Brychotherium* is referred to as "African *Sinopa*"). The weakly supported, very basal

1736   teratodontine placement of *Furodon* is not radically inconsistent with the parsimony-based

1737   results of Rana et al. (2015), which placed Teratodontinae as the sister clade to Hyainailourinae,

1738   and *Furodon* as the basal-most sister group of Hyainailourinae, implying that basal-most

1739 hyainailourines and teratodontines might be very similar morphologically. Solé et al.'s (2014b)

1740 analysis placed *Furodon* far from Teratodontinae, at the base of Hyainailourinae in a

1741 hyainailourine-koholiine clade; note, however, that Solé et al. (2014b) sampled far fewer taxa

1742 than did Rana et al. (2015), and the expanded sampling of Rana et al. might help to explain why

1743 their results are more consistent with those presented here.

1744   The position of "Indohyaenodontinae" (*Indohyaenodon*, *Kyawdawia*, *Paratritemnodon*,

1745 and possibly *Metasinopa*, an African genus that is consistently placed in the same vicinity as

1746 "indohyaenodontines") relative to Teratodontinae differs using each method, and has also been

1747 unstable in previous studies that have included these taxa. Solé et al. (2014b) found

1748 Indohyaenodontinae to be the sister group of *Apterodon* + Sinopaninae (which, in their analysis,

1749 includes *Sinopa*, *Tritemnodon*, *Pyrocyon*, and *Prototomus*), while Rana et al. (2015) found that

1750 "indohyaenodontines" were paraphyletic with respect to (Apterodontinae, (Teratodontinae,

1751 Hyainailourinae)). Neither of these analyses sampled *Metasinopa*. The parsimony analysis

1752 presented here did not resolve relationships among indohyaenodontines, but in the Adams

1753 consensus *Indohyaenodon, Kyawdawia, Paratritemnodon*, and the *Brychotherium*

1754 "teratodontine" clade + *Paroxyaena* (P36) fall into a polytomy at the base of a node (P35) shared

1755 with Apterodontinae + Hyainailourinae (P38), and tip-dating analysis supports the hypothesis

1756 that indohyaenodontines are more closely related to Teratodontinae than they are to

1757 Apterodontinae + Hyainailourinae. The ambiguous position of "indohyaenodontines" and

1758 teratodontines bears similarities to the "Afroasian proviverrine" clade recovered by Egi et al.

1759 (2005), which included *Dissopsalis* + *Anasinopa* as the sister clade of

1760 (*Paratritemnodon*,(*Masrasector*, *Kyawdawia*)). The fact that expanded sampling of taxa and

1761 characters, first by Rana et al. (2015), and now by this study, congruently recovers

1762 "indohyaenodontines" and teratodontines close to Apterodontinae and Hyainailourinae suggests

1763 that the still poorly documented "indohyaenodontines" are likely to be of great importance for

1764 understanding the origin and dispersal of multiple Paleogene Afro-Arabian lineages.

1765

1766 **Phylogenetic position of *Akhnatenavus* and Hyainailourinae**

1767   In every phylogenetic analysis performed in this study, *Akhnatenavus nefertiticyon* was

1768 placed as the sister taxon of early Oligocene *Akhnatenavus leptognathus*. This *Akhnatenavus*

1769 clade was recovered by every analysis as a sister group of Oligo-Miocene Afro-Arabian

1770 hyainailourines, either as the exclusive sister clade to the younger Afro-Arabian hyainailourines

1771 (standard Bayesian inference B66 and tip-dating Bayesian inference T66) or as part of a basal

1772 polytomy with those taxa and *"Pterodon" africanus* (parsimony analysis P48). In every analysis,

1773 North American *Hemipsalodon* and European *Kerberos* were recovered as sister taxa to the

1774 Afro-Arabian clade that includes *Akhnatenavus*, with European *Pterodon dasyuroides* and

1775 African *Metapterodon kaiseri* occupying even more basal positions in Hyainailourinae. In Solé

1776 et al. (2014b) *Akhnatenavus* was placed as the sister taxon to *Megistotherium*, with Afro-Arabian

1777 *Pterodon* species being that clade's sister group. Rana et al. (2015) found no resolution among

1778 hyainailourines, with *Akhnatenavus* falling into a polytomy that also included *Hyainailouros*,

1779 *Koholia*, *Metapterodon*, *Oxyaenoides*, and *Pterodon* (note that, in this analysis, *Oxyaenoides* is

1780 placed with hyaenodontines). In their description of *Kerberos*, Solé et al. (2015) performed a

1781 phylogenetic analysis that included Hyainailourinae and found "*Pterodon*" *phiomensis* to be the

1782 sister group of an unresolved clade that included *Akhnatenavus*, *Isohyaenodon*, and

1783 *Hyainailouros*. Ultimately, earlier phylogenetic studies and the results presented in this study

1784 have supported Holroyd's (1999) decision to erect the genus *Akhnatenavus* rather than keeping

1785   *A. leptognathus* as a species within the genus *Pterodon*, as was originally done by Osborn

1786   (1909).

1787   *Pterodon* is not monophyletic in any of the analyses. *Pterodon dasyuroides* (the type

1788   species of *Pterodon*) was consistently placed in a more basal position than either "*Pterodon*"

1789   *africanus* or "*Pterodon*" *phiomensis*. Furthermore, "*Pterodon*" *africanus* and "*Pterodon*"

1790   *phiomensis* were not recovered as sister taxa using any method in this study. This result is

1791   consistent with the results of Solé et al. (2015) in which *Pterodon dasyuroides* was also placed at

1792   a basal node in Hyainailourinae, with "*Pterodon*" *africanus* in a more deeply nested position, and

1793   "*Pterodon*" *phiomensis* even more deeply nested as the sister taxon to the clade that includes

1794   *Akhnatenavus*. Other studies that have included *Pterodon* have combined multiple species of

1795   *Pterodon* — the *Pterodon* OTUs in Solé et al. (2014b) and Rana et al. (2015) were a

1796   combination of African "*P.*" *africanus*, "*P.*" *phiomensis*, and "*P.*" *syrtos*, while *Pterodon* in

1797   Polly (1996) combines *P. dasyuroides* and "*P.*" *africanus*. The results of Solé et al. (2015) and

1798   the present study strongly suggest that the separate species included in *Pterodon* need to be

1799   reexamined and analyzed as separate OTUs in all future phylogenetic analyses, and that revision

1800   of the genus is in order. In his discussion of "Hyaenodontinae" (which then included *Pterodon*,

1801   *Apterodon*, *Metapterodon*, and *Hyaenodon*), Savage (1965) synonymized North American

1802   *Hemipsalodon* with *Pterodon*. Mellett (1969) disputed this, arguing that *Hemipsalodon* was

1803   distinct from *Pterodon*, though they do share dental and cranial similarities. The results of Solé

1804   et al. (2015) and the analysis presented here support the distinction between these taxa.

1805   In both Bayesian analyses, the major sister clade to Hyainailourinae is Apterodontinae,

1806   and this clade is also found in the Adams consensus derived from the parsimony analysis.

1807   However, in some cases, other taxa that are not distinctly apterodontine or hyainailourine

1808   (*Koholia*, *Orienspterodon*, *Paroxyaena*) intervene or form sister clades of either subfamily. In

1809   the parsimony-based Adams consensus (P39) the consecutive sister clades of Hyainailourinae are

1810   *Orienspterodon* and Apterodontinae alone — *Quasiapterodon* and *Apterodon* — and the latter is

1811   well supported (Bremer = 4), whereas in the standard Bayesian analysis *Koholia*,

1812   *Orienspterodon*, and *Paroxyaena* intervene between Hyainailourinae and Apterodontinae as stem

1813   members of the former clade; again, Apterodontinae is well supported (PP = 0.79). In the tip-

1814   dating analysis, *Koholia*, *Tritemnodon*, and *Paroxyaena* shift to a position along the stem of

1815   Hyainailouridae, outside of Apterodontinae and Hyainailourinae, and *Orienspterodon* is the

1816   sister taxon of Hyainailourinae. This is the first time that *Orienspterodon* has been included in a

1817   phylogenetic analysis and it supports the conclusions of Egi, Tsubamoto & Takai (2007), who

1818   advocated for a close relationship between hyainailourines and *Orienspterodon* rather than a

1819   close relationship between *Orienspterodon*, *Paratritemnodon*, and *Kyawdawia*, as was suggested

1820   by Lewis & Morlo (2010).

1821   Grohé et al. (2012) undertook the first phylogenetic analysis of Apterodontinae and found

1822   that species of *Apterodon* formed a polytomy with *Quasiapterodon* and *Metasinopa*. They did

1823   not include any hyainailourines in their analysis and the sister clade to their Apterodontinae was

1824   *Paratritemnodon* + *Kyawdawia*; both of those Asian taxa are clearly in the phylogenetic

1825   neighborhood of Apterodontinae, but the results of the current analysis indicate that

1826   hyainailourines are probably even more critical for any phylogenetic evaluation of apterodontine

1827   relationships. Solé et al. (2014b) performed the first phylogenetic analysis that included

1828   *Apterodon* alongside hyainailourines. Their study was limited to dental characters, and

1829   *Apterodon* was recovered as the sister clade to Sinopaninae, an assemblage whose monophyly

1830   was not recovered by any of the analyses presented here. More recently, Solé et al. (2015)

1831   illustrated cranial features that are shared by Apterodontinae and Hyainailourinae, and elevated

1832   this group to Hyainailouridae, but these features were not converted into characters for their

1833   phylogenetic analysis, which recovered Apterodontinae and Hyainailourinae in a polytomy with

1834   *Lahimia* and *Boualitomus*. Cranial characters sampled from Polly (1996) were integrated into the

1835   analysis performed by Rana et al. (2015) and that study placed Apterodontinae as the sister clade

1836   to Teratodontinae + Hyainailourinae. The cranial features illustrated by Solé et al. (2015) were

1837   converted into characters for the character-taxon matrix presented here. The matrix also includes

1838   cranial characters from Polly (1996), and several new characters, and the "hyainailourid"

1839   hypothesis (Apterodontinae as the sister clade to Hyainailourinae) is supported, though it is

1840   disrupted in the parsimony analysis by the occasional incursion of "wildcard" taxa. For the sake

1841   of improved communication, we support and encourage the future use of the family-level nomen

1842   Hyainailouridae, which we recommend for the clade that includes *Apterodon macrognathus*,

1843   *Megistotherium osteothlastes*, and their last common ancestor. Furthermore, given the consistent

1844   placement of Teratodontinae as a major sister group of Hyainailouridae using all phylogenetic

1845   methods, we propose the use of the superfamily Hyainailouroidea for the clade that includes

1846   *Apterodon macrognathus*, *Megistotherium osteothlastes*, *Dissopsalis pyroclasticus*, and their last

1847   common ancestor.

1848   One of the more problematic genera that may or may not fall within Hyainailouridae as

1849   defined above is middle-late Eocene *Paroxyaena*. In his discussion of the genus, Lavrov (2007)

1850   suggested that *Paroxyaena* was more closely affiliated with *Pterodon* and *Hemipsalodon* than

1851   with *Hyaenodon*, and that *Hemipsalodon*, *Paroxyaena*, and *Pterodon* belong to a distinct

1852   Paroxyaenini. Solé et al. (2015) placed *Hemipsalodon* in Paroxyaenini with *Paroxyaena*. All

1853   analyses performed in this study found a monophyletic *Paroxyaena*, but not Paroxyaenini as

1854   defined by Solé et al. (2015); instead, *Paroxyaena* is situated in different positions depending on

1855   the method used. In the parsimony analysis, *Paroxyaena* can only be placed as a member of a

1856   clade that also includes hyainailouroids (P31), the relationships of which are largely unresolved,

1857   while standard Bayesian inference places *Paroxyaena* along the stem of Hyainailourinae (B58),

1858   and tip-dating analysis places *Paroxyaena* as a sister taxon of Hyainailouridae (T55). As a taxon

1859   with a long and narrow cranial vault, indistinct postorbital processes, and partially fused

1860   paracones and metacones the phylogenetic position of *Paroxyaena* close to or within

1861   Hyainailouridae seems likely. The M^{1-2} paracone and metacone of *Paroxyaena* are more

1862   divergent than most hyainailourids and the morphology of the molars may be one source of

1863   instability for the genus in the character-taxon matrix used in this analysis.

1864

1865   **Phylogeny of Hyaenodontida**

1866   In this analysis the possible basal hyaenodontidan *Tinerhodon*, a late Paleocene taxon

1867   from Morocco, was found to be more closely related to *Cimolestes* than to Hyaenodontida,

1868   though it should be noted that outgroup sampling is limited and this relationship will need to be

1869   reevaluated again as the matrix used here is eventually expanded to include other non-

1870   hyaenodontidans. *Tinerhodon* was considered by McKenna & Bell (1997) to be part of

1871   Cimolestidae, but Gheerbrant et al. (2006) disputed its cimolestid affinities, suggesting that it

1872   was a basal hyaenodontidan based on comparisons to *Boualitomus*. Subsequent studies (Solé,

1873   2013; Solé, Falconnet & Yves, 2014a; Solé et al., 2014b; Solé et al., 2015) found *Tinerhodon* to

1874   be the sister group of Hyaenodontida while Rana et al. (2015) found *Tinerhodon* to be the sister

1875   taxon of *Lahimia + Boualitomus*, a clade that occupied multiple positions in their analysis. None

1876   of the analyses performed here recover *Lahimia* and *Boualitomus* in such a basal position, and

1877   none place *Tinerhodon* as the sister taxon to Hyaenodontida to the exclusion of *Cimolestes*.

1878   *Tinerhodon* has large metaconids that project well above the paraconids, well-developed talonid

1879   cusps that include an additional cusp along the entocristid, and wide talonids basins, characters

1880   not shared with *Boualitomus* and *Lahimia*; the placement of these taxa in separate clades is

1881   consistent with the gross morphology of the dentition. Currently, *Tinerhodon* is only known from

1882   isolated lower teeth, and more morphological information from upper teeth would help to further

1883   test the phylogenetic position of this Afro-Arabian taxon, as it may either have important

1884   biogeographic implications for Hyaenodontida, or be of no relevance to the clade.

1885   Crochet (1988) erected the subfamily Koholiinae to contain *Koholia*, which was, at the

1886   time, the oldest-known Afro-Arabian hyaenodontidan. Solé et al. (2009) added *Boualitomus* and

1887   *Lahimia* to Koholiinae based on wear patterns inferred from the fragmentary upper dentition of

1888   *Koholia* that were used to reconstruct the lower dentition and make comparisons to *Lahimia*.

1889   Solé et al. (2014b) later found a monophyletic Koholiinae that also included *Metapterodon*,

1890   which together were placed as the sister clade to Hyainailourinae. None of the phylogenetic

1891   analyses presented here recover a monophyletic Koholiinae. Instead, *Koholia* is either in an

1892   unresolved position relative to other hyainailouroids (using parsimony), closely affiliated with

1893   Hyainailourinae (using standard Bayesian inference), or is a sister group of Hyainailouridae to

1894   the exclusion of Teratodontinae (using Bayesian tip-dating). The monophyly of *Lahimia* +

1895   *Boualitomus*, on the other hand, is strongly supported in both Bayesian analyses, in which it is

1896   placed outside of Hyainailouroidea. The other alleged "koholiine," *Metapterodon* (the only

1897   "koholiine" known from upper and lower dentitions), is placed with hyainailourines in both

1898   Bayesian analyses, with tip-dating suggesting a close relationship with *Pterodon dasyuroides*; a

1899   placement with hyainailourines is also present in the parsimony-based Adams consensus.

1900   The tip-dating approach employed here (a first for Hyaenodontida) is of particular

1901   interest given the great age of *Lahimia*, because some have proposed an African origin of

1902   hyaenodontidans solely on the basis of the antiquity of *Lahimia*; however, in practice, the

1903   expected phylogenetic pattern that would support such an African origin (i.e., paraphyly of

1904   multiple African taxa with respect to non-African taxa) has not been found in any phylogenetic

1905   analysis that included these species. Even using tip-dating, *Lahimia* was consistently highly

1906   nested within Hyaenodontida, a result consistent with Rana et al. (2015), who also found

1907   *Lahimia* deeply nested in some MPTs. This result might be expected based on the dentition of

1908   *Lahimia* — the lower molar metaconids are subequal in height to the paraconid, unlike taxa such

1909   as *Cimolestes*, *Tinerhodon*, and *Eoproviverra*, which have taller metaconids than paraconids.

1910   The talonid basin of *Lahimia* is also very narrow compared to the trigonid, and reduced

1911   compared to taxa positioned more basally in the analyses presented here. A deeply nested

1912   *Lahimia* nevertheless implies multiple, unsampled ghost lineages of hyaenodontidans reaching

1913   into the earliest Paleocene and Late Cretaceous. In the tip-dating analysis, *Lahimia +*

1914   *Boualitomus* was resolved in a more basal position than it is in standard Bayesian and Parsimony

1915   analysis, supported by a very relatively rapidly evolving branch, though all basal branches

1916   (except the branch supporting the *Sinopa* clade + Hyaenodontidae) are rapidly evolving. These

1917   rapid basal rates are consistent with an explosive radiation of hyaenodontidans during the

1918   Paleocene, and we interpret this to be an adaptive radiation, that may have involved filling

1919   vacant carnivore niche space on multiple continents before evolutionary rates slowed in the early

1920   Eocene, indicative of more stable, occupied niche space (e.g., Simpson, 1953).

1921   One of the clades consistently resolved as more basal than *Lahimia* and *Boualitomus* and

1922   all other Afro-Arabian taxa is Proviverrinae/Hyaenodontinae, a clade supported by rapidly

1923   evolving branches that emerge very early in the evolution of Hyaenodontida. A close relationship

1924   between Hyaenodontinae and some European proviverrines was first demonstrated by Polly

1925   (1996) when *Eurotherium* was resolved as the sister taxon to *Propterodon + Hyaenodon*. Contra

1926   Solé (2013) and Solé, Falconnet & Yves (2014a) who found *Proviverra* and *Eurotherium* were

1927   part of a monophyletic Proviverrinae, Polly (1996) proposed *Proviverra* as the sister taxon to all

1928   more deeply nested hyaenodontidans and *Eurotherium* as closely related to *Propterodon* and

1929   *Hyaenodon*. Rana et al. (2015) were the first to include *Propterodon* and *Hyaenodon* in a

1930   phylogenetic analysis since Polly (1996); they also included many more proviverrines than Polly

1931   (1996) and found a monophyletic, entirely European Proviverrinae as the sister clade to

1932   Hyaenodontinae. *Proviverra* is the most deeply nested proviverrine in their analysis and

1933   *Eurotherium* is also deeply nested. The entire clade Hyaenodontinae + Proviverrinae in Rana et

1934   al. (2015) is deeply nested within Hyaenodontida, with a stem including North American

1935   "sinopanines" and Limnocyoninae, *Arfia*, and possibly *Lahimia* placed even more basally, near

1936   the root of Hyaenodontida. The results presented in this analysis resolve Proviverrinae near the

1937   root of Hyaenodontida (Parsimony and standard Bayesian analysis) or as a paraphyletic group of

1938   stem taxa relative to Hyaenodontinae. *Eoproviverra* is resolved by parsimony and standard

1939   Bayesian analysis as the sister group of all other Hyaenodontida, but is more deeply nested when

1940   evolutionary rates are incorporated into the analysis.

1941   Solé (2013) and Solé, Falconnet & Yves (2014a) proposed multiple clades within

1942   "proviverrines" including Sinopaninae (including *Sinopa*, *Prototomus*, *Tritemnodon*, and

1943   *Galecyon*), Arfianinae (synonymous with the genus *Arfia*), and Proviverrinae. Rana et al. (2015)

1944   did not recover a monophyletic Sinopaninae, instead placing *Prototomus* as a group that is

1945   paraphyletic with respect to all non-arfianine, non-limnocyonine hyaenodontidans; the remaining

1946   "sinopanines" were placed as basal stem members of a Hyaenodontinae + Proviverrinae clade.

1947   None of the methods employed here support a monophyletic Sinopaninae, and the positions of

1948   the "sinopanine" taxa are highly variable depending on the method applied. *Tritemnodon*, a

1949   North American taxon with partially fused upper molar paracones and metacones, and paracones

1950   that are taller than metacones, is placed along the stem of Hyainailouroidea using standard

1951   Bayesian analysis and as a stem hyainailourid (as the sister taxon of *Koholia*) using tip-dating.

1952   The *Galecyon + Gazinocyon* clade occupies more basal positions, in close phylogenetic

1953   proximity to Limnocyoninae. Both Bayesian methods place *Sinopa* in a clade with *Arfia* and

1954   *Prototomus*. In the standard Bayesian analysis, this clade is more closely related to

1955   Hyainailouroidea than to Hyaenodontinae, but tip-dating places *Sinopa*, *Prototomus*, and *Arfia* in

1956   a sister clade relationship with Hyaenodontinae. Clearly these Eocene North American taxa are

1957   vital for understanding the evolution of major radiations of hyaenodontidans and further study of

1958   these taxa is required as demonstrated by Zack & Rose (2015).

1959

1960   **Biogeographic History of Hyaenodontida**

1961   Each topology and each biogeographic method yielded consistent biogeographic origins

1962   for several constituent clades within Hyaenodontida. Proviverrinae/Hyaenodontinae is

1963   unambiguously European in origin and Hyaenodontinae unambiguously originates in Asia.

1964   Across all analyses, Limnocyoninae, *Sinopa*, and the clade *Gazinocyon + Galecyon* originated in

1965   North America. Teratodontinae, Apterodontinae, and derived Hyainailourinae (from the node

1966   shared with *Akhnatenavus*) are unambiguously Afro-Arabian in origin, but the biogeographic

1967   origins of Hyainailouridae and Hyainailouroidea are uncertain. Most significantly, the origin of

1968   Hyaenodontida across all analyses is reconstructed with an ancestral area in either Europe or

1969   North America and an Afro-Arabian origin is not likely for Hyaenodontida using any of the

1970   methods or topologies employed in this analysis. The nodes closest to the root of Hyaenodontida

1971   are weakly supported, but the earliest Afro-Arabian taxon (*Lahimia*) and earliest Asian taxon

1972   (*Prolimnocyon chowi*) are consistently recovered in deeply nested positions. A European or

1973   North American origin of Hyaenodontida is problematic because hyaenodontidans are unknown

1974   in Europe and North America before the Paleocene/Eocene boundary (Gingerich & Deutsch,

1975   1989; Gunnell, 1998; Zack, 2011; Solé, 2013), though, unlike North America, the Paleocene of

1976   Europe is still not well sampled. Tip-dating analysis indicates that the Paleocene was a period of

1977   rapid evolution for Hyaenodontida when many of the major hyaenodontidan clades originated.

1978   This explosive radiation is not fully captured in the fossil record. It also remains the case that

1979   Asia and Afro-Arabia are particularly poorly sampled, with some geological intervals, like the

1980   late Paleocene, only represented by a few, sparse localities (Meng, Zhai & Wyss, 1998; Seiffert,

1981   2010) that may yet yield important fossils for understanding the origins of Hyaenodontida. Asia,

1982   in particular, is situated as a kind of keystone between the other continental areas and very early

1983   dispersals to North America or Europe from Asia may explain the sudden ~~Paleocene/~~Eocene

1984   emergence of the group in the Europe and North America, which shared a connection as

1985   indicated by common hyaenodontidan taxa (*Arfia*, *Galecyon*, *Prototomus*) between the

1986   continents. Another confounding factor in understanding the possible European roots of

1987   Hyaenodontida is the fragmentary biogeography and and geography of Europe during the early

1988   Paleocene and early Eocene with different faunal zones spread across the continent (Hooker,

1989   2010; Solé, 2013; Solé, Falconnet & Yves, 2014a) with unsampled or isolated regions possibly

1990   serving as the center of origin for early Hyaenodontida.

1991   One goal of this study was to test the Afro-Arabian origin hypothesis for Hyaenodontida

1992   advocated by multiple authors (Gingerich & Deutsch, 1989; Gheerbrant et al., 2006; Morlo et al.,

1993   2013; Solé et al., 2014b), which has never been tested using a phylogenetic analysis and explicit

1994   biogeographic method with assumptions defined. The most recent argument for an Afro-Arabian

1995   origin hypothesis was based on the discovery of *Lahimia*, and the assumption that this taxon is

1996   basal within Hyaenodontida or represents an early-diverging clade ("Koholiinae") from

1997   Hyaenodontida (Grohé et al., 2012; Morlo et al., 2013; Solé et al., 2014b). The study by Rana et

1998   al. (2015) and the results presented here do not support *Lahimia* as a particularly basal

1999   hyaenodontidan, but rather as a basal member of the clade that ultimately gave rise to

2000   Hyainailouroidea. Notably, *Lahimia* and *Boualitomus* were consistently recovered at more basal

2001   nodes than Asian "indohyaenodontines," whose placements either within, or basal to,

2002   Hyainailouroidea indicate that they may be critically important for understanding the

2003   biogeographic origins of Hyainailouroidea and its Afro-Arabian sub-clades. Across all

2004   topologies, *Lahimia* and *Boualitomus* represent an independent dispersal to Afro-Arabia from

2005   taxa with North American or European roots.

2006   Multiple dispersal events within Hyainailouridae are required given the topologies

2007   presented here, but the directions of most are not yet clear due to phylogenetic ambiguity at the

2008   base of the clade. All analyses support a dispersal from Afro-Arabia to Europe that led to

2009   *Apterodon gaudryi*. Both Bayesian analyses support a dispersal from Afro-Arabia to Asia to

2010   account for the presence of *Orienspterodon* in Myanmar, and the Bayesian topologies support

2011   four separate dispersals during the middle Eocene from Afro-Arabia to account for the presence

2012   of *Kerberos*, *Paroxyaena*, and *Pterodon dasyuroides* in Europe, and *Hemipsalodon* in North

2013   America. Perhaps the lineage that led to *Hemipsalodon* crossed through Europe, following the

2014   same dispersal pathway used by *Kerberos*, a closely related European taxon; it is also possible,

2015   given the very weak statistical support for the paraphyly of *Hemipsalodon*, *Kerberos*, and

2016   *Pterodon dasyuroides* with respect to Afro-Arabian taxa, that additional material of these species

2017   will reveal that they are in fact a monophyletic radiation derived from a single out-of-Africa

2018   Eocene dispersal.

2019   The biogeographic history of Teratodontinae, Apterodontinae, and Hyainailourinae is

2020   complicated by the differences between the tip-dating topology and the standard Bayesian and

2021   maximum parsimony topologies. Instead of occupying stem positions relative to the Afro-

2022   Arabian clades, the indohyaenodontines are weakly supported as closely related only to

2023   Teratodontinae in the tip-dating tree, implying that the common ancestor of Indohyaenodontinae

2024   dispersed from Afro-Arabia to Asia during the late Paleocene or early Eocene and the ancestor of

2025   *Metasinopa* dispersed from Asia to Afro-Arabia at some point after the late early Eocene (late

2026   Ypresian). Dispersal from Asia to Afro-Arabia during the Ypresian is possible in multiple

2027   mammalian lineages, potentially but not unambiguously including the zegdoumyid-like ancestor

2028   of anomaluroid rodents, the ancestor of caenopithecine adapiform primates, and the ancestor of

2029   more crownward strepsirrhine primates (Seiffert, 2012), though dispersal from Europe is also

2030   possible (see below). If the ancestors of *Metasinopa* and *Orienspterodon* dispersed from Asia

2031   during the middle Eocene this would coincide with the interval when hystricognathous rodents

2032   and anthropoid primates also likely dispersed from Asia to Afro-Arabia, and when the

2033   anomaluroid rodent *Pondaungimys* dispersed from Afro-Arabia to Asia (Sallam et al., 2010;

2034   Seiffert, 2012; Marivaux et al., 2015).

2035   Using BBM, the common node of "Indohyaenodontinae" + Hyainailouroidea is

2036   reconstructed as North American (parsimony; P31), Asian (standard Bayesian, B42), or North

2037   American (tip-dating, T53). These conflicting reconstructions make it difficult to confidently

2038   assert the ultimate origins of these clades, though there is evidence of dispersal between Afro-

2039   Arabia and Europe as initially proposed in early studies of Fayum Hyaenodontida (Andrews,

2040   1904, 1906; Osborn, 1909; Schlosser, 1911). Gheerbrant & Rage (2006) note a minor exchange

2041   event from Europe to Afro-Arabia near the Lutetian/Bartonian boundary that includes

2042   caenopithecine adapiform and anchomomyin primates, and the European origin of African

2043   caenopithecines was supported by the phylogenetic analyses of Seiffert et al. (2015). The

2044   dispersal of the ancestor of *Paroxyaena* from Afro-Arabia to Europe (as supported by both

2045   Bayesian analyses) may have occurred during this interval, following the same dispersal route as

2046   *Kerberos*, *Hemipsalodon*, and *Pterodon dasyuroides*. The successful dispersal of hyainailourines

2047   to Europe and North America from Afro-Arabia during the middle Eocene has interesting

2048   implications for the structure of the hypercarnivorous niche at the time of the dispersal because

2049   the hypercarnivorous niche the was already occupied on both continents by early species of

2050   *Hyaenodon* (Mellet, 1977; Lange-Badré, 1979).

2051   Multiple relationships recovered in the tip-dating analysis support exchange between

2052   North America and Europe near the PETM (Paleocene-Eocene Thermal Maximum), as

2053   suggested by Smith & Smith (2001). The divergence between North American *Pyrocyon* and

2054   European *Preregidens* reaches across the PETM, as does the divergence between *Prototomus*

2055   *minimus* and *Prototomus phobos*, and the divergence of the clade *Arfia*, *Sinopa*, and *Prototomus*

2056   from a node reconstructed with likely European and North American origins (T2). The

2057   connection between North America and Europe during this interval is further supported by the

2058   European species of *Arfia*, *A. gingerichi*, that was not included in this analysis (Smith & Smith,

2059   2001). There is also a species of *Galecyon*, *G. galus,* from Europe (Solé, Falconnet & Yves,

2060   2014a). The *Galecyon* lineage stretches across the PETM and the ancestor of *Galecyon* likely

2061   originated before this interval and dispersed between Europe and North America.

2062   The nodes supporting *Prolimnocyon chowi* and *Sinopa jilinia*, both Asian taxa, are

2063   reconstructed with North American origins, evidence of exchange from North America to Asia

2064   during the late Paleocene and early Eocene. Exchange between Europe and Asia is implied by

2065   the close relationship between Hyaenodontinae, reconstructed with an Asian origin, and

2066   *Oxyaenoides*, reconstructed with a European origin. The West Siberian Sea was a major

2067   epicontinental seaway that separated Europe from Asia, limiting direct fauna exchange between

2068   these continents, but early Eocene exchange likely occurred, as documented in Perissodactyla

2069   (Hooker & Dashzeveg, 2003), Primates (Smith, Rose & Gingerich, 2006), and Rodentia (Badiola

2070   et al., 2009). The ancestor of Hyaenodontinae may have dispersed directly from Europe to Asia

2071   during this interval. Alternatively, Rana et al. (2015) recovered Hyaenodontinae as the sister

2072   clade to a monophyletic Proviverrinae. The stem of this clade includes North American taxa and

2073   Hyaenodontinae is ambiguously resolved with a North American or European origin. Further

2074   analyses will test the sister-taxon relationships to Hyaenodontinae. *Hyaenodon* is resolved with

2075   an Asian origin across all analyses with dispersal to Europe and North America during the late

2076   Eocene, and endemic radiations of the genus occurred after dispersal in Europe (Bastl, Nagel &

2077   Peigné, 2014) and North America (Mellet, 1977).

2078

2079   **The Evolution of Hypercarnivory within Hyaenodontida**

2080   The dental specializations of hyaenodontidans — such as extended postparacristids and

2081   preprotocristids, elongate metastyles, and buccolingually compressed metacones — indicate that

2082   the group was adapted, like modern carnivorans, to a primarily faunivorous diet (Van

2083　Valkenburgh, 1999). But just as some lineages of carnivorans are more dentally specialized for

2084　carnivory than others, so too were some lineages of hyaenodontidans. Hypercarnivory in modern

2085　carnivores is used to refer to animals that acquire 70% or more of their calories from meat, in

2086　contrast to generalist carnivores, which eat 50%–60% meat and complete the diet with plant

2087　matter and invertebrates (Van Valkenburgh, 1988, 1989). Dental adaptations correlate with the

2088　dietary shift from generalist to hypercarnivore, including the mesiodistal lengthening of the

2089　carnassial complex, reduction and simplification of the talonid, reduction of the protocone, and

2090　loss of the metaconid (Holliday, 2010).

2091　　　　The first attempts to classify subgroups within Hyaenodontida were based on the degree

2092　of specialization in the dentition, particularly in the morphological specialization of the

2093　carnassial complex. "Proviverrinae" contained the less dentally specialized, or generalist taxa,

2094　and "Hyaenodontinae" contained the more specialized, hypercarnivorous taxa (Matthew, 1909,

2095　1915). The distinction between "Proviverrinae," the hyaenodontidans with prominent metaconids

2096　and unfused paracones and metacones, and "Hyaenodontinae," the hyaenodontidans with no

2097　metaconids and fused paracones and metacones, was utilized through most of the 20th century

2098　(Matthes, 1952; Savage, 1965; Van Valen, 1965; Barry, 1988). In this scheme, *Pterodon* and

2099　*Hyaenodon* were closely related based on their hypercarnivorous dentition (Barry, 1988). The

2100　genus *Pterodon* was defined by a groove between the paracone and metacone while *Hyaenodon*

2101　was recognized by its apparent fusion of these cusps (Savage, 1965). The arrangement caused

2102　some debate over how to classify taxa that did not neatly fit the dichotomy, like *Apterodon,*

2103　which has a reduced metaconid but separated paracones and metacones (Van Valen, 1965;

2104　Szalay, 1967) and *Dissopsalis*, which has long, sectorial metastyles and metacones but retains

2105　the metaconid on M_2 and has a paracone that is reduced and not entirely fused to the metacone

2106   (Barry, 1988). Using cranial and postcranial characters, Polly (1996) demonstrated that

2107   *Hyaenodon* and *Pterodon* evolved specialized, hypercarnivorous shearing dentition (lost the

2108   metaconid and fused the paracone and metacone) independent of one another, and each lineage

2109   arose from separate "proviverrine" ancestors. In Polly (1996), *Dissopsalis* is the sister taxon to

2110   Hyainailourinae, with its elongate metastyle and prominent metacone reflecting the possible

2111   ancestral condition that led to the fused paracone and metacone of *Pterodon*, while *Eurotherium*

2112   is the sister taxon to *Propterodon* + Hyaenodontinae, with its divergent paracone and metacone

2113   possibly reflecting the ancestral morphology of its sister clade. Solé et al. (2015) detailed

2114   additional cranial features that distinguish Hyainailourinae from Hyaenodontinae, further

2115   emphasizing the ancient divergence of the two lineages with specialized, or hypercarnivorous

2116   dentition. With the separate origins of *Hyaenodon* and *Pterodon* supported by the present study

2117   and by Rana et al. (2015), the morphology of the carnassial complex in each lineage is worthy of

2118   reexamination.

2119   Originally, the dental adaptations of *Pterodon* and *Hyaenodon* were assumed to be part of

2120   an evolutionary sequence. *Pterodon*, with incompletely fused paracones and metacones, was

2121   viewed as the ancestral condition for *Hyaenodon* (Matthew 1915; Van Valen, 1967), which

2122   completely fused the paracone and metacone. However, carnivorous mammals have not adapted

2123   to hypercarnivory in the exact same way in every lineage that has evolved specialized shearing

2124   dentition, particularly in the arrangement of the metacone and paracone. Furthermore, with the

2125   establishment of Hyainailourinae and Hyaenodontinae as functionally convergent clades, it is

2126   possible to recognize that these two lineages converged on hypercarnivory through

2127   fundamentally different arrangements of the paracone, metacone, and metastyle, which in turn

2128   affects the occlusal morphology of the lower molars.

2129   In Carnivora the carnassial complex is formed between P^4 and M_1. The upper carnassial

2130   blade stretches between the elongate metastyle of P^4 and the buccolingually compressed

2131   postparacrista. This differs from the arrangement of the carnassials in carnivorous metatherians,

2132   which adapted the tricuspate molars into the upper carnassial rather than the bicuspate premolars.

2133   Borhyaenoid metatherians were the dominant carnivores in South America from the Paleocene

2134   through the Pliocene (Rose, 2006), and, like hyaenodontidans, borhyaenoids formed a shearing

2135   carnassial complex between multiple upper and lower molars rather than one carnassial complex

2136   between a premolar and molar as in Carnivora. In borhyaenoids (i.e., Miocene *Pseudolycopsis*

2137   and *Lycopsis*) the upper carnassial is formed through mesiodistal elongation of the metacone and

2138   metastyle rather than the paracone and metastyle as in carnivorans (Van Valen, 1967; Muizon &

2139   Lange-Badré, 1997). The paracone apex in borhyaenoids is distinct from the metacone, and

2140   much shorter than the taller shearing metacone. Borhyaenoids are not closely related to

2141   Dasyuromorphia, the Australian radiation of carnivorous marsupials that includes *Thylacinus*,

2142   but dasyuromorphians converged on the same shearing morphology as borhyaenoids. In

2143   Dasyuromorphia the paracone is retained as a distinct, reduced cusp and the metacone is

2144   mesiodistally elongate and buccolingually compressed, forming the tallest cusp of the trigon. The

2145   postmetacrista is sharp and slopes to meet the sectorial metastyle. This borhyaenoid and

2146   dasyuromorphian-style carnassial, with an augmented metacone and reduced paracone, is the

2147   same carnassial arrangement exhibited by many hyaenodontidans, including *Hyaenodon*,

2148   *Eurotherium*, *Dissopsalis*, and *Brychotherium* (Fig. 23). *Hyaenodon* differs from *Eurotherium*,

2149   *Dissopsalis*, and *Brychotherium* in the degree of fusion between the paracone and metacone. In

2150   *Hyaenodon*, the paracone is a small, vestigial structure that fuses to the mesial metacone.

2151   *Hyaenodon* upper molars are often heavily worn but, in recently erupted M^1, the distinct, small

2152   paracone is easily distinguished and it is even more evident in dP^4. The paracone typically forms

2153   a small ridge on the mesial surface of M^2 though it is easily worn away. *Eurotherium*, a middle

2154   Eocene taxon in the Proviverrinae/Hyaenodontinae clade, represents the likely ancestral

2155   morphology of the upper dentition of *Hyaenodon*, with the metacone more mesiodistally

2156   elongate and taller than the paracone. *Oxyaenoides* is the sister taxon to Hyaenodontinae and it

2157   also has a derived hypercarnivorous dentition with a tall metacone and extended metastyle. In

2158   *Eurotherium*, *Oxyaenoides*, and *Hyaenodon*, the paracone apex parallels the metacone apex,

2159   pointing ventrally. The arrangement of the upper molar carnassial cusps differs from the likely

2160   ancestral condition of the upper dentition, exemplified by *Proviverra* in Fig. 23. In *Proviverra*,

2161   the paracone and metacone are subequal in height and not buccolingually compressed. Rana et

2162   al. (2015) resolved Proviverrinae as the sister clade to Hyaenodontinae. In this scenario,

2163   metacone-dominated hypercarnivorous carnassials are convergent in Hyaenodontinae and in

2164   Proviverrinae.

2165   The arrangement of the paracone and metacone are fundamentally different in

2166   Hyainailourinae. Instead of the metacone forming the tallest piercing cusp, the paracone is the

2167   tallest cusp, and this arrangement is exemplified by *Pterodon dasyuroides* and *Akhnatenavus* in

2168   Fig. 23. Muizon & Lange-Badré (1997) noted the difference in paracone height in *Hyaenodon*

2169   and *Pterodon* but they did not place the distinction into a larger phylogenetic context. In

2170   hyainailourines, the metacone is fused to the distal face of the paracone. The postmetacrista

2171   becomes homologous to the P^4 postparacrista in Carnivora. The paracone is also the tallest cusp

2172   of the trigon in *Tritemnodon*, an early Eocene taxon from North America and, based on the

2173   results of this analysis, probably part of the clade that includes Apterodontinae and

2174   Hyainailourinae. The trigons of *Tritemnodon* differ from those of *Pterodon* and *Akhnatenavus* by

2175   retaining a distinct apex on the metacone and a wider notch between the metacone and paracone.

2176   This arrangement represents the likely ancestral condition to the hyainailourine carnassial

2177   complex. Apterodontinae shares a taller paracone than metacone with Hyainailourinae.

2178   Teratodontinae was consistently recovered in this study as part of the sister clade to the

2179   Apterodontinae and Hyainailourine. However, the dentition of Teratodontinae is arranged more

2180   like the dentition of borhyaenoids and derived proviverrines/hyaenodontines than it is like

2181   hyainailourines. In *Brychotherium* the metacone is slightly taller than the paracone and the

2182   metacone more mesiodistally elongate than the paracone. In *Dissopsalis* the metacone is much

2183   taller and more elongate than the tiny paracone, which points slightly mesially rather than

2184   directly perpendicular to the alveolar plane. The recovery of *Dissopsalis* as part of a separate

2185   clade from Hyainailourinae differs from Polly (1996) whose topology recovered a sister-taxon

2186   relationship between *Dissopsalis* and Hyainailourinae. The topologies presented in this study

2187   imply that *Dissopsalis* provides evidence for yet another (third) convergence upon specialized

2188   hypercarnivory in Hyaenodontida.

2189   The different arrangements of the upper carnassial influence the morphology of the

2190   trigonid on the lower molars. In Hyaenodontinae, the paraconid is almost mesial to the

2191   protoconid and the postparacristid and preprotocristid are nearly parallel to the mandibular

2192   corpus, reflecting the morphology of the postmetacrista and metastyle, which nearly parallel the

2193   alveolar margin. In Hyainailourinae, the paraconid is set lingual relative to the protoconid, giving

2194   the postparacristid and preprotocristid carnassial an oblique shearing angle relative to the

2195   mandibular corpus. This trigonid arrangement shears past a postmetacrista that is slightly

2196   lingually inflected at the carnassial notch, accommodating the wide base of the paracone.

2197   Through biogeographic analysis and tip-dating analysis, the evolution of hypercarnivory

2198   in Hyaenodontinae, Proviverrinae, Hyainailourinae, and Teratodontinae can be reconstructed in

2199   place and time. These conclusions are a preliminary discussion of evolutionary trends inferred

2200   from this novel topology, and more detailed ancestral state reconstructions based on dental

2201   morphology would be an appropriate direction for future studies. Solé, Falconnet & Yves

2202   (2014a) observed a general increase in body size and dental specialization in Proviverrinae

2203   through the Eocene, a trend supported by this analysis, which recovers the clade that includes

2204   *Eurotherium* as European in origin and dentally specialized like Hyaenodontinae.

2205   Hyaenodontinae is even more specialized than *Eurotherium*, and likely originated in Asia during

2206   the early Eocene. Then the hypercarnivorous *Hyaenodon* dispersed from Asia to Europe and

2207   North America where endemic radiations occurred (Mellet, 1977; Bastl, Nagel & Peigné, 2014).

2208   Hyainailourinae likely originated in Afro-Arabia and the carnassial morphology dominated by

2209   the paracone rather than the metacone also likely originated in Afro-Arabia. Hypercarnivory

2210   evolved a second time in Afro-Arabia in the lineage that lead to *Dissopsalis* and *Anasinopa*,

2211   which both possess carnassials dominated by metacones that were taller than paracones. Given

2212   the time-calibrated tip-dating topology, this lineage diverged from *Masrasector*, a less dentally

2213   specialized taxon, during the late Eocene, and *Dissopsalis* diverged from *Anasinopa*, a less-

2214   specialized carnivore, during the late Oligocene. *Dissopsalis* is at the end of the most rapidly

2215   evolving branch of any hyaenodontidan taxon in the Oligocene or Miocene at 1.34% change/Ma

2216   (followed by *Quasiapterodon* at 1.13% change/Ma and *Isohyaenodon* at 1.03% change/Ma). The

2217   increased rate of morphological change in *Dissopsalis* is expected to have slightly predated, or

2218   coincided with, the arrival of Carnivora in Afro-Arabia. This may reflect a general trend to

2219   hypercarnivory that left generalist niche space open for the earliest carnivoran immigrants like

2220   amphicyonids and the ancestors of *Mioprionodon* to exploit (Rasmussen & Gutierrez, 2009), or

2221   rapid morphological change through the evolution of *Dissopsalis* may reflect niche specialization

2222   in carnivores as immigrant taxa crowded the carnivorous niche (Van Valkenburgh, Wang &

2223   Damuth, 2004). The last-surviving hyaenodontidans of the Miocene — *Isohyaenodon*,

2224   *Megistotherium*, and *Dissopsalis* — were each highly specialized carnivores, and each lineage

2225   may have been ecologically vulnerable to extinction as an apex carnivore (Van Valkenburgh,

2226   2007) and morphologically unable to explore novel morphospace with such specialized

2227   dentitions, as demonstrated in studies that examine the ecological and morphological flexibility

2228   of hypercarnivores and their generalist sister taxa (Holliday & Steppan, 2004; Holliday, 2010).

2229   These data can now be used to explore the timing and the ecological context of hypercarnivorous

2230   specialization in Hyaenodontida across four continents and can be compared to the timing and

2231   location of dental specialization in the other Paleogene carnivore lineages, such as Oxyaenida,

2232   Carnivoramorpha, and Mesonychia.

2233

2234   CONCLUSIONS

2235

2236   The character-taxon matrix utilized for this analysis sampled from each hyaenodontidan

2237   lineage that has been proposed, both to place the newly described latest Eocene species

2238   *Brychotherium ephalmos* and *Akhnatenavus nefertiticyon* in a phylogenetic context, and to

2239   rigorously test the hypothesis that Hyaenodontida first arose in Afro-Arabia. All three

2240   phylogenetic methods used here supported the monophyly of the clades Apterodontinae,

2241   Hyainailourinae, Limnocyoninae, *Galecyon + Gazinocyon*, as well as the clade that includes

2242   Hyaenodontinae and some European "proviverrines" (sensu Solé, 2013). Teratodontinae was not

2243   recovered in every MPT, but is supported by a majority of them and in both the standard

2244   Bayesian and Bayesian tip-dating analyses. *B. ephalmos* is one of the most completely known

2245   teratodontines, and is either deeply nested with Miocene taxa (parsimony and standard Bayesian

2246   results) or is a basal form that branched off from other teratodontines in the middle Eocene (tip-

2247   dating results). *Akhnatenavus* is resolved by all methods as a basal member of a hyainailourine

2248   clade that also includes Oligocene African *"Pterodon"* and younger Miocene hyainailourines.

2249   All analyses also recovered the origin of Hyaenodontida as having occurred on northern

2250   continents, either Europe or North America. Proviverrinae/Hyaenodontinae is consistently

2251   recovered as an early-diverging branch with European origins. The earliest diverging nodes in

2252   Hyaenodontida also include largely North American clades like *Arfia* and Limnocyoninae. A

2253   hyaenodontidan origin in Europe or North America is problematic as the group is not known on

2254   those landmasses before the PETM, but Asia and Afro-Arabia, both of which have poor

2255   Paleocene records and as such have repeatedly been envisioned as the likely home of as-yet

2256   unsampled Paleocene hyaenodontidan ghost lineages, have no support as continents of origin

2257   based on the branching patterns recovered here. The presence of *Lahimia* in the middle

2258   Paleocene of Africa, and *Tinerhodon* in the late Paleocene, are intriguing evidence of early Afro-

2259   Arabian hyaenodontidan diversity in Afro-Arabia, but neither is resolved as a sister group of all

2260   other hyaenodontidans, or in a basal enough position to influence the geographic reconstruction

2261   for the hyaenodontidan root node.

2262   Even with more Paleocene fossils from Asia and Afro-Arabia, tip-dating analysis implies

2263   that the early evolutionary history of Hyaenodontida was an explosive adaptive radiation and,

2264   without more compelling evidence for the basal branching sequence in the group, it may be

2265   difficult to identify the exact geographic origin of the clade with any confidence. The early

2266   evolution of Hyaenodontida apparently echoed the larger-scale trend of K/Pg radiations in

2267   mammals (Beck & Lee, 2014) and birds (Lee et al., 2014) in which rapid morphological change

2268   occurred over a short period of geological time, potentially leaving little or no time for the

2269   accumulation of morphological synapomorphies that might otherwise support basal branches.

2270   This rapid period of early radiation led to the establishment of endemic clades on different

2271   continents. The early biogeographic history of the group is difficult to unravel, but once the

2272   major clades were established, there appears to have been little large-scale exchange of taxa

2273   between continents. Immediately after the PETM there were genera common to North America

2274   and Europe, but these shared genera did not persist in Europe, and Solé, Falconnet & Yves

2275   (2014a) demonstrated that endemic European proviverrines occupied vacant niche space left by

2276   genera common to both continents. Dispersal was apparently most likely during the middle and

2277   late Paleocene, then only occurred sporadically through the Eocene, mostly as pulses between

2278   Afro-Arabia and the northern continents in Hyainailourinae and Apterodontinae. No proviverrine

2279   is known to have dispersed from Europe to North America, Afro-Arabia, or Asia. Teratodontines

2280   and indohyaenodontines were limited to Afro-Arabia and Asia. Limnocyoninae is a North

2281   American clade that dispersed into Asia during the late Paleocene. On each of these continents,

2282   different lineages adapted to different carnivorous niches, and hypercarnivory emerged

2283   independently at least once in Eurasia and twice in Afro-Arabia.

2284   Description of the new taxa *Brychotherium ephalmos* and *Akhnatenavus nefertiticyon*

2285   increases the diversity of the Fayum carnivore fauna and further expands the total faunal

2286   diversity of the Afro-Arabia before the continent established a filtered contact with Eurasia

2287   through the late Oligocene and early Miocene. Better documentation of endemic clades like

2288   Hyainailourinae and Teratodontinae is necessary to understand the ecological context that the

2289   earliest Eurasian immigrant carnivorans encountered. Only with a detailed understanding of the

2290   early evolution of Hyaenodontida in Afro-Arabia is it possible to assess the ecological factors

2291   that may have led to the ultimate extinction of this widespread and morphologically diverse

2292   group of carnivores.

2293

2294   ACKNOWLEDGEMENTS

2295

2316

2317   LITERATURE CITED

2318

2319   Andrews CW. 1904. Further notes on the mammals of the Eocene of Egypt. *Geological*
2320   *Magazine* 5:109–115 and 157–162. DOI: http://dx.doi.org/10.1017/S001675680012343X.
2321
2322   Andrews CW. 1906. *A descriptive catalogue of the Tertiary Vertebrata of the Fayum, Egypt*.
2323   London: British Museum of Natural History. DOI: http://dx.doi.org/10.5962/bhl.title.55134.
2324
2325   Archibald JK, Mort ME, Crawford DJ. 2003. Bayesian inference of phylogeny: a non-technical
2326   primer. *Taxon* 52:187–191.
2327
2328   Arcila D, Pyron RA, Tyler JC, Ortí G, Betancur-R R. 2015. An evaluation of fossil tip-dating
2329   versus node-age calibrations in tetraodontiform fishes (Teleostei: Percomorphaceae). *Molecular*
2330   *Phylogenetics and Evolution* 82:131–145. DOI: 10.1016/j.ympev.2014.10.011.
2331
2332   Badiola A, Checa L, Curesta MA, Quer R, Hooker JJ, Astibia H. 2009. The role of new Iberian
2333   finds in understanding European Eocene mammalian paleobiogeography. *Geological Acta*
2334   7:243–258. DOI: 10.1344/105.000000281.
2335
2336   Barry JC. 1988. *Dissopsalis*, a middle and late Miocene proviverrine creodont (Mammalia) from
2337   Pakistan and Kenya. *Journal of Vertebrate Paleontology* 8:25–45. DOI:
2338   10.1080/02724634.1988.10011682.
2339
2340   Bastl K, Nagel D, Peigné S. 2014. Milk tooth morphology of small-sized *Hyaenodon*
2341   (Hyaenodontidae, Mammalia) from the European Oligocene — evidence of a *Hyaenodon* lineage
2342   in Europe. *Palaeontographica, Abt. A: Palaeozoology - Stratigraphy* 303:61–84.
2343   DOI: 10.1127/pala/303/2014/61.
2344
2345   Beck RMD, Lee MSY. 2014. Ancient dates or accelerated rates? Morphological clocks and the
2346   antiquity of placental mammals. *Proceedings of the Royal Society B* 281:20141278. DOI:
2347   10.1098/rspb.2014.1278.
2348

2349 Bown TM, Kraus MJ. 1988. Geology and paleoenvironment of the Oligocene Jebel Qatrani
2350 Formation and adjacent rocks, Fayum Depression, Egypt. *U. S. Geological Survey Professional*
2351 *Paper* 1452:1–64. DOI: http://pubs.er.usgs.gov/publication/pp1452
2352
2353 Bremer K. 1994. Branch support and tree stability. *Cladistics* 10:295–304. DOI: 10.1111/j.1096-
2354 0031.1994.tb00179.x.
2355
2356 Brooks DR. 1990. Parsimony analysis in historical biogeography and coevolution:
2357 methodological and theoretical update. *Systematic Biology* 39:14–30. DOI: 10.2307/2992205.
2358
2359 Clarke JA, Middleton KM. 2008. Mosaicism, modules, and the evolution of birds: results from a
2360 Bayesian approach to the study of morphological evolution using discrete character data.
2361 *Systematic Biology* 57:185–201. DOI: 10.1080/10635150802022231.
2362
2363 Close RA, Friedman M, Lloyd GT, Benson RBJ. 2015. Evidence for a Mid-Jurassic adaptive
2364 radiation in mammals. *Current Biology* 25.1–6. DOI:
2365 http://dx.doi.org/10.1016/j.cub.2015.06.047
2366
2367 Colbert EH. 1933. The skull of *Dissopsalis carnifex* Pilgrim, a Miocene creodont from India.
2368 *American Museum Novitates* 603:1–8.
2369
2370 Cope ED. 1875. Systematic catalogue of Vertebrata of the Eocene of New Mexico, collected in
2371 1874. *Geographical Explorations and Surveys West of the 100th Meridian* 4:37–282. DOI:
2372 http://dx.doi.org/10.5962/bhl.title.104563.
2373
2374 Cope ED. 1884. The Creodonta. *American Naturalist* 18:255–267, 344–353, 478–485. DOI:
2375 10.1086/273635.
2376
2377 Crochet J-Y. 1988. Le plus ancien créodonte africain: *Koholia atlasense* nov. gen., nov. sp.
2378 (Eocène inférieur d'El Kohol, Atlas saharien, Algérie). *Comptes Rendus de l'Académie des*
2379 *Sciences, Paris, Série II* 307:1795–1798.
2380
2381 Dembo M, Matzke NJ, Mooers AØ, Collard M. 2015. Bayesian analysis of a morphological
2382 supermatrix sheds light on controversial fossil hominin relationships. *Proceedings of the Royal*
2383 *Society B* 282:20150943. DOI: http://dx.doi.org/10.1098/rspb.2015.0943.
2384
2385 Egi N, Tsubamoto T, Takai M. 2007. Systematic status of Asian "*Pterodon*" and early evolution
2386 of hyaenaelurine hyaenodontid creodonts. *Journal of Paleontology* 81:770–778. DOI:
2387 DOI: http://dx.doi.org/10.1666/pleo0022-3360(2007)081[0770:SSOAPA]2.0.CO;2.
2388
2389
2390 Egi N, Holroyd PA, Tsubamoto T, Soe AN, Takai M, Ciochon RL. 2005. Proviverrine
2391 hyaenodontids (Creodonta: Mammalia) from the Eocene of Myanmar and a phylogenetic
2392 analysis of the proviverrines from the para-Tethys area. *Journal of Systematic Palaeontology*
2393 3:337–358. DOI: 10.1017/S1477201905001707
2394

2395 Felsenstein J. 1978. Cases in which parsimony and compatibility methods will be positively
2396 misleading. *Systematic Zoology* 27:401–410. DOI: 10.1093/sysbio/27.4.401.
2397
2398 Felsenstein J. 1985. Confidence limits on phylogenies: an approach using the bootstrap.
2399 *Evolution* 39:783–791. DOI: 10.2307/2408678.
2400
2401 Finarelli JA, Flynn JJ. 2009. Brain-size evolution and sociality in Carnivora. *Proceedings of the
2402 National Academy of Sciences, U.S.A.* 106:9345–9349. DOI: 10.1073/pnas.0901780106.
2403
2404 Friscia A, Van Valkenburgh B. 2010. Ecomorphology of North American Eocene carnivores:
2405 evidence for competition between carnivorans and creodonts. In: Goswami A, Friscia A, eds.
2406 *Carnivoran Evolution: New Views on Phylogeny, Form, and Function.* Cambridge: Cambridge
2407 University Press, 311–241. DOI: 10.1017/CB09781139193436.012.
2408
2409 Gaina C, Torsvik TH, van Hinsbergen DJJ, Medvedev S, Werner SC, Labails C. 2013. The
2410 African plate: a history of oceanic crust accretion and subduction since the Jurassic.
2411 *Tectonophysics* 604:4–25. DOI: 10.1016/j.tecto.2013.05.037.
2412
2413 Gheerbrant E, Rage J-C. 2006. Paleobiogeography of Africa: how distinct from Gondwana and
2414 Laurasia? *Paleogeography, Paleoclimatology, Palaeoecology* 241:224–246. DOI:
2415 10.1016/j.palaeo.2006.03.016.
2416
2417 Gheerbrant E, Iarochene M, Amaghzaz M, Bouya B. 2006. Early African hyaenodontid
2418 mammals and their bearing on the origin of the Creodonta. *Geological Magazine* 143:475–489.
2419 DOI: 10.1017/S0016756806002032.
2420
2421 Gingerich PD, Deutsch HA. 1989. Systematics and evolution of early Eocene Hyaenodontidae
2422 (Mammalia, Creodonta) in the Clarks Fork Basin, Wyoming. *Contributions from the Museum of
2423 Paleontology, The University of Michigan* 27:327–391.DOI:
2424 http://hdl.handle.net/2027.42/48535.
2425
2426 Godinot, M. 1981. Les mammiféres de Rians (Éocéne inférieur, Provence). *Palaeovertebrata*
2427 10:43–126.
2428
2429 Goloboff PA, Farris JS, Nixon KC. 2008. TNT, a free program for phylogenetic analysis.
2430 *Cladistics* 24:774–786. DOI: 10.1111/j.1096-0031.2008.00217.x
2431
2432 Gorscak E, O'Connor PM. 2016. Time-calibrated models support congruency between
2433 Cretaceous continental rifting and titanosaurian evolutionary history. *Biology Letters*
2434 12:20151047. DOI: 10.1098/rsbl.2015.1047
2435
2436 Grohé C, Morlo M, Chaimanee Y, Blondel C, Coster P, Valentin X, Salem M, Bilal AA, Jaeger
2437 J-J, Brunet M. 2012. New Apterodontinae (Hyaenodontida) from the Eocene locality of Dur At-
2438 Talah (Libya): systematic, paleoecological and phylogenetical implications. *PLOS ONE*
2439 7(11):e49054. DOI: 10.1371/journal.pone.0049054.
2440

2441 Gunnell GF. 1998. Creodonta. In: Janis CM, Scott KM, Jacobs LL, eds. *Evolution of the Tertiary*
2442 *Mammals of North America. Volume 1: Terrestrial Carnivores, Ungulates, and Ungulate like*
2443 *Mammals*. Cambridge: Cambridge University Press, 91–109.
2444
2445 Gunnell GF, Gingerich PD. 1991. Systematics and evolution of late Paleocene and early Eocene
2446 Oxyaenidae (Mammalia, Creodonta) in the Clarks Fork Basin, Wyoming. *Contributions from*
2447 *the Museum of Paleontology, The University of Michigan* 28:141–180.
2448
2449 Gunnell GF, Seiffert ER, Simons EL. 2008. New bats (Mammalia: Chiroptera) from the late
2450 Eocene and early Oligocene, Fayum Depression, Egypt. *Journal of Vertebrate Paleontology*
2451 28:1–11. DOI: 10.1671/0272-4634(2008)28[1:NBMCFT]2.0.CO;2
2452
2453 Halliday TJD, Upchurch P, Goswami A. 2015. Resolving the relationships of Paleocene
2454 placental mammals. *Biological Reviews*. DOI: 10.1111/brv.12242
2455
2456 Holliday JA. 2010. Evolution of Carnivora: identifying a morphological bias. In: Goswami A,
2457 Friscia A, eds. *Carnivoran Evolution: New Views on Phylogeny, Form, and Function*.
2458 Cambridge: Cambridge University Press, 189–224. DOI:
2459 http://dx.doi.org/10.1017/CBO9781139193436.008.
2460
2461
2462 Holliday JA, Steppan SJ. 2004. Evolution of hypercarnivory: the effect of specialization on
2463 morphological and taxonomic diversity. *Paleobiology* 30:108–128. DOI: 10.1666/0094-
2464 8373(2004)030<0108:EOHTEO>2.0.CO;2
2465
2466 Holroyd PA. 1994. An examination of dispersal origins of Fayum Mammalia. Ph.D. dissertation,
2467 Duke University.
2468
2469 Holroyd PA. 1999. New Pterodontinae (Creodonta: Hyaenodontidae) from the late Eocene–early
2470 Oligocene Jebel Qatrani Formation, Fayum Province, Egypt. *PaleoBios* 19(2):1–18.
2471
2472 Hooker JJ. 2010. The mammal fauna of the early Eocene Blackheath Formation of Abbey Wood,
2473 London. *Monograph of the Palaeontographical Society, London* 165:1–162.
2474
2475 Hooker JJ, Dashzeveg D. 2003. Evidence for direct mammalian faunal interchange between
2476 Europe and Asian near the Paleocene–Eocene boundary. *Geological Society of America Special*
2477 *Paper* 369:479–500. DOI: 10.1130/0-8137-2369-8.479.
2478
2479 Huelsenbeck JP, Larget B, Miller RE, Ronquist F. 2002. Potential application and pitfalls of
2480 Bayesian inference of phylogeny. *Systematic Biology* 51:673–688.
2481 DOI: 10.1080/10635150290102366
2482
2483 Ji Q, Luo Z-X, Yuan C-X, Wible JR, Zhang J-P, Georgi JA. 2002. The earliest known eutherian
2484 mammal. *Nature* 416:816–822. doi:10.1038/416816a.
2485

2486 Kappelman J, Simons EL, Swisher III CC. 1992. New age determinations for the Eocene–
2487 Oligocene boundary sediments in the Fayum Depression, northern Egypt. *Journal of Geology*
2488 100:647–668. DOI: 10.1086/629619.
2489
2490 Kearney M, Clark JM. 2003. Problems due to missing data in phylogenetic analyses including
2491 fossils: a critical review. *Journal of Vertebrate Paleontology* 23:263–274. DOI: 10.1671/0272-
2492 4634(2003)023[0263:PDTMDI]2.0.CO;2.
2493
2494 Kielan-Jaworowska Z, Cifelli RL, Luo Z-X. 2004. *Mammals from the Age of Dinosaurs*. New
2495 York: Columbia University Press.
2496
2497 Kocsis L, Gheerbrant E, Mouflih M, Capetta H, Yans J, Amaghzaz M. 2014. Comprehensive
2498 stable isotope investigation of marine biogenic apatite from the late Cretaceous–early Eocene
2499 phosphate series of Morocco. *Palaeogeography, Palaeoclimatology, Palaeoecology* 394:74–78.
2500 DOI: 10.1016/j.palaeo.2013.11.002.
2501
2502 Lange-Badré B. 1979. Les créodontes (Mammalia) d'Europe occidentale de l'Éocène supérieur à
2503 l'Oligocène supérieur. *Mémoires du Muséum National d'Histoire Naturelle* 42:1–249.
2504
2505 Lavrov AV. 2007. A new species of *Paroxyaena* (Hyaenodontidae, Creodonta) from
2506 Phosphorites of Quercy, Late Eocene, France. *Paleontological Journal* 41:298–311. DOI:
2507 10.1134/S0031030107040144.
2508
2509 Lee M, Cau A, Naish D, Dyke GJ. 2014. Morphological clocks in paleontology, and a mid-
2510 Cretaceous origin of crown Aves. *Systematic Biology* 63:442–449. DOI: 10.1093/sysbio/syt110.
2511
2512 Lepage T, Bryant D, Philippe H, Lartillot N. 2007. A general comparison of relaxed molecular
2513 clock models. *Molecular Biology and Evolution* 24:2669–2680. DOI: 10.1093/molbev/msm193.
2514
2515 Lewis ME, Morlo M. 2010. Creodonta. In: Werdelin L, Sanders W, eds. *Cenozoic Mammals of*
2516 *Africa*. Berkeley: University of California Press, 543–560.
2517
2518 Lewis PO. 2001. A likelihood approach to estimating phylogeny from discrete morphological
2519 character data. *Systematic Biology* 50:913–925. DOI: 10.1080/106351501753462876.
2520
2521 Lillegraven JA. 1969. Latest Cretaceous mammals of upper part of the Edmonton Formation of
2522 Alberta, Canada, and review of marsupial–placental dichotomy in mammalian evolution.
2523 *Paleontological Contribution of the University of Kansas* 50:1–122.
2524
2525 Maddison WP, Maddison DR. 2015. Mesquite: a modular system for evolutionary analysis 3.03.
2526
2527 Marivaux L, Essid E, Marzougui W, Ammar HK, Merzeraud, Tabuce GR, Vianey-Liaud M.
2528 2015. The early evolutionary history of anomaluroid rodents in Africa: new dental remains of a
2529 zegdoumyid (Zegdoumyidae, Anomaluroidea) from the Eocene of Tunisia. *Zoologica Scripta*
2530 44:117–134. DOI: 10.1111/zsc.12095.
2531

2532   Matthes HW. 1952. Die Creodontier aus der mitteleozänen Braunkohle des Geiseltales.
2533   *Hallesches Jahrbuch für Mitteldeutsche Erdgeschichte* 1:201–240.
2534
2535   Matthew WD. 1901. Additional observations on Creodonta. *Bulletin of the American Museum of*
2536   *Natural History* 14:1–38. URI: http://hdl.handle.net/2246/1542.
2537
2538   Matthew WD. 1906. The osteology of *Sinopa*, a creodont mammal of the middle Eocene.
2539   *Memoirs of the American Museum of Natural History* 9:291–576. DOI:
2540   http://dx.doi.org/10.5479/si.00963801.30-1449.203.
2541
2542   Matthew WD. 1909. The Carnivora and Insectivora of the Bridger Basin, middle Eocene.
2543   *Memoirs of the American Museum of Natural History* 9:291–576. URI:
2544   http://hdl.handle.net/2246/5744.
2545
2546   Matthew WD. 1915. A revision of the lower Eocene Wasatch and Wind River faunas, Part 1,
2547   Order Ferae (Carnivora), suborder Creodonta. *Bulletin of the American Museum of Natural*
2548   *History* 34:4–103.
2549
2550   McKenna MC, Bell SK. 1997. *Classification of Mammals above the Species Level*. New York:
2551   Colombia University Press.
2552
2553   Mellett JS. 1969. A skull of *Hemipsalodon* (Mammalia, Deltatheridia) from the Clarno
2554   Formation of Oregon. *American Museum Novitates* 387:1–19. URI:
2555   http://hdl.handle.net/2246/2597.
2556
2557   Mellett JS. 1977. Paleobiology of North American *Hyaenodon* (Mammalia, Creodonta).
2558   *Contributions to Vertebrate Evolution* 1:1–134.
2559
2560   Meng J, Zhai R, Wyss AR. 1998. The late Paleocene Bayan Ulan fauna of inner Mongolia,
2561   China. In: Beard KC, Dawson MR, eds. *Dawn of the Age of Mammals in Asia*. Pittsburgh:
2562   Bulletin of Carnegie Museum of Natural History, 148–185.
2563
2564   Miller KG, Browning JV, Aubry M-P, Wade BS, Katz ME, Kulpecz AA, Wright JD. 2008.
2565   Eocene–Oligocene global climate and sea-level changes: St. Stephens Quarry, Alabama.
2566   *Geological Society of America Bulletin* 120:34–53. DOI: 10.1130/B26105.1.
2567
2568   Miller MA, Pfeiffer W, Schwartz T. 2010. Creating the CIPRES Science Gateway for inference
2569   of large phylogenetic trees. In: *Proceedings of the Gateway Computing Environments (GCE)*
2570   *Workshop, New Orleans*, 1–8. DOI: 10.1109/GCE.2010.5676129.
2571
2572   Morlo M. 1999. Niche structure and evolution in creodont (Mammalia) faunas of the European
2573   and North American Eocene. *Geobios* 32:297–305. DOI: 10.1016/S0016-6995(99)80043-6.
2574
2575   Morlo M, Gunnell GF. 2003. Small limnocyonines (Hyaenodontidae, Mammalia) from the
2576   Bridgerian middle Eocene of Wyoming: *Thinocyon*, *Prolimnocyon*, and *Iridodon*, new genus.

2577   *Contributions from the Museum of Paleontology, The University of Michigan* 31:43–78. DOI:
2578   DOI: 10.1671/0272-4634(2005)025[0251:NSOLMC]2.0.CO;2.
2579
2580
2581   Morlo M, Gunnell GF, Nagel D. 2010. Ecomorphological analysis of carnivore guilds in the
2582   Eocene through Miocene of Laurasia. In: Goswami A, Friscia A, eds. *Carnivoran Evolution:*
2583   *New Views on Phylogeny, Form, and Function*. Cambridge: Cambridge University Press, 269–
2584   310. DOI: 10.1017/CBO9781139193436.011.
2585
2586   Morlo M, Bastl K, Wenhao W, Schaal SFK. 2013. The first species of *Sinopa* (Hyaenodontida,
2587   Mammalia) from outside of North America: implications for the history of the genus in the
2588   Eocene of Asia and North America. *Palaeontology* 57:111–125. DOI: 10.1111/pala.12052.
2589
2590   Muizon C de, Lange-Badré B. 1997. Carnivorous dental adaptations in tribosphenic mammals
2591   and phylogenetic reconstruction. *Lethaia* 30:353–366. DOI: 10.1111/j.1502-
2592   3931.1997.tb00481.x.
2593
2594   O'Leary MA, Bloch JI, Flynn JJ, Gaudin TJ, Giallombardo A, Giannini NP, Goldberg SL,
2595   Kraatz BP, Luo Z-X, Meng J, Ni X, Novacek MJ, Perini FA, Randall ZS, Rougier GW, Sargis
2596   EJ, Silcox MT, Simmons NB, Spaulding M, Velazco PM, Weksler M, Wible JR, Cirranello AL.
2597   2013. The placental mammal ancestor and the post-K–Pg radiation of placentals. *Science*
2598   339:662–667. DOI: 10.1126/science.1229237.
2599
2600   Osborn HF. 1909. New carnivorous mammals from the Fayum Oligocene, Egypt. *Bulletin of the*
2601   *American Museum of Natural History* 26:415–424.
2602
2603   Partridge TC. 2010. Tectonics and geomorphology of Africa during the Phanerozoic. In:
2604   Werdelin L, Sanders W, eds. *Cenozoic Mammals of Africa*. Berkeley: University of California
2605   Press, 3–17.
2606
2607   Pilgrim GE. 1932. The fossil Carnivora of India. *Memoirs of the Geological Survey of India.*
2608   *Palaeontologica Indica* 18:1–232. DOI: 10.1017/S0016756800096448.
2609
2610   Polly PD. 1996. The skeleton of *Gazinocyon vulpeculus* gen. et comb. nov. and the cladistic
2611   relationships of Hyaenodontidae (Eutheria, Mammalia). *Journal of Vertebrate Paleontology*
2612   16:303–319. DOI: 10.1080/02724634.1996.10011318.
2613
2614   Prevosti FJ, Chemisquy MA. 2010. The impact of missing data on real morphological
2615   phylogenies: influence of the number and distribution of missing entries. *Cladistics* 26:326–339.
2616   DOI: 10.1111/j.1096-0031.2009.00289.x.
2617
2618   Pyron RA. 2011. Divergence time estimation using fossils as terminal taxa and the origins of
2619   Lissamphibia. *Systematic Biology* 60:466–481. DOI: 10.1093/sysbio/syr047.
2620
2621   Rana R, Kumar K, Zack, Solé SF, Rose K, Missiaen KP, Singh L, Sahni A, Smith T. 2015.
2622   Craniodental and postcranial morphology of *Indohyaenodon raoi* from the early Eocene of India,

2623 and its implications for ecology, phylogeny, and biogeography of hyaenodontid mammals.
2624 *Journal of Vertebrate Paleontology*. DOI: 10.1080/02724634.2015.965308
2625
2626 Rasmussen DT, Gutiérrez M. 2009. A mammalian fauna from the late Oligocene of northwestern
2627 Kenya. *Palaeontographica*, Abt A 288:1–52.
2628
2629 Rasmussen DT, Simons EL. 1991. The oldest Egyptian hyracoids (Mammalia: Pliohyracidae):
2630 new species of *Saghatherium* and *Thyrohyrax* from the Fayum. *Neues Jahrbuch für Geologie*
2631 *and Paläontologie, Abhandlungen* 182:187–209.
2632
2633 Ronquist F, Klopfstein S, Vilhelmsen L, Schulmeister S, Murray DL, Rasnitsyn AP. 2012b. A
2634 total-evidence approach to dating with fossils, applied to the early radiation of the Hymenoptera.
2635 *Systematic Biology* 61:973–999. DOI: 10.1093/sysbio/sys058.
2636
2637 Ronquist F, Teslenko M, van der Mark P, Ayres DL, Darling A, Höhna S, Larget B, Liu L,
2638 Suchard MA, Huelsenbeck JP. 2012a. MrBayes 3.2: efficient Bayesian phylogenetic inference
2639 and model choice across a large model space. *Systematic Biology* 61:539–542. DOI:
2640 10.1093/sysbio/sys029.
2641
2642 Rose K. 2006. *The Beginning of the Age of Mammals*. Baltimore: Johns Hopkins University
2643 Press, Baltimore.
2644
2645 Sallam HM, Seiffert ER. 2016. New phiomorph rodents from the latest Eocene of Egypt, and the
2646 impact of Bayesian "clock"-based phylogenetic methods on estimates of basal hystricognath
2647 relationships and biochronology. *PeerJ* 4:e1717. DOI: https://doi.org/10.7717/peerj.1717
2648
2649 Sallam HM, Seiffert ER, Simons EL. 2011. Craniodental morphology and systematics of a new
2650 family of hystricognathous rodents (Gaudeamuridae) from the late Eocene and early Oligocene
2651 of Egypt. *PLOS ONE* 6(2):e16525. DOI:10.1371/journal.pone.0016525
2652
2653 Sallam HM, Seiffert ER, Simons EL. 2012. A basal phiomorph (Rodentia, Hystricognathi) from
2654 the late Eocene of the Fayum Depression, Egypt. *Swiss Journal of Palaeontology* 131:283–301.
2655 DOI: 10.1007/s13358-012-0039-6.
2656
2657 Sallam HM, Seiffert ER, Simons EL, Brindley C. 2010. A large-bodied anomaluroid rodent from
2658 the earliest late Eocene of Egypt: phylogenetic and biogeographic implications. *Journal of*
2659 *Vertebrate Paleontology* 30:1579–1593. DOI: 10.1080/02724634.2010.501439.
2660
2661 Savage RJG. 1965. Fossil mammals of Africa 19: the Miocene Carnivora of East Africa. *Bulletin*
2662 *of the British Museum of Natural History (Geology)* 10:239–316.
2663
2664 Savage RJG. 1973. *Megistotherium,* gigantic hyaenodont from Miocene of Gebel Zelten, Libya.
2665 *Bulletin of the British Museum of Natural History (Geology)* 22:483–511.
2666
2667 Schneider CA, Rasband WS, Eliceiri KW. 2012. NIH Image to ImageJ: 25 years of image
2668 analysis. *Nature Methods* 9:671–675. DOI:10.1038/nmeth.2089.

2669
2670 Schlosser M. 1911. Beiträge zur Kenntnis der oligozänen Landsäugetiere aus dem Fayum,
2671 Ägypten. *Beiträge zur Paläontologie und Geologie Österreich-Ungarns, Wien* 14:51–167. DOI:
2672 10.1086/621934.
2673
2674 Schrago CG, Mello B, Soares AE. 2013. Combining fossil and molecular data to date the
2675 diversification of New World primates. *Journal of Evolutionary Biology* 26:2438–2446. DOI:
2676 10.1111/jeb.12237.
2677
2678 Seiffert ER. 2006. Revised age estimates for the later Paleogene mammal faunas of Egypt and
2679 Oman. *Proceedings of the National Academy of Sciences, U.S.A.* 103:5000–5005. DOI:
2680 10.1073/pnas.0600689103.
2681
2682
2683 Seiffert ER. 2007. Evolution and extinction of Afro-Arabian primates near the Eocene–
2684 Oligocene boundary. *Folia Primatologica* 78:314–327. DOI:10.1159/000105147.
2685
2686 Seiffert ER. 2010. The oldest and youngest records of afrosoricid placentals from the Fayum
2687 Depression of northern Egypt. *Acta Palaeontologica Polonica* 55:599–616. doi:
2688 http://dx.doi.org/10.4202/app.2010.0023.
2689
2690 Seiffert ER. 2012. Early primate evolution in Afro-Arabia. *Evolutionary Anthropology* 21:239–
2691 253. DOI: 10.1002/evan.21335.
2692
2693 Seiffert ER., and E. L. Simons. 2000. *Widanelfarasia*, a diminutive placental from the late
2694 Eocene of Egypt. *Proceedings of the National Academy of Sciences, U.S.A.* 97:2646–2651. DOI:
2695 10.1073/pnas.040549797.
2696
2697 Seiffert ER, Costeur L, Boyer DM. 2015. Primate tarsals from Egerkingen, Switzerland,
2698 attributable to the middle Eocene adapiform *Caenopithecus lemuroides*. *PeerJ* 3:e1036. DOI:
2699 https://doi.org/10.7717/peerj.1036
2700
2701 Seiffert ER, Simons EL, Ryan TM, Bown TM, Attia Y. 2007. New remains of Eocene and
2702 Oligocene Afrosoricida (Afrotheria) and the origin(s) of afrosoricid zalambdodonty. *Journal of
2703 Vertebrate Paleontology* 27:963–972. DOI: 10.1671/0272-
2704 4634(2007)27[963:NROEAO]2.0.CO;2
2705
2706 Simons EL. 1990. Discovery of the oldest known anthropoidean skull from the Paleogene of
2707 Egypt. *Science* 247:1567–1569. DOI: 10.1126/science.2108499.
2708
2709 Simons EL. 1997. Preliminary description of the cranium of *Proteopithecus sylviae*, an Egyptian
2710 late Eocene anthropoidean primate. *Proceedings of the National Academy of Sciences, U.S.A.*
2711 94:14970–14975. DOI: 10.1073/pnas.94.26.14970.
2712
2713 Simons EL, Gingerich PD. 1974. New carnivorous mammals from the Oligocene of Egypt.
2714 *Annals of the Geological Survey of Egypt* 4:157–166.

2715
2716 Simons EL, Rasmussen DT. 1996. Skull of *Catopithecus browni*, an early Tertiary catarrhine.
2717 *American Journal of Physical Anthropology* 100:261–292. DOI: DOI: 10.1002/(SICI)1096-
2718 8644(199606)100:2<261::AID-AJPA7>3.0.CO;2-#.
2719
2720 Simons EL, Cornero S, Bown TM. 1996. The taphonomy of fossil vertebrate quarry L-41, upper
2721 Eocene, Fayum Province, Egypt. In: *Proceedings of the Geological Survey of Egypt Centennial*
2722 *Conference, Cairo*, 785–791.
2723
2724 Simons EL, Seiffert ER, Chatrath PS, Attia Y. 2001. Earliest record of a parapithecid anthropoid
2725 from the Jebel Qatrani Formation, northern Egypt. *Folia Primatologica* 72:316–331. DOI:
2726 10.1159/000052748.
2727
2728 Simpson GG. 1953. *The Major Features of Evolution.* New York: Columbia University Press.
2729
2730 Slowinski JB. 1993. "Unordered" versus "ordered" characters. *Systematic Biology* 42:155–165.
2731 DOI: 10.1093/sysbio/42.2.155.
2732
2733 Smith, T, Smith R. 2001. The creodonts (Mammalia, Ferae) from the Paleocene–Eocene
2734 transition in Belgium (Tienen Formation, MP7). *Belgian Journal of Zoology* 131:117–135. doi:
2735 10.1080/11035890001221148.
2736
2737 Smith T, Rose KD, Gingerich PD. 2006. Rapid Asia–Europe–North America geographic
2738 dispersal of earliest Eocene primate *Teilhardina* during the Paleocene–Eocene Thermal
2739 Maximum. *Proceedings of the National Academy of Sciences, U.S.A.*103:11223–11227. DOI:
2740 10.1073/pnas.0511296103.
2741
2742 Solé F. 2013. New proviverrine genus from the early Eocene of Europe and the first phylogeny
2743 of late Palaeocene–middle Eocene hyaenodontidans (Mammalia). *Journal of Systematic*
2744 *Palaeontology* 11:375–398. DOI: 10.1080/14772019.2012.686927.
2745
2746 Solé F, Falconnet J, Yves L. 2014a. New proviverrines (Hyaenodontida) from the early Eocene
2747 of Europe; phylogeny and ecological evolution of the Proviverrinae. *Zoological Journal of the*
2748 *Linnean Society* 171:878–917. DOI: 10.1111/zoj.12155.
2749
2750 Solé F, Gheerbrant E, Mbarek A, Bouya B. 2009. Further evidence of the African antiquity of
2751 hyaenodontid ("Creodonta", Mammalia) evolution. *Zoological Journal of the Linnean Society*
2752 156:827–846. DOI: 10.1111/j.1096-3642.2008.00501.x.
2753
2754 Solé, F, Amson E, Borths M, Vidalenc D, Morlo M, Bastl K. 2015. A new large hyainailourine
2755 from the Bartonian of Europe and its bearings on the evolution and ecology of massive
2756 hyaenodonts (Mammalia). PLOS ONE 10(10):e0141941. DOI: 10.1371/journal.pone.0141941
2757
2758 Solé, F, Lhuillier J, Adaci M, Bensalah M, Mahboubi M, Tabuce R. 2014b. The hyaenodontidans
2759 from the Gour Lazib area (?early Eocene, Algeria): implications concerning the systematics and

the origin of the Hyainailourinae and Teratodontinae. *Journal of Systematic Paleontology* 12:303–322. DOI: 10.1080/14772019.2013.795196.

Spaulding M, Flynn JJ. 2012. Phylogeny of the Carnivoramorpha: the impact of postcranial characters. *Journal of Systematic Palaeontology* 10:653–677. DOI: 10.1080/14772019.2011.630681.

Spaulding M, O'Leary MA, Gatesy J. 2009. Relationships of Cetacea (Artiodactyla) among mammals: increased taxon sampling alters interpretations of key fossils and character evolution. *PLOS ONE* 4(9):e7062. DOI: 10.1371/journal.pone.0007062.

Stanhope MJ, Waddell VG, Madsen O, de Jong WW, Hedges SB, Cleven GC, Kao D, Springer MS. 1998. Molecular evidence for multiple origins of Insectivora and for a new order of endemic African insectivore mammals. *Proceedings of the National Academy of Sciences, U.S.A.* 95:9967–9972. DOI: 10.1073/pnas.95.17.9967.

Strong EE, Lipscomb D. 1999. Character coding and inapplicable data. *Cladistics* 15:363–371. DOI: 10.1111/j.1096-0031.1999.tb00272.x.

Swofford DL. 2003. PAUP*. Phylogenetic Analysis Using Parsimony (*and other methods). Version 4. Sinauer Associates, Sunderland, Massachusetts.

Szalay FS. 1967. The affinities of *Apterodon* (Mammalia, Deltatheridia, Hyaenodontidae). *American Museum Novitates* 2293:1–17.

Van Valen L. 1965. Some European Proviverrinae (Mammalia, Deltatheridia). *Paleontology* 8:638–665.

Van Valen L. 1966. Deltatheridia, a new order of mammals. *Bulletin of the American Museum of Natural History* 132:1–126. URI: http://hdl.handle.net/2246/1126.

Van Valen L. 1967. New Paleocene insectivores and insectivore classification. *Bulletin of the American Museum of Natural History* 135:217–284. URI: http://hdl.handle.net/2246/358.

Van Valkenburgh B. 1988. Trophic diversity in past and present guilds of large predatory mammals. *Paleobiology* 14:155–173. DOI: http://dx.doi.org/10.1017/S0094837300011891.

Van Valkenburgh B. 1989. Carnivore dental adaptations and diet: a study of trophic diversity within guilds. In: Gittleman JL, ed. *Carnivore Behavior, Ecology and Evolution*. Ithaca: Cornell University Press, 410–436. DOI: 10.1007/978-1-4613-0855-3_16.

Van Valkenburgh B. 1990. Skeletal and dental predictors of body mass in carnivores. In: Damuth J, MacFadden BJ, eds. *Body Size in Mammalian Paleobiology: Estimation and Biological Implications*. New York: Cambridge University Press, 181–206

2805 Van Valkenburgh B. 1999. Major patterns in the history of carnivorous mammals. *Annual*
2806 *Review of Earth and Planetary Sciences* 27:463–493. DOI: 10.1146/annurev.earth.27.1.463.
2807
2808 Van Valkenburgh B. 2007. Déjà vu: the evolution of feeding morphologies in the Carnivora.
2809 *Integrative and Comparative Biology* 47:147–163. DOI: 10.1093/icb/icm016.
2810
2811 Van Valkenburgh B, Wang X, Damuth J. 2004. Cope's rule, hypercarnivory, and extinction in
2812 North American canids. *Science* 306:101–104. DOI: 10.1126/science.1102417.
2813
2814 Wesley-Hunt GD, Flynn JJ. 2005. Phylogeny of the Carnivora: basal relationships among the
2815 carnivoramorphans, and assessment of the position of 'Miacoidea' relative to Carnivora. *Journal*
2816 *of Systematic Palaeontology* 3:1–28. DOI: http://dx.doi.org/10.1017/S1477201904001518.
2817
2818 Wible JR, Rougier GW, Novacek MJ, Asher RJ. 2007. Cretaceous eutherians and Laurasian
2819 origin for placental mammals near the K/T boundary. *Nature* 447:1003–1006. DOI:
2820 10.1038/nature05854.
2821
2822
2823 Wible JR, Rougier GW, Novacek MJ, Asher RJ. 2009. The eutherian mammal *Maelestes*
2824 *gobiensis* from the late Cretaceous of Mongolia and the phylogeny of Cretaceous Eutheria.
2825 *Bulletin of the American Museum of Natural History* 327:1–123.
2826 DOI: http://dx.doi.org/10.1206/623.1.
2827
2828 Wiens JJ. 2003. Missing data, incomplete taxa, and phylogenetic accuracy. *Systematic Biology*
2829 52:528–538. DOI: 10.1080/10635150390218330.
2830
2831 Wiens, JJ, Moen DS. 2008. Missing data and the accuracy of Bayesian phylogenetics. *Journal of*
2832 *Systematics and Evolution* 46:307–314. DOI: 10.3724/SP.J.1002.2008.08040.
2833
2834 Wood HM, Matzke NJ, Gillespie RG, Griswold CE. 2013. Treating fossils as terminal taxa in
2835 divergence time estimation reveals ancient vicariance patterns in the palpimanoid spiders.
2836 *Systematic Biology* 62:264–284. DOI: 10.1093/sysbio/sys092.
2837
2838 Yu Y, Harris AJ, Blair C, He X. 2015. RASP (Reconstruct Ancestral State in Phylogenies): a
2839 tool for historical biogeography. *Molecular Phylogenetics and Evolution* 87:46–49.
2840 DOI: 10.1016/j.ympev.2015.03.008.
2841
2842 Zack SP. 2011. New species of the rare early Eocene creodont *Galecyon* and the radiation of the
2843 early Hyaenodontidae. *Journal of Paleontology* 85:315–336. DOI: http://dx.doi.org/10.1666/10-
2844 093.1.
2845
2846 Zack SP, Rose KD. 2015. The postcranial skeleton of *Galecyon*: evidence for morphological and
2847 locomotor diversity in early Hyaenodontidae (Mammalia, Hyaenodontida). *Journal of Vertebrate*
2848 *Paleontology*, 35: e1001492, DOI: 10.1080/02724634.2014.1001492.

Figure 1(on next page)

Map of the Fayum Depression, Egypt

A, Map of the Fayum Depression, Egypt. Stars indicate quarries. Red star indicates L-41 (latest Priabonian, ~34 Ma) in the Jebel Qatrani Formation (Fm.). Well-defined formational contacts (Qasr el-Sagha Fm./Jebel Qatrani Fm. and Jebel Qatrani Fm./Khashab Fm.) are indicated by solid lines. The older and more ambiguous formational boundary (Birket Qarun Fm./Qasr el-Sagha Fm.) is indicated by a dashed line. **B**, Fayum field crew excavating at Quarry L-41 by carefully removing sheets of mudstone to expose fossils.
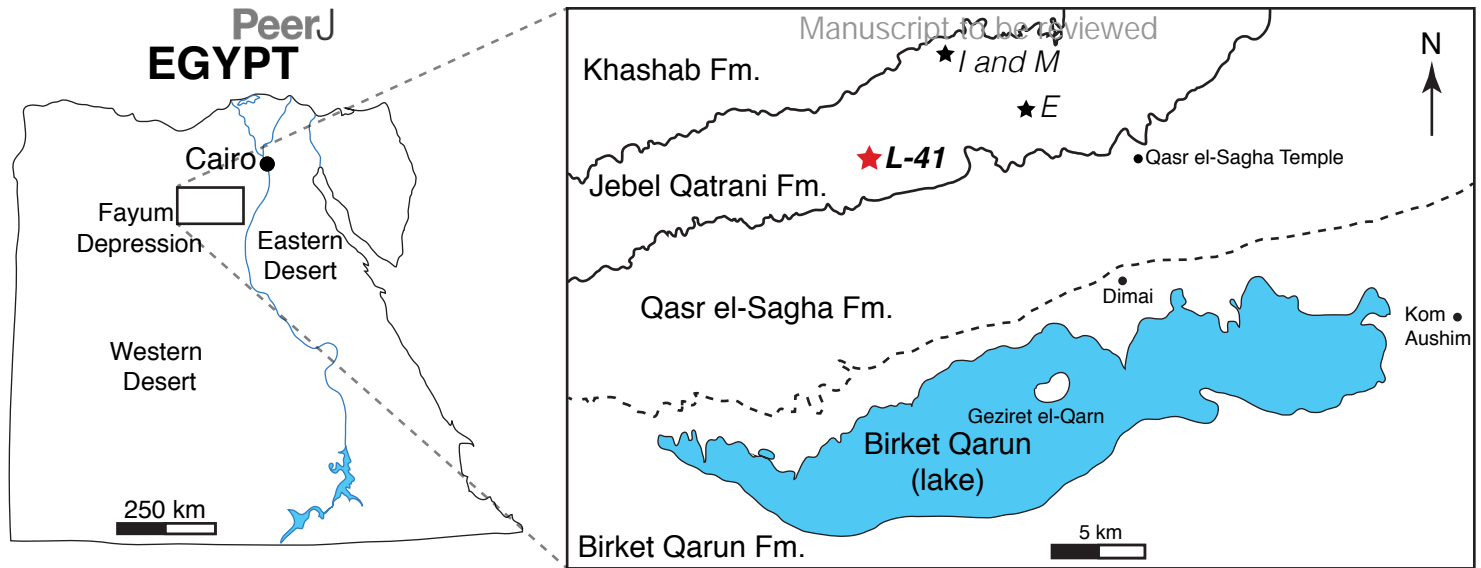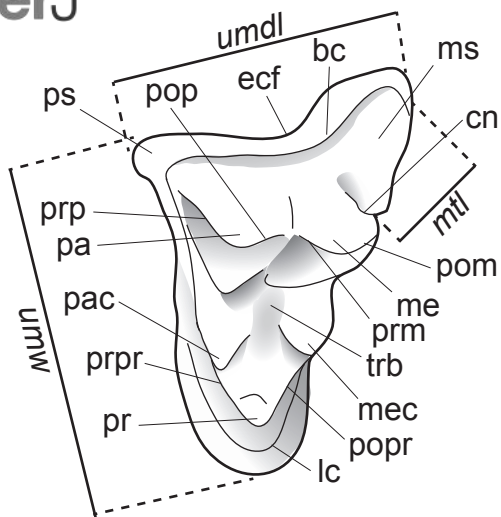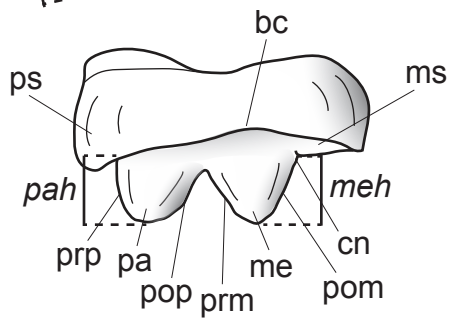
Figure 2(on next page)

Dental nomenclature used in this study

Upper left M² and lower left M₃ of *Proviverra typica* (**A**–**E**) and *Pterodon dasyuroides* (**F**-**J**) showing dental terminology and measurements used in this study. **A**, *Proviverra typica* M² in occlusal and **B**, buccal views and M₃ in **C**, occlusal **D**, lingual, and **E**, buccal views. **F**, *Pterodon dasyuroides* M² in occlusal and **G**, buccal views and M₃ in **H**, occlusal **I**, lingual, and **J**, buccal views. Measurements are indicated in italics. **Abbreviations**: **ak**, anterior keel; **bc**, buccal cingulum; **bcd**; buccal cingulid; **cn**, carnassial notch; **co**, cristid obliqua; **ecf**, ectoflexus; **ed**, entoconid; **ecd**, entocristid; **hd**, hypoconid; **hld**, hypoconulid; **lc**, lingual cingulum; *lmdl*, lower molar mesiodistal length; *meh*, metacone height beyond metastyle; **me**, metacone; **mec**, metaconule; **med**, metaconid; **ms**, metastyle; *mtl*, metastyle mesiodistal length; **pa**, paracone; **pac**, paraconule; **pad**, paraconid; *pah*, paracone height beyond metastyle; **pom**, postmetacrista; **pop**, postparacrista; **popad**; postparacristid; **popr**, postprotocrista; **pr**, protocone; **prd**, protoconid; **prm**, premetacrista; **prp**, preparacrista; **prpr**, preprotocrista; **prprd**; preprotocristid; **ps**, parastyle; **tab**, talon basin; **tadb**, talonid basin; *tall*, talonid mesiodistal length; *talw*, talonid buccolingual width; **trb**, trigon basin; **trdb**, trigonid basin *tril*, trigonid mesiodistal length; *triw*, trigonid buccolingual width; *umdl*, upper molar mesiodistal length; *umw*, upper molar buccolingual width.
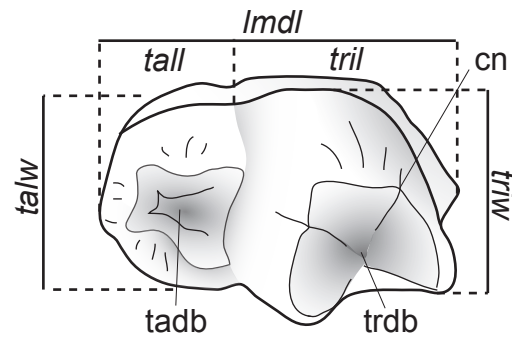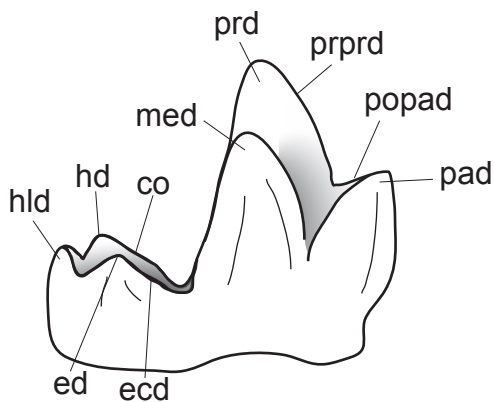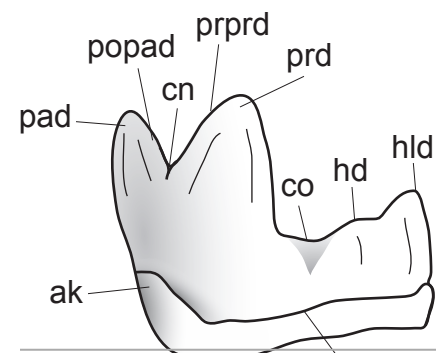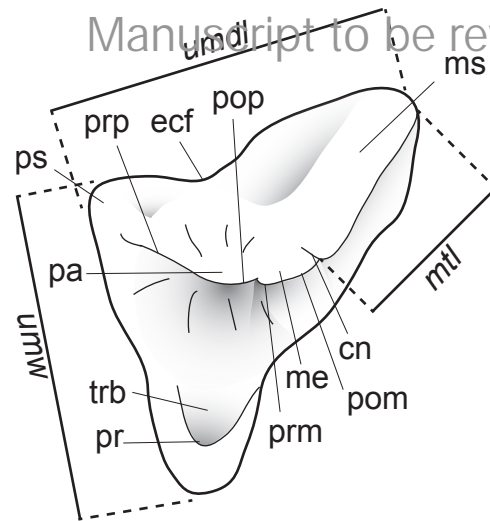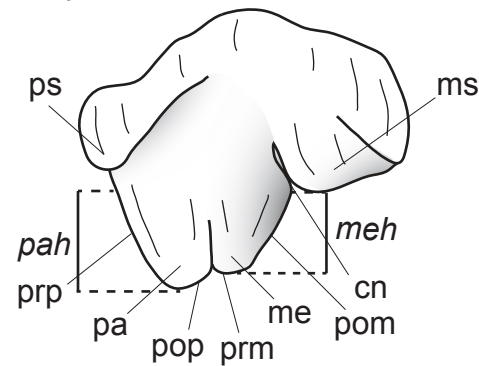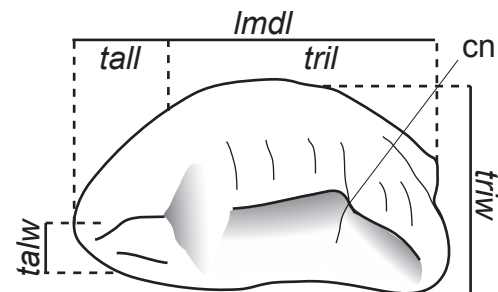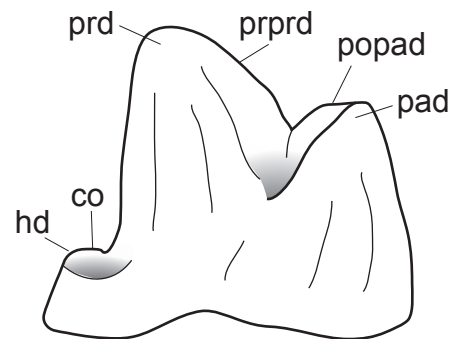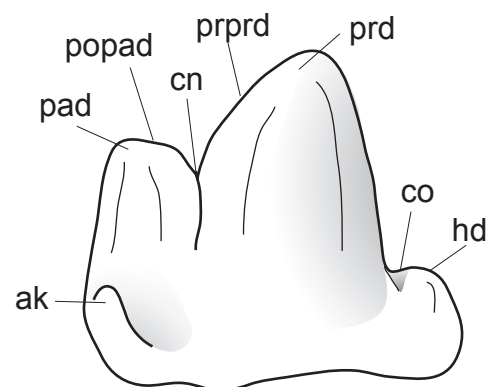
Figure 3(on next page)

Brychotherium ephalmos DPC 11990 rostrum

Brychotherium ephalmos gen. et sp. nov. DPC 11990, rostrum with left and right P^4–M^3 and alveoli for right and left I^2–P^3. **A**, ventral view; **B**, dorsal view; **C**, left lateral view; **D**, right lateral view. Specimen crushed mediolaterally with left maxilla shifted anteriorly relative to right maxilla.

Figure 4(on next page)

Brychotherium ephalmos DPC 11990 sketch and model

Brychotherium ephalmos gen. et sp. nov. DPC 11990; rostrum with P^4–M^3 with left and right P^4-M^3: and alveolus for right and left I^2–P^3. Sketch on the left (subscript 1) and digital model on the right (subscript 2): **A**, ventral view; **B**, dorsal view; **C**, left lateral view; **D**, right lateral view. Solid lines indicate definite sutures, dotted lines indicate interpreted sutures that have been obscured by crushing. Digital model is a volume rendering in Avizo based on the model available at MorphoSource.

Figure 5(on next page)

Brychotherium ephalmos holotype DPC 17627 rostrum

Brychotherium ephalmos gen. et sp. nov. DPC 17627, rostrum with left canine, dP^4-M^3 (M^3 erupting) and alveolus for dP^3 and right P^4-M^2; specimen photographs on the left (subscript 1) and digital model on the right (subscript 2): **A**, occlusal view of left dentition, buccal aspect of right dentition visible; **B**, buccal view of left dentition, protocones of right P^4-M^2 and M^2 paracone and metacone visible; **C**, lingual view of left dentition, buccal aspect of right dentition visible. Postmortem distortion involuted right side of rostrum. Occlusal portions of right dentition protrude through left maxilla. Digital model is a volume rendering in Avizo based on the model available at MorphoSource.

Figure 6(on next page)

Brychotherium ephalmos holotype DPC 17627 dentary

Brychotherium ephalmos gen. et sp. nov. DPC 17627, right dentary with P_4-M_3; specimen photographs on the left (subscript 1) and digital model on the right (subscript 2); **A**, occlusal view; **B**, lingual view; **C**, buccal view. Digital model is a volume rendering in Avizo based on the model available at MorphoSource.

Figure 7 (on next page)

Brychotherium ephalmos holotype CGM 83750 dentary

Brychotherium ephalmos gen. et sp. nov. CGM 83750, right dentary with C–M_3; specimen photos on the left (subscript 1) and digital model images on the right (subscript 2); **A**, occlusal view; **B**, lingual view; **C**, buccal view. Digital model is a volume rendering in Avizo based on the model available at MorphoSource.

Figure 8(on next page)

Brychotherium ephalmos DPC 11569A right dentary

Brychotherium ephalmos gen. et sp. nov. DPC 11569A, right dentary with C, P_2–M_3; specimen photos on the left (subscript 1) and digital model images on the right (subscript 2); **A**, occlusal view; **B**, lingual view; **C**, buccal view. Digital model is a volume rendering in Avizo based on the model available at MorphoSource.

Figure 9(on next page)

Brychotherium ephalmos DPC 11569B left dentary

Brychotherium ephalmos gen. et sp. nov. DPC 11569B, left dentary with C, P_2–M_3; specimen photos on the left (subscript 1) and digital model images on the right (subscript 2); **A**, occlusal view; **B**, lingual view; **C**, buccal view. Digital model is a volume rendering in Avizo based on the model available at MorphoSource.

Figure 10(on next page)

Akhnatenavus nefertiticyon cranium CGM 83735

Akhnatenavus nefertitcyon sp. nov. holotype CGM 83735, cranium with right canine, P^3–M^3 and alveolus of P^2 and left P^2, P^4, M^2; **A**, right lateral view; **B**, dorsal view; **C**, left lateral view. Postmortem distortion mediolaterally crushed the specimen with the left dentition involuted. Specimen also preserves atlas (cervical vertebra 1) appressed to the basicranium and a proximal rib appressed to the right parietal.

Figure 11(on next page)

Akhnatenavus nefertiticyon cranium CGM 83735 labeled

Akhnatenavus nefertiticyon sp. nov. CGM 83735, cranium sketch (subscript 1) and digital model (subscript 2) with right canine, P^3-M^3 and left P^2, P^4, M^2; **A**, right lateral view; **B**, dorsal view; **C**, left lateral view. Dotted lines indicate uncertain sutures or boundaries. Unlabeled regions are fragmentary. **Abbreviations**: **l.,** left; **r.,** right; **inf. orb. f.**, infraorbital foramen; **mand. fossa**, mandibular fossa; **r. occ. condyle**, right occipital condyle. Digital model is a volume rendering in Avizo based on the model available at MorphoSource.

Figure 12(on next page)

Akhnatenavus nefertiticyon CGM 83735 dentition detail

Akhnatenavus nefertiticyon sp. nov. CGM 83735 photographs (subscript 1) and digital model images (subscript 2) of right P^3–M^3; **A**, occlusal view. DPC 13518, left M^1; **B**, occlusal-lingual view.

Figure 13(on next page)

Akhnatenavus nefertiticyon DPC 18242 cranium

Akhnatenavus nefertiticyon sp. nov., DPC 18242, palate with left P^2-M^2 and P^1 roots and right M^1 and P^1–P^4 roots; **A**, ventral view; **B**, dorsal view; **C**, left lateral view; **D**, right lateral view. Postmortem distortion involuted the right maxilla and dorsoventrally compressed the cranium.

Figure 14(on next page)

Akhnatenavus nefertiticyon DPC 18242 cranium labeled

Akhnatenavus nefertiticyon sp. nov., DPC 18242, digital model images of palate with left P^2-M^2 and P^1 roots and right M^1 and P^1–P^4 roots; **A**, ventral view; **B**, dorsal view; **C**, left lateral view; **D**, right lateral view. Postmortem distortion involuted the right maxilla and dorsoventrally compressed the cranium. Digital model is a volume rendering in Avizo based on the model available at MorphoSource.

Figure 15(on next page)

Akhnatenavus nefertiticyon DPC 18242 and DPC 13518 dentition detail

Akhnatenavus nefertiticyon sp. nov., detail from DPC 18242 of left P^2–M^2; photographs of dental specimen on the left (subscript 1) and digital model images on the right (subscript 2); **A**, occlusal view; **B**, buccal view; DPC 13518, isolated left M^1 in **C**, occlusal; **D**, buccal, and **E**, lingual view. Digital model is a volume rendering in Avizo based on the model available at MorphoSource.

Figure 16(on next page)

Strict and Adams consensus trees

A, Strict consensus tree and **B,** Adams consensus tree of 650 most parsimonious trees (1029 steps, consistency index (CI) = 0.187, retention index (RI) = 0.613, rescaled consistency index (RC) = 0.114). P# corresponds to the node to the right of the label in the strict consensus tree and are used in the discussion of clades and the biogeographic analyses. Bremer support values (range 1–10) right of relevant node in the strict consensus tree. Bootstrap support values (range 50%–100%) right of relevant node and italicized. Only clades supported by greater than 50% bootstrap support are labeled with bootstrap values. Major clades identified by this study are indicated by the round boxes with the name enclosed or overlapping the boundaries of the box. Dashed branches indicate branches recovered in the Adams consensus but not in the strict consensus tree.
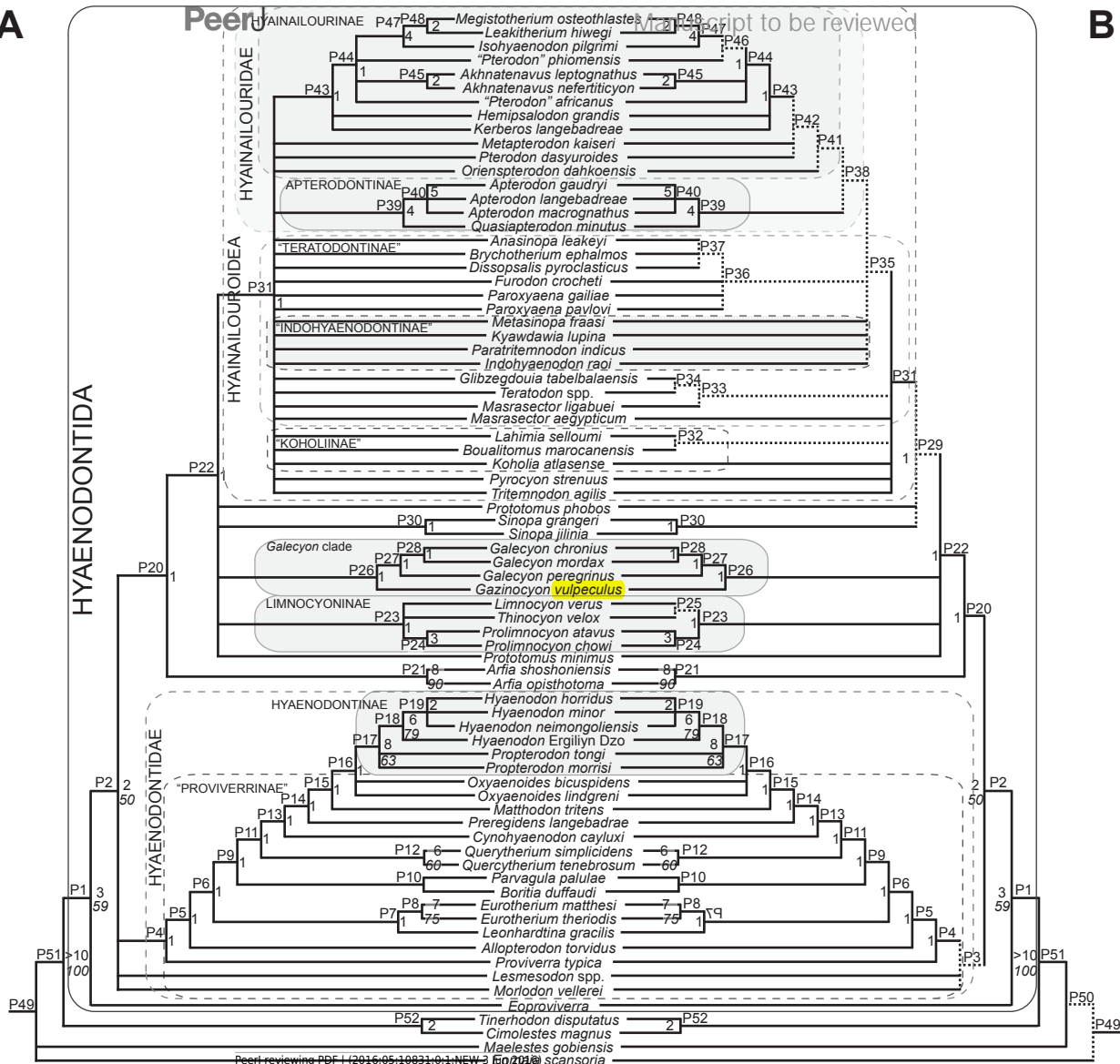
Figure 17(on next page)

Agreement subtree and Adams consensus

A, Agreement subtree of 650 most parsimonious trees compared with **B,** Adams consensus tree. Taxa colored grey are not part of the agreement subtree. Dashed branch indicates the branch was not recovered in the strict consensus tree.
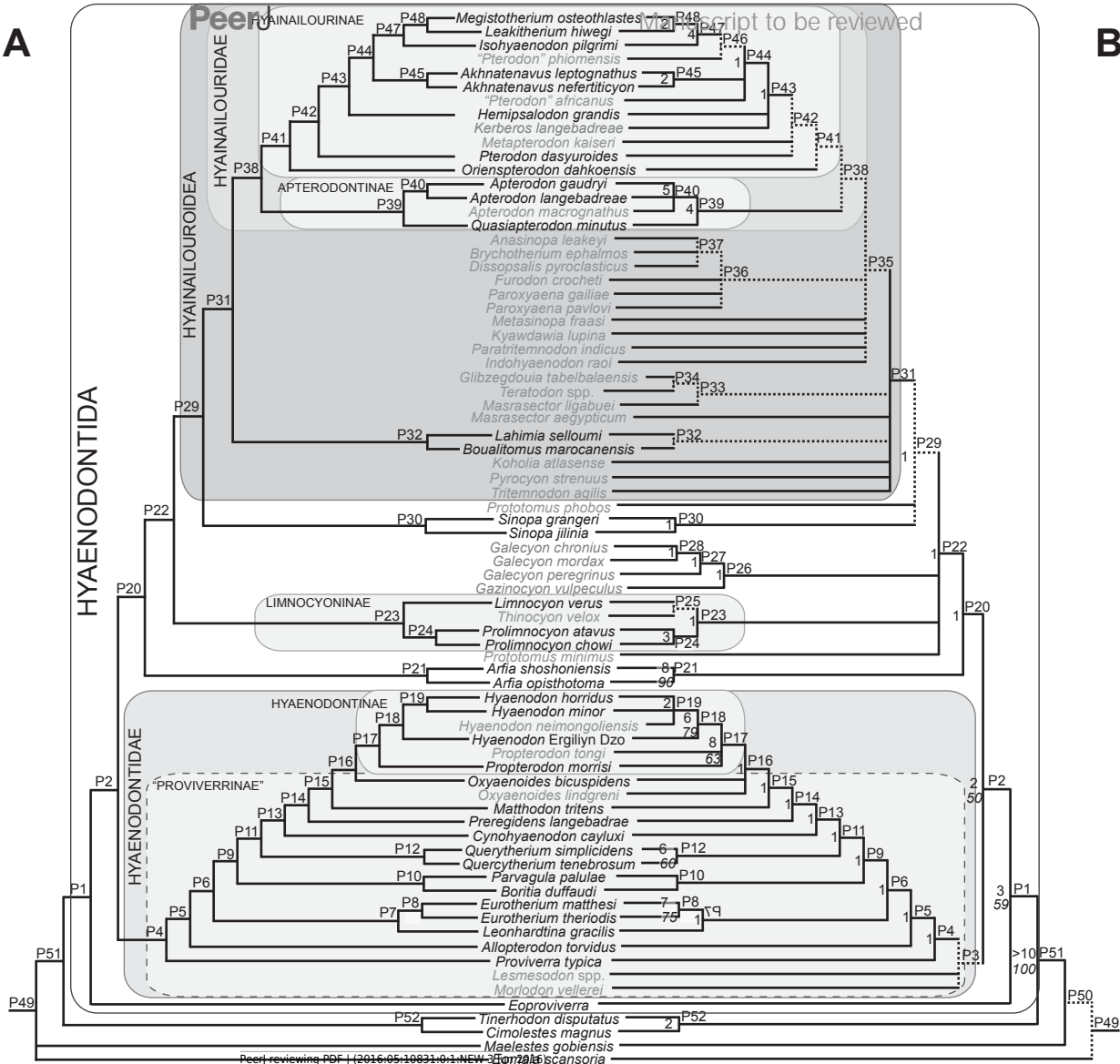
Figure 18(on next page)

Standard Bayesian "allcompat" tree

"allcompat" standard Bayesian tree. B# correspond to the node to the <mark>right</mark> of the label and are used in the discussion and in the biogeographic analyses to reference the clade. Posterior Probabilities (PP) correspond to the node to the left of value. Strength of PP support summarized by color. Major clades identified by this study are indicated by the round boxes with the clade name enclosed or overlapping the boundaries of the box.
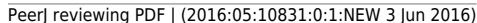
Figure 19 (on next page)

Bayesian tip-dating "allcompat" tree

"allcompat" Bayesian tip-dating tree. T# correspond to Table 4 and biogeography results. Posterior probability (PP) shown in italics to the right or below relevant node. Divergence dates represent mean divergence date for clades and taxa. Branch colors correspond to legend for relative median rate (% change/Ma) along branches. Most rapidly evolving clades are shown in warm colors. The mean age recovered by the analysis is shown as a vertical line on the estimated age range for each terminal taxon. See Table S2 for sources of the age ranges used in the tip-dating analysis. Major clades identified by this study are indicated by the round boxes with the clade name enclosed or overlapping the boundaries of the box.

PeerJ

Figure 20(on next page)

BBM biogeographic analysis of strict consensus tree

Results from Bayesian Binary MCMC (BBM) biogeographic analysis performed on the strict consensus tree based on maximum parsimony analysis. Proportion of circle corresponds to likelihood of node originating from continental area. P# corresponds to clade rows in Table S5 where the reconstructed biogeographic origin for each clade is listed using parsimony optimization (PO), and % likelihood for each area using likelihood optimization (LO) and BBM. Green = Afro-Arabia; Purple = Asia; Red = Europe; Blue = North America; Gray = continents without hyaenodontidans.

Branch collapses in strict consensus

Early Eocene ~50 Ma

HYAINAILOURINAE

P48 — *Megistotherium osteothlastes*
P47 — *Leakitherium hiwegi*
— *Isohyaenodon pilgrimi*
P44 — *"Pterodon" phiomensis*
P45 — *Akhnatenavus leptognathus*
— *Akhnatenavus nefertiticyon*
P43 — *"Pterodon" africanus*
— *Hemipsalodon grandis*
— *Kerberos langebadreae*
— *Metapterodon kaiseri*
— *Pterodon dasyuroides*
— *Orienspterodon dahkoensis*

APTERODONTINAE
P40 — *Apterodon gaudryi*
P39 — *Apterodon langebadreae*
— *Apterodon macrognathus*
— *Quasiapterodon minutus*

"TERATODONTINAE"
— *Anasinopa leakeyi*
— *Brychotherium ephalmos*
— *Dissopsalis pyroclasticus*
P31 — *Furodon crocheti*
— *Paroxyaena gailiae*
— *Paroxyaena pavlovi*

"INDOHYAENODONTINAE"
— *Metasinopa fraasi*
— *Kyawdawia lupina*
— *Paratritemnodon indicus*
— *Indohyaenodon raoi*
— *Glibzegdouia tabelbalaensis*
— *Teratodon* spp.
— *Masrasector ligabuei*
— *Masrasector aegypticum*

"KOHOLIINAE"
— *Lahimia selloumi*
— *Boualitomus marocanensis*
— *Koholia atlasense*
— *Pyrocyon strenuus*
— *Tritemnodon agilis*
— *Prototomus phobos*
P30 — *Sinopa grangeri*
— *Sinopa jilinia*

Galecyon clade
P28 — *Galecyon chronius*
P27 — *Galecyon mordax*
P26 — *Galecyon peregrinus*
— *Gazinocyon vulpeculus*

LIMNOCYONINAE
— *Limnocyon verus*
P23 — *Thinocyon velox*
— *Prolimnocyon atavus*
P24 — *Prolimnocyon chowi*
— *Prototomus minimus*
P21 — *Arfia shoshoniensis*
— *Arfia opisthotoma*

HYAENODONTINAE
P19 — *Hyaenodon horridus*
P18 — *Hyaenodon minor*
P17 — *Hyaenodon neimongoliensis*
— *Hyaenodon* Ergiliyn Dzo
P16 — *Propterodon tongi*
— *Propterodon morrisi*

"PROVIVERRINAE"
P15 — *Oxyaenoides bicuspidens*
P14 — *Oxyaenoides lindgreni*
P13 — *Matthodon tritens*
P11 — *Preregidens langebadrae*
— *Cynohyaenodon cayluxi*
P9 — P12 — *Quercytherium simplicidens*
— *Quercytherium tenebrosum*
P6 — P10 — *Parvagula palulae*
— *Boritia duffaudi*
P5 — *Eurotherium matthesi*
P7 — P8 — *Eurotherium theriodis*
— *Leonhardtina gracilis*
P4 — *Allopterodon torvidus*
— *Proviverra typica*
— *Lesmesodon* spp.
— *Morlodon vellerei*
— *Eoproviverra*
P52 — *Tinerhodon disputatus*
— *Cimolestes magnus*
— *Maelestes gobiensis*
— *Eomaia scansoria*

P2 — P1 — P51 — P49 — P20 — P22 — P31

HYAINAILOUROIDEA / HYAINAILOURIDAE

HYAENODONTIDAE

Figure 21 (on next page)

BBM biogeographic analysis of standard Bayesian tree

Results from Bayesian Binary MCMC (BBM) biogeographic analysis performed on the standard Bayesian "allcompat" consensus tree. Proportion of circle corresponds to likelihood of node originating from continental area. B# corresponds to clade rows in Table S6 where the reconstructed biogeographic origin for each clade is listed using parsimony optimization (PO), and % likelihood for each area using likelihood optimization (LO) and BBM. Green = Afro-Arabia; Purple = Asia; Red = Europe; Blue = North America; Gray = continents without hyaenodontidans.

PeerJ

Early Eocene ~50 Ma

HYAINAILOURINAE

B71 *Megistotherium osteothlastes*
B70 *Leakitherium hiwegi*
B69 *Isohyaenodon pilgrimi*
B68 *"Pterodon" phiomensis*
B66 *"Pterodon" africanus*
B65 *Akhnatenavus leptognathus*
B67 *Akhnatenavus nefertiticyon*
B64 *Hemipsalodon grandis*
B63 *Kerberos langebadreae*
B62 *Metapterodon kaiseri*
B61 *Pterodon dasyuroides*
B60 *Koholia atlasense*
B58 *Orienspterodon dahkoensis*
B59 *Paroxyaena gailiae*
Paroxyaena pavlovi

APTERODONTINAE
B57 *Apterodon gaudryi*
B56 *Apterodon langebadreae*
B55 *Apterodon macrognathus*
Quasiapterodon minutus

TERATODONTINAE
B53 *Dissopsalis pyroclasticus*
B51 *Brychotherium ephalmos*
Anasinopa leakeyi
B52 *Furodon crocheti*
B50 *Teratodon spp.*
B49 *Glibzegdouia tabelbalaensis*
B48 *Masrasector aegypticum*
Masrasector ligabuei
Metasinopa fraasi

"INDOHYAENODONTINAE"
Paratritemnodon indicus
Kyawdawia lupina
Indohyaenodon raoi
Tritemnodon agilis
B40 *Lahimia selloumi*
Boualitomus marocanensis
Pyrocyon strenuus
Preregidens langebadrae

Galecyon clade
B36 *Galecyon chronius*
B35 *Galecyon mordax*
B34 *Galecyon peregrinus*
Gazinocyon vulpeculus

LIMNOCYONINAE
B32 *Limnocyon verus*
Thinocyon velox
B30 *Prolimnocyon atavus*
B31 *Prolimnocyon chowi*

Sinopa clade
B28 *Arfia shoshoniensis*
B26 *Arfia opisthotoma*
Sinopa grangeri
B27 *Sinopa jilinia*
Prototomus phobos
Prototomus minimus

HYAENODONTINAE
B22 *Hyaenodon horridus*
B21 *Hyaenodon minor*
B20 *Hyaenodon neimongoliensis*
B19 *Hyaenodon* Ergiliyn Dzo
B18 *Propterodon tongi*
Propterodon morrisi

"PROVIVERRINAE"
B17 *Oxyaenoides bicuspidens*
Oxyaenoides lindgreni
B13 *Matthodon tritens*
B14 *Eurotherium matthesi*
Eurotherium theriodis
Leonhardtina gracilis
Cynohyaenodon cayluxi
B10 *Quercytherium simplicidens*
Quercytherium tenebrosum
Allopterodon torvidus
Boritia duffaudi
Proviverra typica

HYAENODONTIDAE

Morlodon vellerei
B3 *Lesmesodon*
Parvagula palulae
Eoproviverra
B74 *Tinerhodon disputatus*
Cimolestes magnus
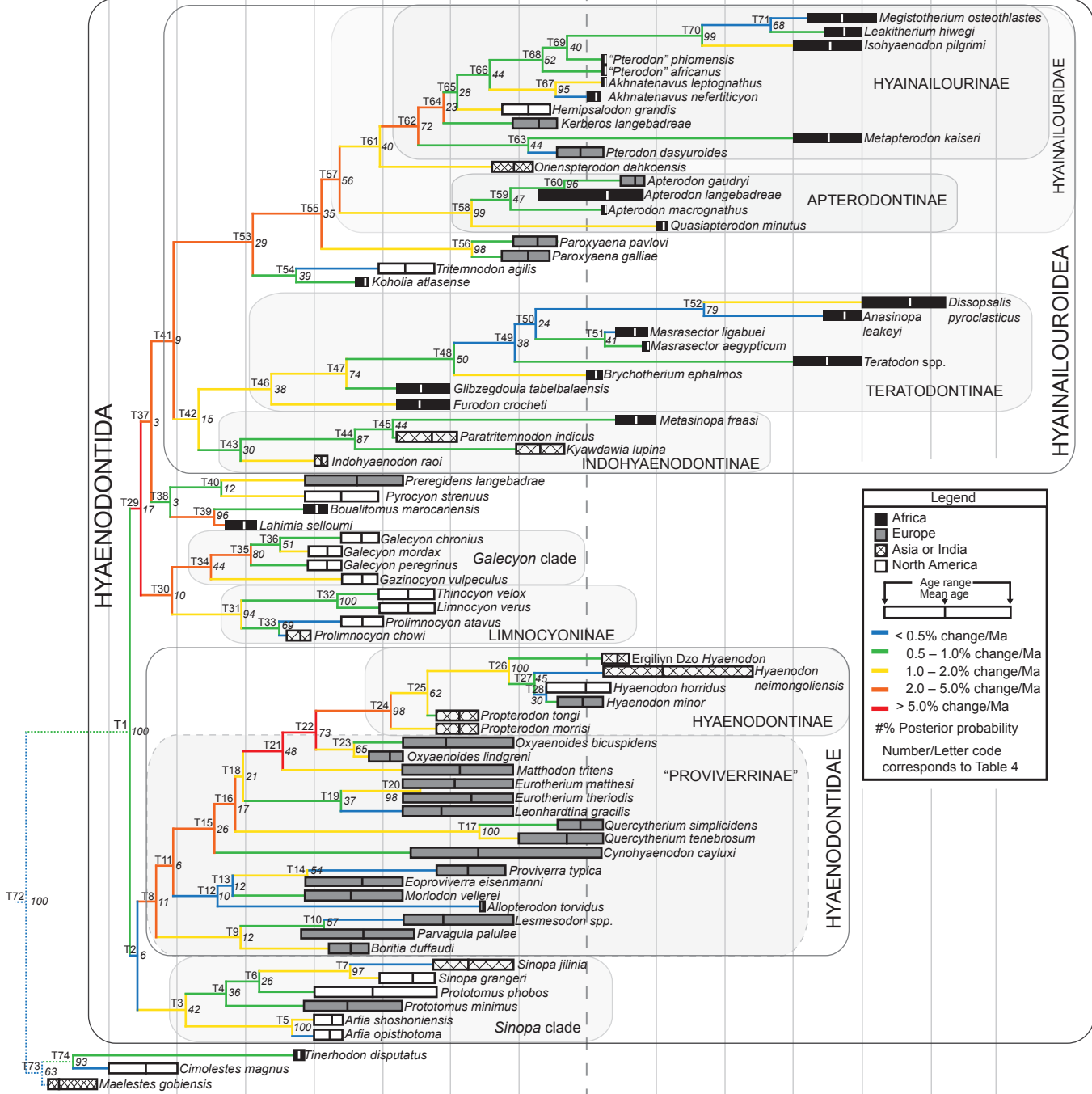*Maelestes gobiensis*
Eomaia scansoria

Figure 22(on next page)

BBM biogeographic applied to Bayesian tip-dating tree

Results from Bayesian Binary MCMC (BBM) biogeographic analysis performed on the Bayesian tip-dating "allcompat" consensus tree. Proportion of circle corresponds to likelihood of node originating from continental area. T# corresponds to clade rows in Table S7 where the reconstructed biogeographic origin for each clade is listed for parsimony optimization (PO), and % likelihood for each area using likelihood optimization (LO) and BBM. Green = Afro-Arabia; Purple = Asia; Red = Europe; Blue = North Americ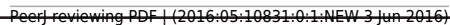a; Gray = continents without hyaenodontidans. Red vertical dashed lines indicate dispersal intervals discussed by Gheerbrant & Rage (2006). Gray vertical dashed line indicates age of L-41.
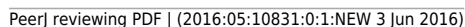
Figure 23(on next page)

Carnassial specialization in Hyaenodontida

Comparison of carnassial specialization in Hyaenodontida. Sketches show M^2 of each taxon (name to the right of the tooth) in buccal view. Mesial direction is to the right of the image; distal direction is to the left. M^1 and M^2 for *Hyaenodon* shown. Schematized tree, including divergence estimates, are based on the tip-dating topology. *Proviverra* represents the unspecialized, condition of the upper molars in Hyaenodontida. *Sinopa* is slightly more specialized with a more buccolingually compressed paracone and metacone. *Eurotherium* represents the more specialized carnivorous dentition with the upper carnassial blade formed between the metacone and metastyle and the paracone is smaller, but unfused to the metacone. *Hyaenodon* represents a very specialized shearing dentition. The metacone is taller than the paracone and the paracone is fused to the mesial aspect of the metacone. Teratodontinae independently evolved specialized carnassial morphology from Hyaenodontinae, but their dental morphology is convergent with the metacone taller than the paracone in Teratodontinae, as expressed in the specialized *Dissopsalis* and less specialized *Brychotherium.* Hyainailourinae also converged on specialized, hypercarnivore-like dentition, but in this lineage the paracone is taller than the metacone and the metacone is fused to the distal aspect of the paracone. While not specialized for hypercarnivorous shearing, *Apterodon* also has taller paracones than metacones. **M**, metacone; **P**, paracone. Timeline abbreviations correspond to the first letter for each stage shown in Figs. 19 and 22.

Paleocene			Eocene				Oligocene		Miocene						
D	S	T	Y	L	B	P	R	C	A	B	L	S	T	M	

HYAINAILOURINAE

Akhnatenavus nefertiticyon

M   P

Pterodon dasyuroides

M   P

APTERODONTINAE

Apterodon macrognathus

M   P

Tritemnodon agilis

M   P

TERATODONTINAE

Dissopsalis pyroclasticus

M   P

Brychotherium ephalmos

M   P

HYAENODONTINAE

Hyaenodon neimongoliensis

M   M   P

Hyaenodon horridus

M   M   P

"PROVIVERRINAE"

Eurotherium matthesi

M   P

"PROVIVERRINAE"

Proviverra typica

M   P

Sinopa grangeri

M   P

Table 1 (on next page)

Specimen measurements for the upper dentition of *Brychotherium ephalmos*

Length, maximum mesiodistal length; **Width**, maximum buccolingual width; **Metastyle length**, maximum mesiodistal length from base of the paracone (premolars) or metacone (molars); **Paracone Height**, paracone height from alveolar margin to the apex; **Metacone Height**, metacone height from alveolar margin to the apex; **Paracone Length**, paracone mesiodistal length at base of cusp; **Metacone Length**, metacone mesiodistal length at base of cusp.

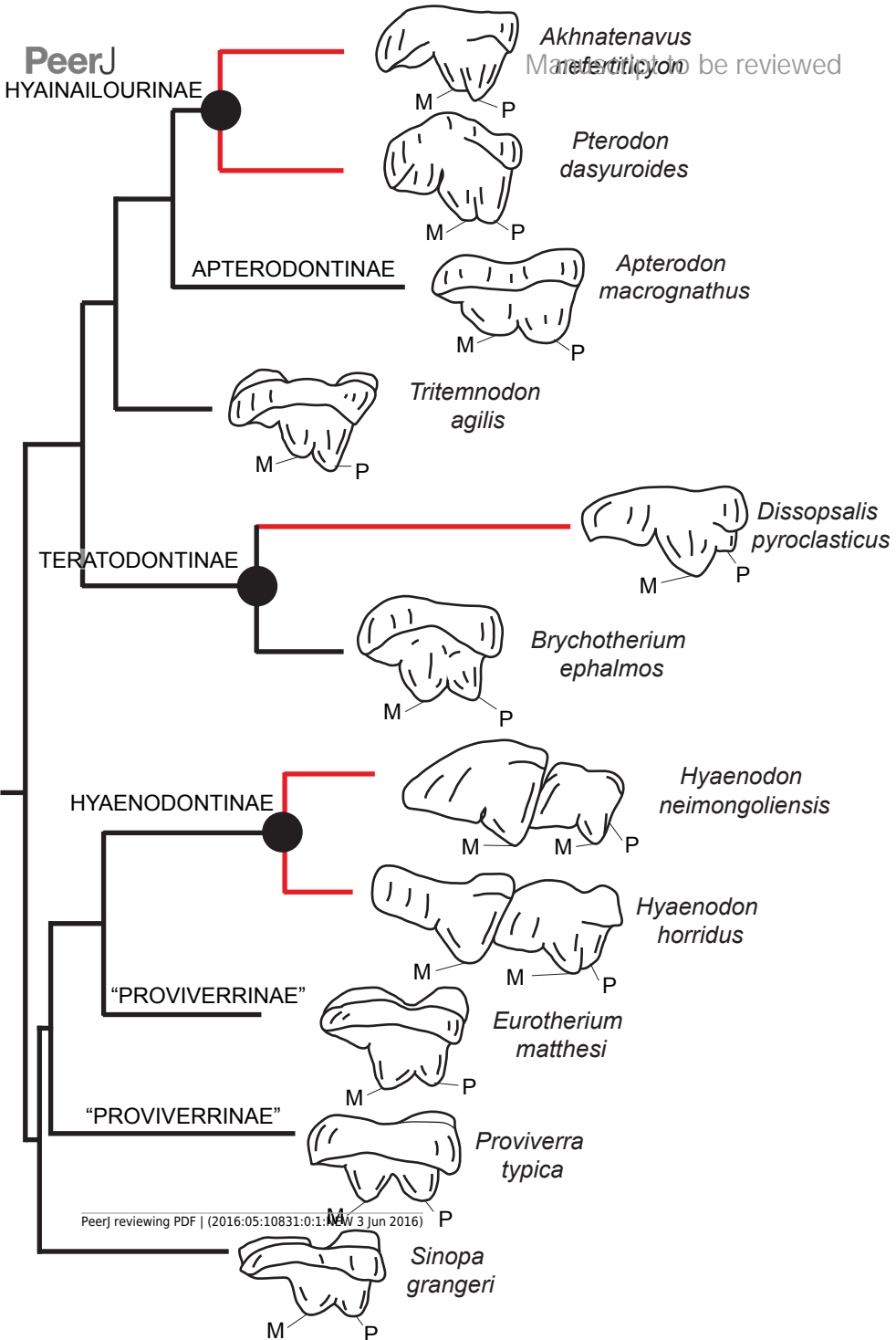| *Brychotherium ephalmos*	Element	Length	Width	Metastyle Length	Paracone Height	Metacone Height	Paracone base length	Metacone base length
DPC 11990	P^4	7.12	6.53	2.4	—	—	3.72	—
(left side)	M^1	8.44	7.42	3.87	2.46	3.01	2.21	2.48
	M^2	9.66	9.65	4.35	3.3	4.67	2.3	2.94
	M^3	3.37	11	—	1.93	~0.83	2.03	0.9
DPC 17627	dP^4	7.72	5.95	3.36	—	—	1.67	2.75
(left side)	M^1	8.73	7.05	4.13	2.47	3.21	1.81	2.89
	M^2	9.91	9.82	4.74	3.54	4.55	2.22	3.47

1
2

Table 2 (on next page)

Specimen measurements of the lower dentition of *Brychotherium ephalmos*

Max. length, maximum mesiodistal length; **Max. trigonid length**, maximum mesiodistal length of trigonid; **Max. talonid length**, maximum mesiodistal length of talonid; **Max. trigonid width**, maximum buccolingual width of trigonid; **Max. talonid width**, maximum buccolingual talonid width; **Talonid height**, tallest point on talonid to alveolar margin; **Paraconid height**, apex of paraconid to alveolar margin; **Protoconid height**, maximum height from cristid obliqua to cusp apex. **Std. Dev.,** standard deviation. Measurements preceeded by "~" indicate measurement taken from a heavily worn cusp. Summary statistics only include specimens with minimal wear.

Brychotherium ephalmos	Element	Max. length	Max. trigonid length	Max. talonid length	Max. trigonid width	Max. talonid width	Talonid height	Paraconid height	Protoconid height
DPC 17627	P_4	7.15	5.48	1.49	3.65	3.18	3.54	2.6	6.08
	M_1	7.56	4.85	2.52	4.18	3.2	2.98	~4.17	5.8
	M_2	9.55	5.4	3.86	5.1	3.47	3.08	6.23	8.85
	M_3	10.19	7.22	2.8	5.12	2.31	2.55	7.12	9.48
CGM 83750	C	5.75	—	—	—	—	—	—	—
	P_1	5.33	3.63	1.45	2.1	2.21	1.52	—	~2.62
	P_2	6.52	5.06	1.47	3.08	2.85	1.48	2.67	~3.8
	P_3	6.7	5.45	1.23	3.31	3.13	2.1	1.8	~3.7
	P_4	7.01	5.21	1.86	3.6	3.57	2.7	2.8	~4.75
	M_1	6.25	4.24	2.06	3.89	3.49	2.67	~2.16	~3.6
	M_2	8.17	5.29	2.57	4.61	3.97	2.95	~3.98	~5.95
	M_3	9.35	6.49	2.97	5.43	3.55	2.69	5.23	7.29
DPC 11569A	C	5.35	—	—	—	—	—	—	—
	P_2	5.18	4.33	0.81	2.51	1.69	0.61	—	3.4
	P_3	6.37	5.2	1.02	2.5	1.72	1.07	1.09	~3.10
	P_4	6.94	5.55	1.41	3.1	2.19	2.37	1.62	5.21
	M_1	6.06	3.77	2.35	3.02	2.34	2.24	~3.83	~4.33
	M_2	~7.68	5.07	~2.57	4.13	~2.27	—	4.46	6.52
	M_3	9.68	6.81	2.81	4.92	2.46	1.93	5.91	8.24
DPC 11569B	C	4.38	—	—	—	—	—	—	—
	P_2	~4.6	—	1.17	2.31	1.84	0.78	—	—
	P_3	6.68	5.05	1.68	2.31	2.1	1.31	1.13	3.6
	P_4	—	—	~1.66	—	2.46	~1.76	—	—
	M_1	6.16	4.07	2.09	2.73	2.28	2.39	~3.20	~4.95
	M_2	7.52	4.95	2.62	3.95	2.42	2.88	4.54	6.32
	M_3	9.07	6.52	2.54	4.69	2.19	1.77	5.87	7.74

Tooth Length	C	P_1	P_2	P_3	P_4	M_1	M_2	M_3
N	3	1	2	3	3	4	3	4
Mean (Std. Dev.)	5.16 (0.70)	5.33	5.85 (0.95)	6.58 (0.19)	7.03 (0.11)	6.51 (0.71)	8.41 (1.04)	9.57 (0.48)

1

Table 3 (on next page)

Specimen measurements for the upper dentition of *Akhnatenavus nefertiticyon*

Length, total mesiodistal length; **Width**, total buccolingual width; **Metastyle length**, mesiodistal length from base of the paracone (premolars) or metacone (molars); **Paracone Height,** from alveolar margin to the apex; **Metacone Height**, from alveolar margin to the apex; **Para/Meta base length**, mesiodistal length of base of both paracone and metacone. **Std. Dev.,** standard deviation. Summary statistics only include specimens with minimal wear.

Akhnatenavus nefertiticyon	Element	Length	Width	Metastyle length	Paracone height	Metacone height	Para/Meta base length
DPC 18242	P^2	9.18	4.08	1.37	6.2	—	5.66
(left side)	P^3	10.09	5.22	2.18	6.3	—	6.58
	P^4	10.94	8.54	2.96	6.25	—	6.09
	M^1	14.08	11.08	6.6	5.57	4.63	7.21
	M^2	15.3	12.8	6.9	7.27	6.07	7.44
(right side)	M^1	13.5	—	5.1	7.37	5.9	5.37
CGM 83735	C	9.95	—	—	—	—	—
(right side)	P^3	10.98	4.44	2.34	—	—	6.03
	P^4	11.98	9.15	3.65	—	—	5.71
	M^1	13.28	9.78	5.33	—	—	5.72
	M^2	15.14	13.5	7.28	—	—	7.04
	M^3	2.49	—	—	—	—	—
(left side)	P^2	9.51	—	2.44	5.95	—	—
	P^4	11.79	—	3.49	—	—	—
	M^1	13.34	—	5.5	—	—	—
	M^2	15.18	—	5.91	7.87	5.54	7.15
DPC 13518	M^1	14.73	9.5	6.37	5.41	4.41	6.96

Tooth Length		P^2	P^3	P^4	M^1	M^2	M^3
N		2	2	3	5	3	1
Mean (Std. Dev.)		9.35 (0.23)	10.54 (0.63)	11.57 (0.55)	13.79 (0.62)	15.21 (0.08)	2.49

1